Quantitative analysis of non-cooperative transboundary river basins

Thèse

Nicolas Avisse

Doctorat en génie des eaux
Philosophiæ doctor (Ph. D.)

Québec, Canada

Quantitative analysis of non-cooperative transboundary river basins

Thèse

Nicolas Avisse

Sous la direction de:

Amaury Tilmant, directeur de recherche

Résumé

Le partage de l'eau dans des bassins versants transfrontaliers est un problème complexe, en particulier lorsqu'il n'y a pas de tradition de coopération entre les pays riverains dans d'autres domaines non liés à l'eau tels que le commerce. De plus, à mesure que les ressources en eau se développent et que le changement climatique est une nouvelle source de risque, le manque d'informations partagées quant aux débits hydrologiques et aux décisions humaines et institutionnelles sur la gestion des ressources rend de plus en plus difficile la distinction entre facteurs naturels et anthropiques dans le dérèglement d'un régime hydrologique.

Des tentatives de récupération de données hydrologiques dans des régions difficiles d'accès ont été réalisées avec succès en utilisant la télédétection. Mais l'application de cette technique pour la modélisation des systèmes d'eau (notamment pour caractériser des infrastructures ou des comportements d'usagers) reste difficile puisqu'elle nécessite d'importantes observations et interactions avec les gestionnaires de la ressource sur le terrain. La portée de la plupart des techniques de modélisation est également limitée par leur incapacité à gérer la multitude d'institutions en charge des ressources en eau, ou l'impact de leurs intérêts spécifiques et souvent opposés sur la ressource en elle-même. Pendant des décennies, ce manque de données détaillées et de techniques de modélisation appropriées a conduit de nombreuses études sur des bassins versants internationaux non gérés de façon concertée à rester qualitatives ou conceptuelles. Cette incapacité à comprendre et à quantifier de manière indépendante les causes de changements hydrologiques est particulièrement frustrante pour des décideurs politiques.

Dans le bassin du Yarmouk, par exemple, qui est partagé entre la Syrie, la Jordanie et Israël, le débit annuel moyen correspond aujourd'hui à moins de 15 % de celui qui a précédé la période de développement, et ce malgré la signature d'accords bilatéraux entre la Syrie et la Jordanie (1987) et entre la Jordanie et Israël (1994). Cette situation a conduit les pays riverains à développer chacun leur propre théorie, contestée, concernant l'effondrement du débit du Yarmouk.

En prenant ce bassin comme étude de cas, cette thèse de doctorat vise à analyser quantitativement des changements hydrologiques dans des bassins versants transfrontaliers, non gérés de façon concertée, complexes institutionnellement, et aménagés à l'excès. Cet objectif passe par deux activités de recherche principales : (*i*) le suivi de la retenue d'eau de petits barrages dans des zones inaccessibles – comme première étape à la caractérisation d'un système multi-réservoirs ; et (*ii*) la simulation et

l'analyse de scénarios, dans le but d'étudier de manière quantitative des changements hydrologiques dans un bassin versant. Les résultats indiquent que des facteurs naturels et anthropiques sont responsables de la chute du débit du Yarmouk et évaluent leur contribution à cet effet en combinant télédétection, simulation multi-agent et analyse de scénarios.

Abstract

Sharing waters in a transboundary river basin is challenging, especially when there is no tradition of cooperation between riparian countries in other, non water-related, issues such as trade. Moreover, as water resources are being developed and climate change is a new source of risk, the lack of shared information on hydrological flows and human/institutional decisions on resources management implies that it is increasingly difficult to distinguish between natural and anthropogenic factors affecting a flow regime.

Attempts to retrieve hydrological data in hardly accessible areas have successfully been made using remote sensing. But the use of this technique for water systems modeling efforts, and particularly for characterizing infrastructure or understand water user behaviors, remains challenging as it requires extensive on-the-ground observations and interactions with water resources managers. The scope of most modeling techniques is also limited by their inability to handle the multiplicity of institutions dealing with water, or the impact of their specific and often competing interests on water resources. For decades, this lack of detailed data and suitable modeling techniques has led many studies on non-cooperatively managed international river basins to remain qualitative or conceptual, and has therefore frustrated policy makers for not being able to independently understand and quantify the causes of hydrological changes.

In the Yarmouk River basin, for example, which is shared between Syria, Jordan and Israel, the annual outflow now corresponds to less than 15% of that of pre-development era, despite the signature of bilateral agreements between Syria and Jordan (1987), and between Jordan and Israel (1994). This state of affairs has led riparian countries to develop their own, contested, narratives regarding the collapse of the Yarmouk flow.

Taking the Yarmouk basin as a case-study, this Ph.D. thesis consequently aims at quantitatively analyzing past hydrological changes in non-cooperatively managed, institutionally complex, over-built, transboundary river basins. This objective goes through two main research activities: (*i*) the monitoring of small reservoirs' storage in inaccessible areas, as a start to characterize a multi-reservoir system; and (*ii*) the simulation and analysis of scenarios to quantitatively study changes in a river basin. Results reveal that the contributions of natural and anthropogenic factors to explain the decline of the Yarmouk flows can be identified and then assessed using remote sensing, multi-agent simulation, and scenario analysis.

Contents

List of Tables

List of Figures

Preface

This Ph.D. thesis presents the research that has been performed between January 2014 and December 2017 at the Water Engineering Department of Université Laval under the supervision of Professor Amaury Tilmant. The work also makes part of a Belmont Forum G8 international project on the *Integrated Analysis of Freshwater Resources Sustainability in Jordan*.

The document starts with an introduction of the context and current main challenges related to the management of transboundary water resources, and then gives a summary of the literature review, research activities and main findings conducted and obtained during these four years of research. More detailed information on the work that has been carried out can be found in the following research papers, in which I am first author:

Paper A Avisse, N., Tilmant, A., Müller, M. F., and Zhang, H.: Monitoring small reservoirs' storage with satellite remote sensing in inaccessible areas, Hydrology and Earth System Sciences, 21, 6445–6459, doi:/10:5194/hess-21-6445-2017, 2017.
Status: published

Paper B Avisse, N., Tilmant, A., Rosenberg, D., and Talozi, S.: Quantitative analysis of contested water uses and management in the conflict-torn Yarmouk basin.
Status: manuscript in preparation

I have also contributed to the following papers through my research:

Supplementary paper 1 Zhang, H., Gorelick, S. M., Avisse, N., Tilmant, A., Rajsekhar, D., and Yoon, J.: A New Temperature-Vegetation Triangle Algorithm with Variable Edges (TAVE) for Satellite-Based Actual Evapotranspiration Estimation, Remote Sensing, 8, 735, https://doi.org/doi:10.3390/rs8090735, 2016.
I produced a land use map for southern Syria without any access to ground data. The whole procedure is presented in this thesis in Sect. 3.3.4. The quality of the map was very high but the procedure required many cumbersome steps (see Fig.3.12). For these reasons, the land use map was used to calibrate other land use maps for Jordan, and served as a basis for crop assessment. The French version of the abstract is available in Annex C.

Supplementary paper 2 Müller, M. F., Yoon, J., Gorelick, S. M., Avisse, N., and Tilmant, A.: Impact of the Syrian refugee crisis on land use and transboundary freshwater resources, P. Natl. Acad. Sci. USA, 113, 14932–14937, https://doi.org/doi:10.1073/pnas.1614342113, 2016.
I developed an innovative approach to retrieve storage–area relationships for reservoirs in data-scarce areas, and to characterize the Syrian multi-reservoir system. This work corresponds to earlier stages of the 2-D dynamic classification *and* Statistical correction of elevation *presented in Paper A. The results were not good enough to precisely estimate reservoir storage, but they were perfectly suited for a statistical analysis of storage variations in the Yarmouk River basin. The French version of the abstract is available in Annex D.*

Finally, some of my work has been presented to the following conference oral presentations and posters:

Poster Avisse, N., Lachaut, T., and Tilmant, A.: Consequences of the unilateral management of the Yarmouk waters on transboundary water allocation in the Jordan River basin, Canadian Water Resources Association, Montreal, National Conference 2016.

Oral presentation Avisse, N., Tilmant, A., Zhang, H., Talozi, S., Müller, M. F., Rajsekhar, D., Yoon, J., and Gorelick, S.: Combining Remote Sensing and Multi-Agent Simulation to Assess Alternative Water Management Policies in Conflict-Prone Areas - The Case of the Yarmouk River Basin, American Geophysical Union, San Francisco, Fall Meeting 2016, abstract #H52F-08.

Oral presentation Avisse, N. and Tilmant, A.: Simulation de l'impact de politiques de gestion de l'eau dans des régions soumises à des conflits ou inaccessibles. Application au Bassin Versant du Yarmouk, Institut Eau Développement Société, Québec, Colloque 2017.

Poster Avisse, N. and Tilmant, A.: Combiner télédétection et simulation multi-agents pour soutenir la conception d'accords internationaux efficaces, Réseau Environnement, Lévis, Symposium sur la Gestion de l'Eau 2017.

Poster Avisse, N., Tilmant, A. and Rosenberg D.: Quantitative analysis of contested water uses and management in conflict-torn transboundary river basins, European Geophysical Union, Vienna, EGU General Assembly 2018.

Introduction

0.1 Jordan Water Project – Analysis of Freshwater Resources Sustainability in Jordan

This work has been carried out under a larger project – *Integrated Analysis of Freshwater Resources Sustainability in Jordan*, which has been undertaken in collaboration with different universities: Stanford University (USA; lead), Université Laval (Canada), UFZ and Leipzig University (Germany), Manchester University (UK), King's College (UK), and Jordan University of Science and Technology (Jordan). By gathering engineers, earth scientists and social scientists specialized in fields as various as surface water hydrology, hydrogeology, modeling, programing, remote sensing, system analysis, economics, institution analysis, risk analysis and geography, our objective has been to *develop a quantitative policy-evaluation tool to explore ways to enhance the sustainability of freshwater systems in Jordan* (`https://pangea.stanford.edu/researchgroups/jordan/`).

Through this Jordan Water Project (JWP), we have aimed at building a multi-agent hydro-economic simulation model combining hydrological modules, to represent environmental processes, and human modules, to characterize human and institutional decisions on various hierarchical levels in Jordan and its main neighbors. By simulating a set of potential future scenarios (e.g. climatic or socioeconomic changes) and interventions (e.g. demand-side regulation or supply side enhancement), valuable information can be retrieved to support Jordanian managers' decision making process. Endogenous interactions between human and biophysical modules, and exogenous inputs impacting these modules, are represented in the integrated model representation of Fig. 0.1.

The institutional framework of the JWP is shown in Fig. 0.2. As a member of this project, I have worked on an optimization model of the Water Authority of Jordan (WAJ) freshwater distribution network (see Annex E). Most of my activities inside the project, though, have focused on international aspects, i.e. on interactions between Jordan and its riparians with which common pool water resources are shared. In particular, Jordan shares the Jordan River basin with Lebanon, Syria, Israel, and the Palestinian Territories; and the Disi Aquifer with Saudi Arabia. Yet, the part of the basin covering Lebanon is marginal, there is almost no water left in the Jordan River (water resources in the Palestinian Territories are by any means mostly managed by Israel), and there is no regulation on water abstractions in the Disi Aquifer but on the quality of its water (Jordan and Saudi Arabia, 2015). The

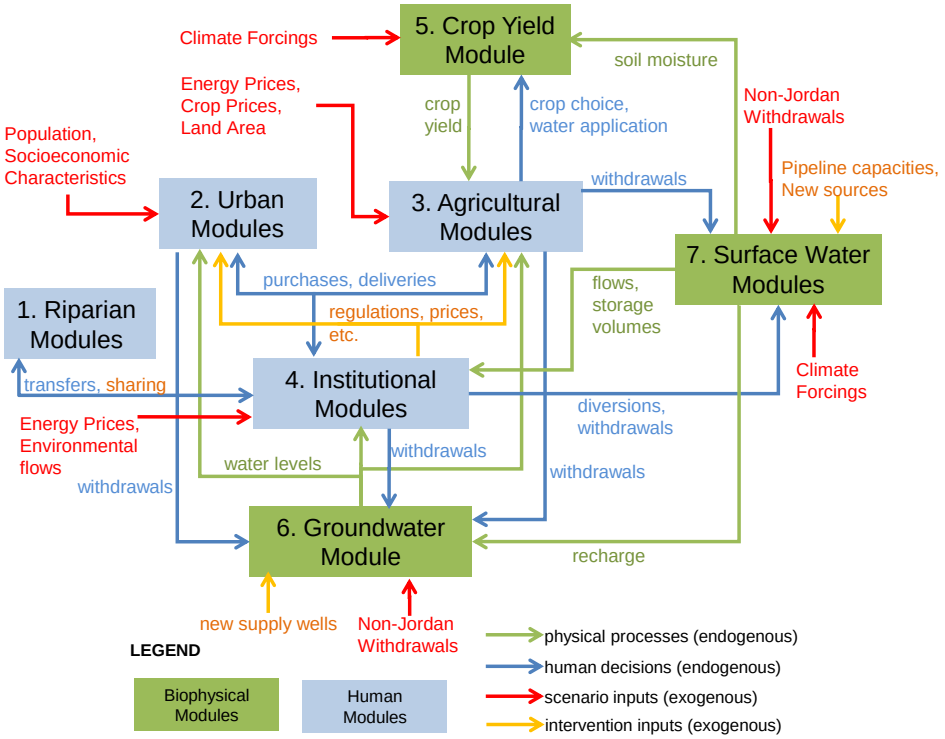

Figure 0.1: Integrated model considered in the Jordan Water Project (Jim Yoon, Stanford University group).

study of international aspects has consequently focused on Syria and Israel, and I have contributed to the JWP multi-agent simulation model by developing management decisions for Jordanian and Israeli institutions as per their Treaty of Peace (Israel and Jordan, 1994).

For these reasons, the Yarmouk River basin, which is shared between the Hashemite Kingdom of Jordan, the Syrian Arab Republic and Israel, has also been taken as a case study for my Ph.D. research.

0.2 Ph.D. context and objectives

One of the main challenges with freshwater resources is to access, transport, and treat these resources at affordable costs to different users. Easily accessible freshwater resources indeed represent only 0.0075% of global water resources on the planet (they are mostly lakes and rivers; Shiklomanov and Rodda, 2003), and the per capita availability of this freshwater keeps decreasing since the beginning of the 20th century due to population growth, rising living standards, and more recently climate change-induced uncertainties. Such large global changes are prone to increase the share of physically scarce water areas (areas physically lacking of water, which have originally mostly been limited to arid parts of the world); but also of economically scarce areas (areas lacking of financial and institutional resources to connect the supply to the demand) since accessing freshwater requires more and more financial resources.

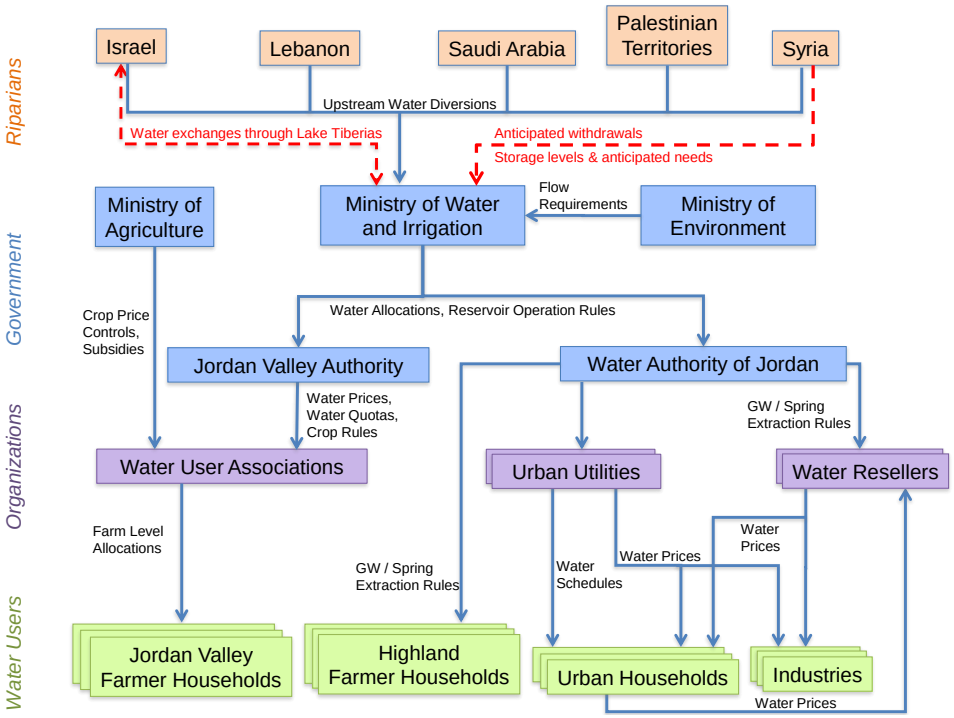

Figure 0.2: Institutional framework considered in the Jordan Water Project (Jim Yoon, Stanford University group).

Decreasing freshwater availability is particularly concerning when water resources are shared between different users and usages (common pool resources), and even more when such users and usages are located in different countries with multiple jurisdictions. In the absence of effective transboundary regulation on surface water resources, upstream riparian countries indeed tend to develop and manage their resources unilaterally without considering the potential externalities (i.e. consequences) on their downstream neighbors. Such situation is a challenge for many interdependent countries: 92 among them have more than 50% of their territory within international basins (Wolf, 2010). In these basins, sharing information on hydrological flows or human activities (e.g. reservoir storage, water diversion or consumption) is often acknowledged as a first step to cooperation. Unfortunately, because this kind of information is generally considered sensitive, countries are often reluctant to release it to their neighbors.

In this data-scarce context, remote sensing has been extensively used for a few decades to retrieve hydrological data in inaccessible areas, either for monitoring or modeling applications. Its coupling to system modeling has however faced numerous limitations for inaccessible areas, as representing anthropogenic activities such as infrastructure, agricultural policies, or reservoir operation, typically requires extensive in situ observations, surveys and interactions with water resources managers. It must be stressed that most modeling techniques are also limited by their inability to handle the multiplicity of institutions and decision-makers that are responsible for water management, as well as the interactions between them or with the resource in itself (Dinar and Wolf, 1994; Giuliani et al., 2015).

Studies that analyzed transboundary water resources systems have then mostly remained qualitative or conceptual, due to the difficulty to address the above-mentioned issues.

The challenge of this Ph.D. has been to develop a modeling framework for quantitatively analyzing past hydrological changes in non-cooperatively managed, institutionally complex, over-built, transboundary river basins. By taking the Yarmouk River basin as a case study, this research has gone through two secondary objectives which are:

1. To characterize the Yarmouk basin's water resources system, and particularly water stored in the multi-reservoir system (**Paper A**), using remote sensing data only.
2. To identify and assess the contributions of natural and anthropogenic factors in the decline of the Yarmouk flows, by combining remote sensing, multi-agent simulation, and scenario analysis (**Paper B**).

This Ph.D. thesis summarizes the findings of my two research papers. Chapter 1 introduces a literature review on cooperation as a way to effectively share common pool resources, and on alternative approaches that have so far been developed for that matter in transboundary basins when shared information is lacking. Chapter 2 presents our case study, the Yarmouk River basin, and the particular issues related to the hydrological changes that have affected its riparian countries. The methodology is then described in Chapter 3, the results are discussed in Chapter 4, and followed by concluding remarks on the research conducted in this Ph.D., on its limitations, and on potential future work.

Chapter 1

Current context and issues

1.1 Water scarcity

When focusing on freshwater resources availability issues, one of the main challenges today is to access, transport and treat these resources at affordable cost to different users. Indeed, only 0.0075% of global water resources are considered easily accessible freshwater (i.e. freshwater lakes and rivers; Table 1.1).

Moreover, since the beginning of the 20th century, the world is witnessing some rapid transformations that are altering the quantity and quality of water resources. With population growth only, per capita freshwater availability has dropped by more than 60% in the last 60 years (Dinar et al., 2007). Considering industrialization and rising living standards, this availability has then certainly decreased even more.

Falkenmark (1989) defined per capita water availability thresholds to characterize a certain pressure on freshwater resources (Table 1.2). These thresholds are widely used today to estimate how vulnerable to water a population is. Two types of water scarcity can actually be distinguished: (i) *physical water scarcity* if not enough freshwater is physically available to meet a population demand, and (ii) *economic water scarcity* if there is not enough financial and institutional resources to access and to distribute freshwater to satisfy the demand. We can see in Fig. 1.1 that physical scarcity typically affects areas in the Middle East and North Africa (MENA), and economic scarcity affects areas that may receive a lot of precipitation (e.g. Equatorial Africa).

Table 1.1: Global distribution of the world's water (from Shiklomanov and Rodda, 2003).

Total water	Saltwater (97.5%)	
	Freshwater (2.5%)	Glaciers (68.7%)
		Groundwater (30.1%)
		Lakes & rivers (0.3%)
		Other (0.9%)

Table 1.2: Conventional definitions of water stress levels (Food and Agriculture Organization, 2012).

Renewable freshwater resources [m^3/cap./yr]	Level of water stress
< 500	Absolute scarcity
500–1,000	Chronic scarcity
1,000–1,700	Regular stress
> 1,700	Occasional or local stress

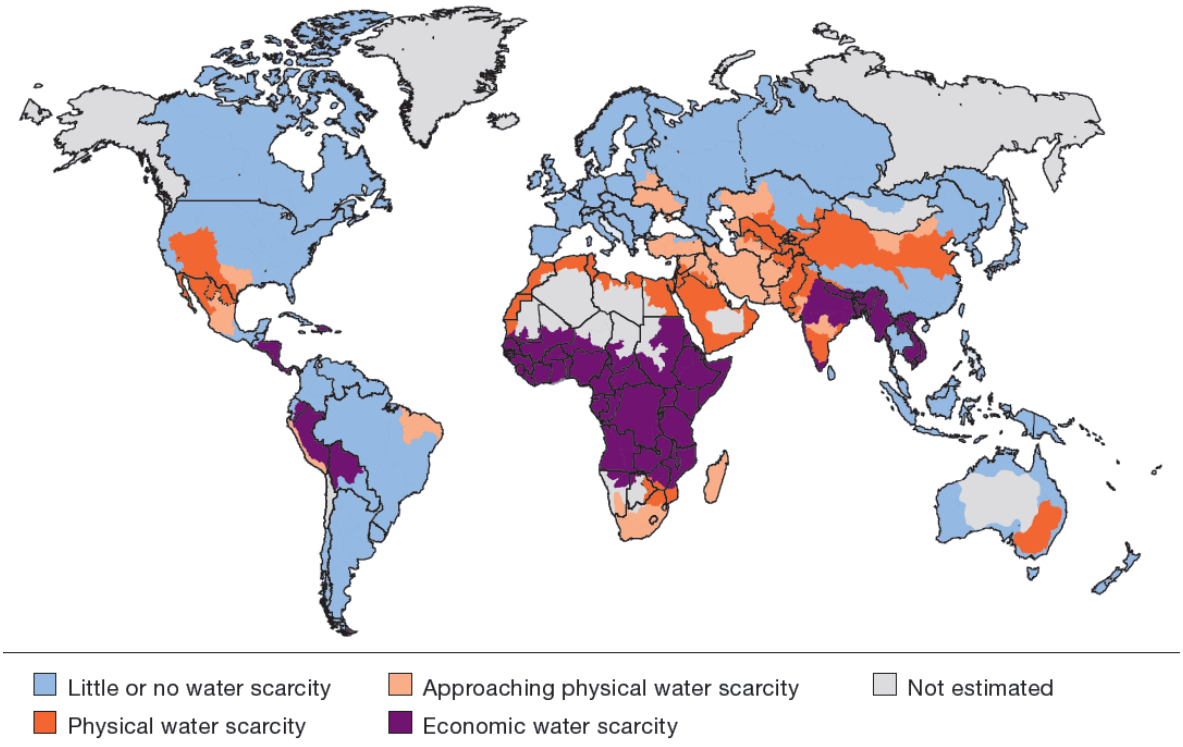

Figure 1.1: Physical and economic water scarcity in the world (Molden et al., 2007).

Table 1.3: Type of goods depending on the level of rivalry and excludability. A usage is rival if the use of the good from a certain party reduces the availability for others; and it is excludable when the use from a certain party prevents the others from using it.

	Rival	Non-rival
Excludable	Private goods	Club goods
Non-excludable	Common goods	Public goods

1.2 Common pool resources

The increasing water stress is raising even more concern when water resources are naturally shared between rival but non-excludable uses (i.e. common pool resources; see Table 1.3) since some parties are relying on others' decisions. In the absence of effective regulation, users often tend to unilaterally manage and develop the resources they can access for their own interests without taking into account the potential externalities (i.e. consequences) that will affect others, or the resource in itself. This important issue, better known as the "Tragedy of the Commons", gained wide popularity with Hardin (1968). In the context of river basins, externalities are most of the time unilateral in the sense that the use from an upstream riparian often affects the availability of downstream users. Therefore, the water management challenge for such basins is often a unilateral externalities problem.

International river basins have particularly been studied as the potential for severe consequences increases with the geographical scale of a dispute (Ashton, 2007). The case of such basins is all the more relevant as 276 river basins cross borders around the world, covering 45% of land area (excluding Antarctica; Wolf, 2010), gathering 40% of the world population, and 60% of the global freshwater flow (UNEP, 2002). However, the risk for a conflict to occur (Fig. 1.2) is more an issue of water scarcity than of geographical scale (Fig. 1.1). The analysis of past international water-related events has indeed shown that violent cases are rare in international basins (Wolf et al., 2003). Water may be a trigger for conflicts, but it is not the only one; and other economic, political, social, historical or environmental aspects need to be considered (Heywood, 2012).

For many years, customary law has been a standard to manage transboundary river basins. It comes from state practices and constitutes implicit agreements supposed to bind all countries sharing the resource. Three main doctrines have historically been called for by riparians depending on the river basin configuration, and on their relationships with neighboring countries (Dellapenna, 1996; Kliot et al., 2001; UNDP, 2006):

Absolute territorial sovereignty also known as **Harmon doctrine**. This doctrine stipulates that riparian countries have exclusive authority on the water flowing down within their territory. In other words, they can manage their waters without considering the effect of potential externalities. This doctrine is typically used by upstream countries, and goes in the opposite direction to current international agreements.

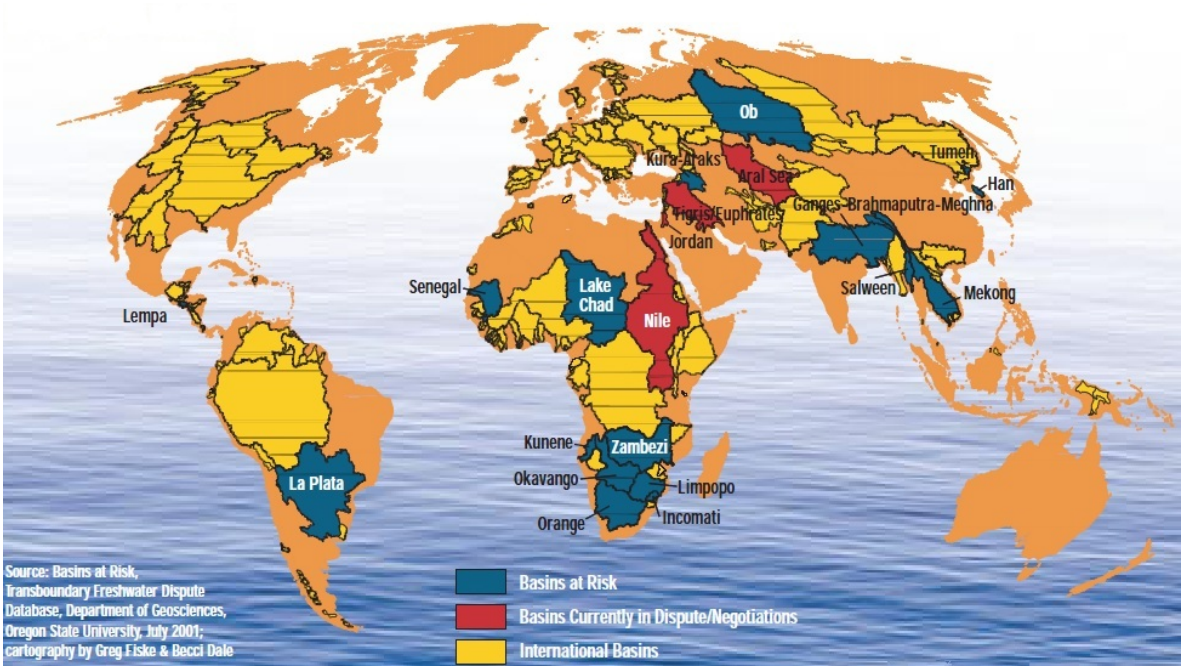

Figure 1.2: Risks of conflict in transboundary river basin (Wolf et al., 2003).

Absolute territorial integrity. It maintains that downstream countries have the right to receive an unaltered river flow from their upstream riparians. This doctrine is exactly the opposite of the absolute territorial sovereignty, but it is seen as too constraining for upstream countries to be applied.

Limited territorial sovereignty. This doctrine claims that each riparian country has sovereignty on the water flowing in its territory, as long as it does not cause significant harm to its neighbors. This principle has been taken over in the building of many international agreements.

Most of the time, these doctrines, though, do not have any acknowledged legitimacy across international river basins. This is the reason why, for a few decades, neighboring countries sharing freshwater resources are more and more encouraged to consider a holistic management of these resources. Managing water in an integrated manner at the river basin scale enables parties to "internalize" externalities (Dinar et al., 2007), so that conflicts can be avoided.

1.3 Managing shared water resources

Methods to solve mutual problems in transboundary basins are sometimes separated in three categories (Jennings et al., 1998): *cooperation* (i.e. working together towards a common objective), *coordination* (i.e. scheduling activities to prevent harmful unilateral decisions and foster beneficial actions), and *negotiation* (i.e. establishing cooperative arrangements acceptable for all parties). These approaches are however presented as different levels of cooperation characterizing a range of more or less realistic

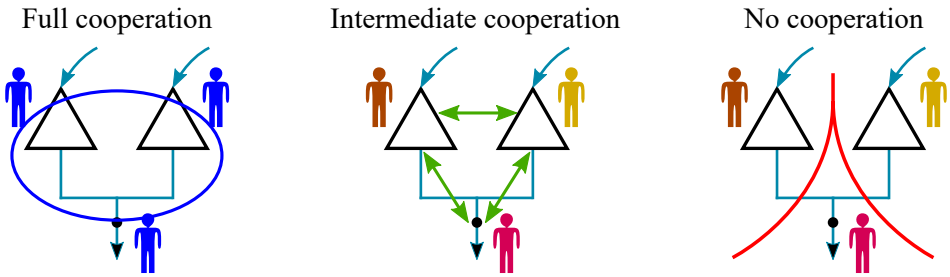

Figure 1.3: Various degrees of cooperation between users/managers in a water resources system.

possibilities depending on the international river basin considered. In this thesis, the word *cooperation* is used as a standard term to characterize this whole range of possibilities (Fig. 1.3).

In a transboundary context, cooperation is often associated to the establishment of international agreements (Wolf et al., 2003; UNDP, 2006) and to the building of transnational basin-wide organisations (Ostrom, 1990; Kliot et al., 2001). Guidelines were first presented by the International Law Association (1966) in the Helsinki Rules on the Uses of the Waters of International Rivers. The International Law Commission (affiliated to the United Nations) took over these principles soon after to prepare the United Nations (1997) *Convention on the law of the non-navigational uses of international watercourses*. It got approved on 21 May 1997 and entered into force on 17 August 2014 after 35 countries ratified it. The main principles are (UNDP, 2006; Dombrowsky, 2007):

- The responsibility to use a shared water in an *equitable and reasonable* way with the aim of reaching "optimal and sustainable utilization thereof and benefits therefrom" (articles 5 & 6).
- The duty to not cause any *significant harm* to riparian parties (article 7). It must be stressed that this point and the previous one meet the doctrine of limited territorial sovereignty.
- The commitment to *cooperate* with riparians, and an incentive to consider the creation of joint mechanisms or commissions to help building this cooperation (article 8).
- The requirement to provide a *prior notification* to riparian countries sharing the same resource before any implementation of a measure likely to affect them significantly (articles 12 to 19).
- The obligation to *protect the rivercourse ecosystem* by avoiding any unreasonable degradation of their own environment or their riparian countries' (articles 20 to 23).

Some regret the lack of explicit tools in the Convention to solve competing claims. It can indeed be noted that only one case involving international rivers has so far been investigated by the International Court of Justice in 55 years (UNDP, 2006). But generally speaking, the Convention is considered as a standard against customary law, and as a basis for building other agreements better suited to address the complexity and variety of issues associated with each transboundary river basin.

In practice, the difficulty to establish any kind of joint management increases with the number of stakeholders and competing interests, particularly when parties are located in different countries with multiple jurisdictions. To better address this complexity, Marty (2001) actually advocates the implementation of bilateral agreements instead of multilateral agreements.

By any means, the existence of cooperative arrangements does not necessarily mean that the "cooperation" will be effective (Underdal, 1992; Zeitoun and Warner, 2006; Zeitoun and Mirumachi, 2008; Selby, 2013). Such regimes, or the studies that are made to build them, may be flouted to benefit more some parties than others (Messerschmid and Selby, 2015). Helm and Sprinz (2000) and Siegfried and Bernauer (2007) have actually developed indices to assess existing regulatory regimes effectiveness by comparing them to non-cooperation and full cooperation scenarios. These baseline situations respectively represent cases in which each manager develops its own water resources system in a decentralized manner independently of the other riparian countries, and in which a single decision-maker is assumed to manage water resources with the aim of maximizing utility at the basin scale. Taking these two extreme scenarios as a reference is also commonly done to assess the value of intermediate (and more realistic) cooperation strategies (Giuliani and Castelletti, 2013).

However, no matter the number of parties involved and the level of complexity of a certain coordination arrangement, cooperation often starts with the sharing of information, either on hydrological flows or management decisions (e.g. reservoir operation or diversion system). Because this information is particularly sensitive in transboundary river basins (Chenoweth and Feitelson, 2001), international cooperation is generally affected by the reluctance of riparian countries to share that data on their part of the basin.

1.4 Circumventing the lack of data

The lack of data issue cannot be narrowed to non-cooperatively managed river basins since it more broadly concerns many remote or inaccessible river basins, if not many river basins in general. Solander et al. (2016) note that there is a scarcity of monitoring data in most parts of the world as many countries cannot financially build gauging stations. Vörösmarty et al. (2001) even notice a decline in available in situ measurements in all parts of the world. And when monitoring systems do exist, there may not be institutions to collect the data or legal means to disseminate it (Alsdorf et al., 2007; Duan and Bastiaanssen, 2013).

Then, the study of non-cooperatively managed river basins, or more generally of remote or inaccessible areas, requires (*i*) to find methods to access information when technical, legal or institutional means are lacking; and (*ii*) to develop modeling tools to interpret this information and to analyze past changes or future potential scenarios.

1.4.1 Remote sensing

Large amounts of spatially distributed data can be retrieved via remote sensing and serve as input data for hydrological models (Lakshmi, 2004; Lettenmaier et al., 2015). Physically based distributed hydrological models are often adopted to take into account the spatial heterogeneity of parameters such as precipitation, evapotranspiration or soil moisture (Stisen et al., 2008; Wanders et al., 2014; Zhang et al., 2016). Efforts performed by Zhu and Woodcock (2014) to continually detect land cover changes can also be noted, as they may prove to be useful for near real-time analysis. Moreover, remote sensing has recently been used to evaluate the spatial pattern performance of hydrological models (e.g. Conradt et al., 2013; Mendiguren et al., 2017) to complement the usual calibration/validation that compares simulated parameters to in situ specific measurements at specific locations (typically flow time series at the outlet of a basin). The goal of this approach is to take into account spatial considerations, instead of temporal ones, for performance evaluation.

As water resources are increasingly developed, remote-sensed information on reservoir storage can also be useful for downstream water users relying on upstream reservoir releases when coordination is lacking (Crétaux et al., 2015). This information also becomes essential to conduct hydrological studies in committed basins, from defining reservoir operation rules in simulation models (Yoon and Beighley, 2015) to assessing the impact of multi-reservoir systems on downstream river discharge (Vörösmarty et al., 1997; Hanasaki et al., 2006; Döll et al., 2009). A lot of research has actually been carried out towards the analysis of surface water bodies, but most approaches have only been applied to reservoirs larger than 100 km^2 (see **Paper A**), which are estimated to represent only 0.54% of reservoirs larger than 0.1 km^2 in the world (Lehner et al., 2011). Studies that analyzed small reservoirs could only get storage capacity estimates by conducting bathymetrical surveys (Sawunyama et al., 2006; Liebe et al., 2009; Rodrigues et al., 2012). As a matter of fact, applying remote sensing to characterize infrastructure or water user behaviors most of the time requires extensive calibration through on-the-ground observations, surveys, and interactions with water resources managers. Such approaches are consequently inapplicable to remote, ungauged or conflict-torn areas.

Assumptions, such as a stationary land use (Pereira-Cardenal et al., 2011), linear or polynomial reservoir elevation–area relationships (Gao et al., 2012; Duan and Bastiaanssen, 2013; Song et al., 2013) or cyclic storage variations (Yoon and Beighley, 2015) are then sometimes made to circumvent the lack of in situ parameters for system modeling applications.

1.4.2 Water resources system modeling techniques

Generally speaking, the modeling of a river basin water resources system is valuable to go beyond qualitative observations or analyses. Modeling techniques can be classified in two main categories: simulation and optimization. Simulation is useful to assess the impact of hypothetical scenarios over a historical period or a planning horizon, while optimization is generally applied to determine the best option among a set of possibilities. Most studies modeling transboundary water resources man-

agement have used three techniques: hydro-economic optimization, game theory and multi-agent simulation.

Hydro-economic optimization

Hydro-economic models are used to represent hydrological, engineering, environmental and economic aspects in a coherent framework. These models take into account both supply and demand, and dynamically allocate water in terms of its economic value for each usage at each time, considering specific environmental and societal constraints. Such an approach is then often used to value the integrated water resources management, based on the principle that "managing water as an economic good is an important way of achieving efficient and equitable use, and of encouraging conservation and protection of water resources", which was developed during the International Conference on Water and the Environment (1992). It can be noted that assigning a value to water also enables to simplify complex multi-objective problems into a single-objective one to be optimized. Modeling parameters are generally integrated in a unified computational framework constituted of arcs and nodes (Harou et al., 2009). Arcs typically stand for rivers, canals or pipes; and nodes for wells, reservoirs, or demand sites. Hydro-economic optimization studies include Rosegrant et al. (2000); Cai et al. (2003); Ringler et al. (2004); Geressu and Harou (2015).

Hydro-economic optimization problems often consist in an objective function to be maximized (or minimized) over a planning period, and subjected to physical, economic and institutional constraints:

$$Z^* = \max_{x_t} \left\{ \mathop{\mathbb{E}}_{q_t} \left[\sum_{t=1}^{T} \alpha_t b_t(w_t, x_t) + \alpha_{T+1} v(w_{T+1}) \right] \right\} \tag{1.1}$$

subject to:

$$g_{t+1}(x_{t+1}) \leq 0 \tag{1.2}$$

$$h_{t+1}(w_{t+1}) \leq 0 \tag{1.3}$$

$$w_{t+1} = f_t(w_t, x_t, q_t) \tag{1.4}$$

where t is the index of stage, T the end of the planning period, b the one-stage benefit function, x the vector of allocation (decision) variables, α the discount factor, w the vector of state variable, v the future expected benefits, q the vector of stochastic inflows, $\mathbb{E}$ the expectation operator, f the transition function from stage t to state $t+1$, g the set of functions constraining the decisions, h the set of functions constraining the state and Z^* the maximum total benefits associated to the optimal allocation $(x_1^*, x_2^*, ..., x_T^*)$. In most of the studies reported in the literature, the formulation is deterministic (the expectation operator $\mathbb{E}$ can be omitted) and the optimization problem is solved using non-linear programing solvers.

However, traditional hydro-economic models rest on the assumption that there is only one decision-maker overlooking the entire situation in the river basin. In the context of transboundary rivers, this is considering a joint, supranational, entity is responsible for allocating water to the different parties, or,

Table 1.4: A water management game: the Prisoner's Dilemma with two players (Dombrowsky, 2007). Considering that each player has the choice between unilaterally defecting (D), or cooperating (C) with the other, no-cooperating is the strictly dominant strategy in the game: it is always more interesting for a player to not cooperate, no matter what the other does (4 > 3 and 2 > 1). Strategies for a Nash equilibrium (N; no player has any incentive to change his position as long as the other does not change his own) and a Pareto equilibrium (P; the situation of a player cannot improve without making another one's worse) respectively characterize the predominance of individual interests and of collective interests. The aggregated welfare optimum P^+ is also presented.

	C	**D**
C	3,**3**$^{P+}$	1,**4**^{P}
D	4,**1**^{P}	2,**2**^{N}

in other words, it corresponds to a fully cooperative management scenario. Since political, social and institutional aspects are of paramount importance in many transboundary river basins, considering a unique decision-maker that follows an economic objective may not be suited to represent the complexity of international basins. But such an approach still provides an upper bound on the economic value of cooperation. Various attempts have been made to derive a lower bound (i.e. the basin-wide net benefits without any cooperation) based on an ad hoc implementation of hydro-economic models. The basic idea is to resolve the optimization problem sequentially, starting with the upstream country, determining the optimal (unilateral) allocations in that country, which are then imposed to the immediately downstream riparian country, and so on (Tilmant and Kinzelbach, 2012). The comparison between the upper and lower bounds provides an estimate of the benefits of cooperation in a transboundary river basin.

Game theory

By mathematically representing conflictive and cooperative interactions between stakeholders sharing a resource (see example in Table 1.4), game theory (GT) enables to characterize more realistic interactions than a traditional hydro-economic model and is considered useful to study transboundary river basins (Madani et al., 2014). GT is based on the assumption that each player is rational and follows its own interests measured in terms of payoffs. Games can then be cooperative (for non-zero-sum games where all players can benefit from certain configurations, which is not always the case; Dufournaud, 1982), or non-cooperative (McKinney and Teasley, 2007; Madani, 2010).

Non-cooperative game theory (NCGT) has been extensively used in transboundary river basins in conflict, with the objective to resolve issues by evaluating conditions that would lead to mutual benefits. Madani and Hipel (2007) have, for instance, applied the method to the Jordan River basin between Lebanon, Syria, Jordan, Palestine, and Israel; Rogers (1969) to the Ganges and Brahmaputra rivers between India and Pakistan; Dufournaud (1982) to the Mekong River basin, Elimam et al. (2008) to the Nile basin between Egypt, Sudan, Ethiopia, and the upstream nations; and Sheikhmohammady et al. (2010) to the Caspian Sea to model negotiations between Azerbaijan, Iran, Kazakhstan, Russia, and Turkmenistan. However, results of NCGT highly depend on the mathematical definition of

each player's behavior, which is typically based on parameters like level of foresight, risk aversion, or knowledge of the other players' preferences (Madani and Hipel, 2011), which may all be difficult to assess. Moreover, while NCGT produces insightful information into strategic behaviors for studying negotiations, for instance, the results remain most of the time qualitative (Madani et al., 2014).

Cooperative game theory (CGT) assumes that parties are already bound, and communicate and exchange information before the game. Decisions are not taken unilaterally but jointly to lead to a Pareto equilibrium. The objective is to address the allocation problem, particularly for water-scarce basins, by developing functional water allocation arrangements (Parrachino et al., 2006; Madani et al., 2014). The approach is quantitative and it is aimed at assessing the value of cooperation under different coalitions in transboundary river basins including the Syr Darya basin between Kyrgyzstan, Uzbekistan, and Kazakhstan (McKinney and Teasley, 2007; Teasley and McKinney, 2011); the Nile basin between Egypt, Sudan, Ethiopia, Uganda, Kenya, Tanzania, Burundi, Rwanda, Democratic Republic of Congo, and Eritrea (Wu and Whittington, 2006); the Tigris and Euphrates river basins between Turkey, Syria, and Irak (Kucukmehmetoglu and Guldmann, 2004); but also in western Middle East for a regional water trade between Egypt, Israel, the West Bank, and the Gaza Strip (Dinar and Wolf, 1994). Studies that used CGT have then worked on resource allocation methods so that the sharing can be more acceptable and produce more benefits to the riparian countries. Typical allocation systems include: (*i*) social welfare maximization – maximization of the basin-wide benefits as described in Eq. 1.1 and the previous section, (*ii*) bankruptcy methods – for fairly sharing a scarce resource between users, e.g. with the Caspian Sea (Sheikhmohammady and Madani, 2008) or the Tigris River between Turkey, Syria and Iraq (Mianabadi et al., 2015), and (*iii*) benefit sharing – for equitably sharing the benefits through water allocations, e.g. on the Eastern Nile river between Ethiopia, South Sudan, Sudan, and Egypt (Arjoon et al., 2016).

Although useful, the scope of such studies is limited by their inability to handle both the multiplicity of institutions dealing with water, and these institutions' specific and often competing interests on water resources. Dinar and Wolf (1994) actually concluded their study by noting that future studies on international water transfers should include more interacting mechanisms and institutions that are responsible for water management.

Multi-agent simulation

Shoham and Leyton-Brown (2009) define multi-agent systems as "systems including agents that have diverging information, or different information or both, and performing in the same environment". The difference with a single-objective optimization problem is that there is no global supervising structure. Agents are autonomous entities that interact with others and take their own decisions. Reynolds (1987), for instance, used multi-agent modeling to simulate a flock of birds: he computationally reproduced its global behavior while developing an agent for each bird moving in accordance with its own perceptions.

Multi-agent system environments can be differentiated on the basis of five parameters:

Deterministic or stochastic i.e. whether the future state of the environment entirely depends on the current state of the system and on the decisions of the agents that are about to be taken

Episodic or sequential i.e. whether current decisions affect all future decisions

Static or dynamic i.e. whether the environment changes when agents are deliberating

Discrete or continuous i.e. whether time is divided into steps during which agents have to take decisions, or continuous

Known or unknown i.e. whether agents have any information on how the environment works

Among all these potential configurations, agent-based modeling (ABM) commonly refers to autonomous intelligent agents in an *episodic* environment, and the term multi-agent simulation (MAS) refers to a more general simulation modeling framework that can fit in any multi-agent system environment.

Multi-agent systems have been applied in various domains: from distributed-artificial intelligence, to economics or linguistics. The technique has quite recently received a lot of attention for environmental applications due to its ability to associate social and organisational aspects to environmental processes – a review of MAS for ecosystem management applications has been conducted by Bousquet and Le Page (2004). Multi-agent systems also capture decision-making at the agent level, be it an institution (e.g. a government agency, a riparian country) or a resource user (e.g. a farmer, a household, an industry) as well as their interactions (Barnaud et al., 2013). It can be noted that MAS therefore addresses the above-mentioned limitations of game theory as it enables the representation of multiple institutions with varying degrees of cooperation (see Fig. 1.3) in heterogeneous conditions (Parker et al., 2003).

It must be stressed that ABM analyses, due to the complexity of their implementation, have only focused on small-scale case studies: Feuillette et al. (2003) simulated water management interventions in the complex and distributed system of the Kairouan water table in Tunisia; Berger and Ringler (2002) and Berger et al. (2007) represented hydrological and socio-economic aspects, and interactions between the resource and its users in micro-basins in Chile to develop new management policies; Becu et al. (2003) coupled hydrological modeling, farming decisions and crop dynamics in a small basin in northern Thailand; and Le et al. (2012), for instance, studied long-term land-use decisions in the Hong Ha basin in Vietnam. Full decentralized optimization methods, such as the complex ABM constraint-based reasoning, could only been applied to simple hypothetical basins (Yang et al., 2009; Giuliani et al., 2015).

Applications to real large-scale basins have then adopted a simpler decentralized sequential optimization instead of the complex ABM formulation – e.g. on the Yellow River basin (Yang et al., 2012) or

on the Zambezi basin through the definition of an intermediate cooperation scenario in which information is exchanged (Giuliani and Castelletti, 2013) –; or have assumed the existence of a centralized institution to collect data from the riparians – e.g. on the Nile basin (Ding et al., 2016).

Because the Yarmouk River basin is non-cooperatively managed, strongly affected by unilateral reservoir management and irrigation development policies through autonomous managers and farmers, and at the same time characterized by institutional interactions through water transfers between Jordan and Israel at the outlet of the basin, the MAS formulation presents significant assets for the modeling of this case-study. The Yarmouk basin, its resources, water users, and water managers, are then described in the following chapter.

Chapter 2

Case study: the Yarmouk River basin

This chapter presents the Yarmouk River basin (YRB). It gives an overview of the history of the basin, and introduces hydrological changes that occurred since the pre-development stage (pre-1960s) and their related consequences on the neighboring countries.

2.1 Historical and hydrological background

The Yarmouk River drains an area of almost 7,000 km^2 on the left bank of the Jordan River, downstream from Lake Tiberias (Fig. 2.1). The river is shared, but not jointly managed, by three countries: Syria, Jordan, and Israel. The drainage area is mostly an open plateau incised by the Yarmouk River and its tributaries, which are flowing in deep gorges before discharging into the Jordan River. Precipitation (473 mm/yr on average; Salameh and Bannayan, 1993) is highly variable and is concentrated during the winter season, from November to April. It mainly occurs in the western part of the basin, on the slopes of the Golan Heights.

In situ measurements of the Yarmouk River flow at the Wahda dam (major dam built on the Yarmouk River) or Maqarin station before the dam's construction, and Adasiya (outlet of the YRB by convention; see Fig. 2.1) are the only ground data available in the basin. For years following the 1960s, three stages can clearly be noticed in the monitoring data from the Jordanian Ministry of Water and Irrigation/Jordan Valley Authority (MWI/JVA) that are presented in Fig. 2.2: (*i*) a stationary regime before 1999; (*ii*) a sharp decrease of both the base flow and the runoff during the period 1999–2012; and (*iii*) the return of the runoff from 2013, when many Syrian refugees fled the civil war (Müller et al., 2016). Quantitatively, the historical annual flow of the Yarmouk River is estimated to have been in the range 450–500 hm^3/yr (million cubic meter per year; Burdon, 1954; Salameh and Bannayan, 1993; Hof, 1998; UN-ESCWA and BGR, 2013), and characterizes the pre-development stage. Over the past, the discharge of the river has decreased by more than 85% to reach 60 hm^3/yr in 2010. With the civil war in Syria, the flow rose to an average of 120 hm^3/yr for the period 2013–2015. Therefore, as most springs and wadis feeding the Yarmouk are located in Syria and the Israel-controlled Golan Heights, Jordan is generally considered as the downstream riparian country suffering the most from

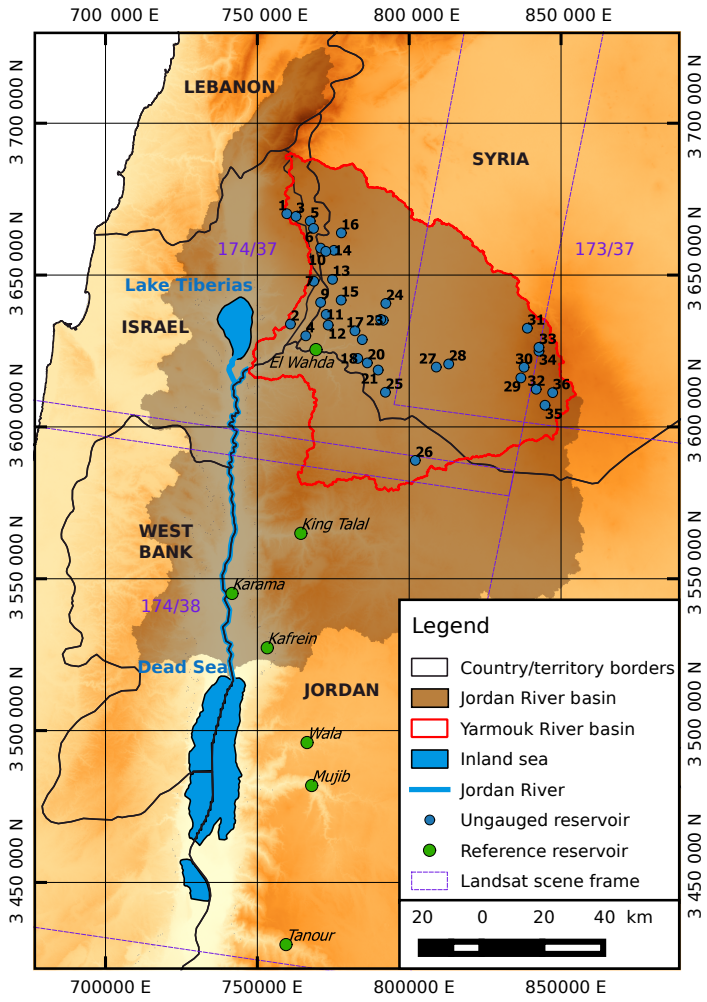

Figure 2.1: The Yarmouk River basin as part of the Jordan River basin, with reservoirs detected using remote sensing (Sect. 3.3.1; see Avisse et al., 2017). Because in situ measurements are accessible for those managed by Jordan, they have been used to validate the method. All coordinates are expressed in the Coordinate Reference System (CRS) WGS 84/UTM zone 36N (EPSG:32636), in which 1 unit equals 1 m.

the river decline.

There are various theories related to the collapse of the Yarmouk flows. Most consider that it was caused by large droughts, increased diversions from the Yarmouk tributaries and groundwater abstractions (UN-ESCWA and BGR, 2013). According to Salameh and Bannayan (1993), rainfall dropped by 30% in the second half of the 20th century, and Beaumont (1997) estimates a natural runoff for the period 1968–1987 inferior by 25% to the one given by Salameh and Bannayan (1993) for the period 1927–1954. According to Kelley et al. (2015), the trend also continued after 1990 with the occurrence of three of the four most severe multi-year droughts in the region in 25 years since 1901. Other analyses overlook climate change aspects and rather consider that the Yarmouk depleted because of excessive water abstractions and uncoordinated construction of dams in the Syrian part of the YRB

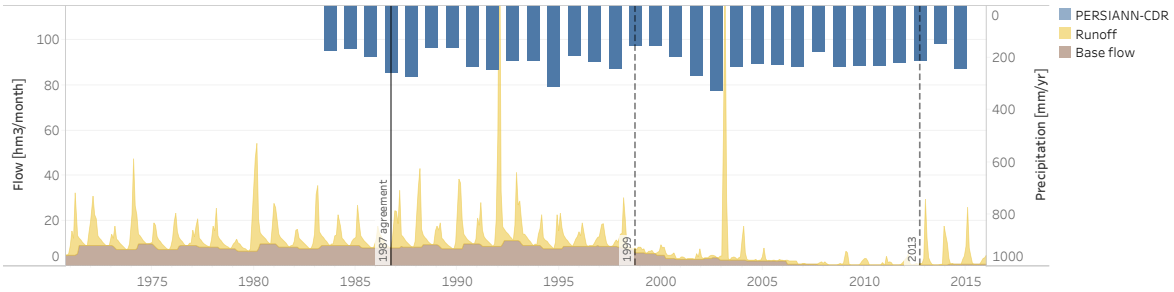

Figure 2.2: Yarmouk River flow – expressed in terms of base flow (moving minimum) and runoff – measured at the station of the Wahda dam by the Jordanian Ministry of Water and Irrigation, and the Jordan Valley Authority; and PERSIANN-CDR precipitation upstream from that station.

(FAO, 2009; Yorke, 2016). It must be stressed that these potential explanations actually reflect the perspectives of the two main riparian countries: Jordan considers that Syria violated their 1987 bilateral agreement by building more dams than what was agreed on, while Syria blames climate change (Hussein, 2017).

2.2 Bilateral agreements

A first bilateral agreement was signed in 1953 between Jordan and Syria (Syria and Jordan, 1953), and updated in 1987 (Syria and Jordan, 1987) essentially to recognize water uses and dams already built in Syria (Rosenberg, 2006; Hussein, 2017). The 1987 version gave the right to Syria to retain water in 28 dams on the Yarmouk basin for a cumulated capacity of 164.64 hm^3, and to access water welling up above the 250 m level above the Wahda dam (less than 0.3% of the YRB area; Rosenberg, 2006), or below the 200 m level below the site of the dam. Jordan got the right to use this reservoir's water to irrigate crops in the Jordan Valley along the King Abdullah Canal (KAC; see Fig. 2.1) essentially, and to supply Amman in freshwater. No explicit limitation regarding groundwater withdrawals is mentioned in the document. Consequently, after considering surface water flow depletions caused by the Syrian reservoirs listed in the 1987 agreement, reduced groundwater triggered by irrigation from springs and projected wells, and irrigation return flows, MWI/JVA (2002) expected inflows to the Wahda dam to attain 117.6 hm^3/yr.

Yet, the flow monitored by MWI/JVA has never reached such a level before the civil war. Wahda has held at most 20 hm^3 (i.e. 18% of its 110 hm^3 capacity) between 2006, when it became operational, and the beginning of the refugees migration in 2013. Consequently, the Yarmouk depletion has affected Jordan's capacity to comply with the Treaty of Peace signed later with Israel (Israel and Jordan, 1994). As per the two water rights on the Yarmouk described in the Israel–Jordan treaty, the hydrological risk is borne by Jordan: no matter the quantity reaching Wahda, (*i*) Israel has the right to a 25 hm^3 annual *allocation* when Jordan gets the rest of the flow; and (*ii*) Jordan has the possibility to store up to 20 hm^3 each year in Lake Tiberias during the Winter Period, and get it back at the entrance of the KAC in the Summer Period (*concession*). Technically, the sharing of water is operated at Adasiya: the flow is

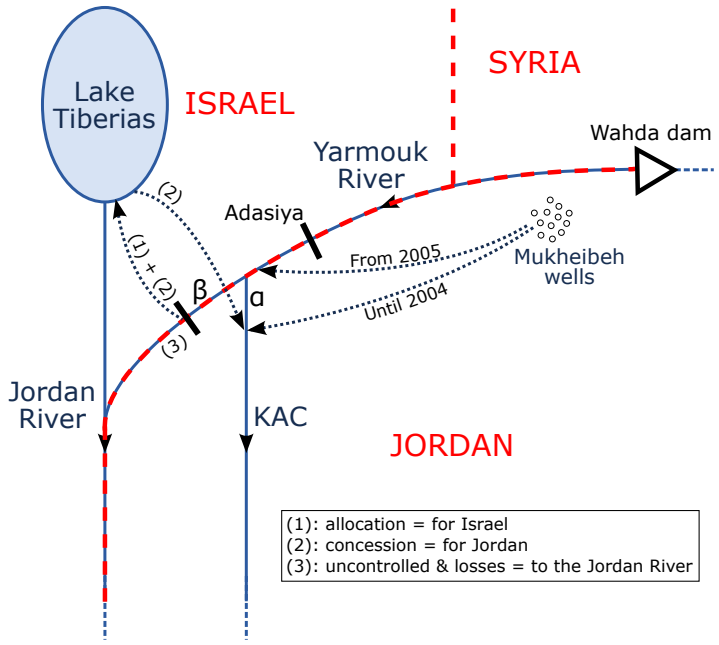

Figure 2.3: Diversion systems downstream from Adasiya.

separated between "alpha", the diversion to the KAC, and "beta", the natural route (Fig. 2.3).

2.3 Agricultural development policies in Syria

As mentioned above, the role of Syria in the Yarmouk decline is still controversial, but not the fact that irrigation increased in its part of the basin since the pre-development stage. Before the 1960s, the Yarmouk and upstream wadis waters were primarily exploited for subsistence agriculture (Courcier et al., 2005), but it changed with the first agrarian reform in 1958 and further highly centralized economic policies towards the development of agriculture (Ababsa, 2013; Ibrahim et al., 2014) at the expense of water resources sustainability (Barnes, 2009). In 1997, irrigation accounted for more than 80% of water use in the Syrian part of the YRB (World Bank, 2001). Aw-Hassan et al. (2014) distinguish three phases in the development of this usage in Syria. In the first one, between 1966 and 1984, irrigation systems expanded. The country started building numerous dams and canals on the Yarmouk tributaries in the upper part of the YRB to increase surface water availability. However, these investments were not sufficient to enable the agricultural production to meet the ever-growing population needs. In the middle of the 1980s, Syria still had to import a large share of basic food supplies (Ababsa, 2013). In the second phase (1985–2000), irrigated crops area kept expanding with the Government's objective to increase food security and ensure self-sufficiency (Salman and Mualla, 2008). Some crops were guaranteed fixed price, and important subsidies for agricultural inputs such as seeds and fertilizers were given to farmers involved in governmental production schemes (Salman and Mualla, 2008; Ababsa, 2013; Aw-Hassan et al., 2014; Ibrahim et al., 2014). Groundwater-irrigated area particularly grew – nationwide, its share rose from 49% in 1985 to 58% in 2000 (Kaisi and

Yasser, 2004) – as farmers could get low interest loans, well licenses were more easily delivered and fuel was strongly subsidized (Gül et al., 2005). But some of these incentives also fostered the growth of illegal groundwater pumping: 50% of wells were unlicensed at the end of the century (World Bank, 2001; Salman and Mualla, 2008). By any means, we can see in Fig. 2.2 that the decrease of the Yarmouk River flow started at the end of this period. The third and last phase defined by Aw-Hassan et al. (2014), from 2001 to 2010, can then be described as a challenging management period for Syria. The Government tried to address groundwater depletion while liberalizing the economy to stimulate investments in the agricultural sector (Ababsa, 2010; Kelley et al., 2015) and ensure food security. As a result, the decrease in the water table level could only be tempered. To these development stages followed the civil war in March 2011, which is still ongoing. This conflict and the 2013 Syrian refugees migration led to a strong reduction in irrigated land area, number of operational wells and reservoir storage in the Syrian part of the YRB (Müller et al., 2016).

2.4 Challenges to quantitatively analyze the basin

While all the above-mentioned studies provide useful information to understand the Yarmouk River flow variations since the end of the pre-development stage, they remain qualitative and basin-wide. Local, quantitative analyses are difficult because of the lack of available data going back as far as 1983 and the ongoing Syrian civil war. To our knowledge, the study conducted by Al-Bakri (2015) on the Jordanian part of the YRB is indeed the only analysis that provides local information on land use and water withdrawals. However, detailed information such as reservoir storage, canal diversions, groundwater withdrawals, crops and irrigation activity is crucial to identify with precision the causes of the Yarmouk River flow decline, and to distinguish consistent study results from widespread politically biased narratives.

Chapter 3

Methodology

This chapter introduces a modeling framework for quantitatively analyzing past changes and future scenarios in transboundary river basins. The approach relies on two components: (*i*) the development of remote sensing-based analysis tools to access information on infrastructures, and on both hydrological and anthropogenic parameters; and (*ii*) the implementation of a MAS system to adequately represent different human and institutional behaviors, and characterize various levels of interactions. Through the combination of these two techniques, one can get a somehow realistic representation of complex water resources systems in non-cooperatively managed river systems.

The chapter starts with a general description of the remote sensing techniques and MAS tools. Sec. 3.3 then provides a more detailed description of the methodology to retrieve the above-listed data from remote sensing products in the Yarmouk basin.

3.1 Remote sensing

Remote sensing is used to retrieve hydrological and anthropogenic data without any detailed on-the-ground measurement, observation, survey, or interaction with water resources managers. Various techniques are applied to get precipitation, to build the multi-reservoir system, to estimate the incremental natural inflows to each reservoir, and to assess water withdrawals.

Precipitation Many remote sensing precipitation datasets exist with different coverage and resolution. The monthly PERSIANN-CDR (Precipitation Estimation from Remotely Sensed Information using Artificial Neural Networks - Climate Data Records) product is used in this study. This global dataset covers the period from January 1983 onwards with a 0.25° spatial resolution.

Dams A method is implemented to locate reservoirs, to assess their maximal storage capacities, and to monitor their storage from 1998 onwards for further validation of the model. It relies on Landsat satellite images for water area estimation, and digital elevation models (DEMs) for topography. Unlike existing approaches, the method does not require any in situ measurement

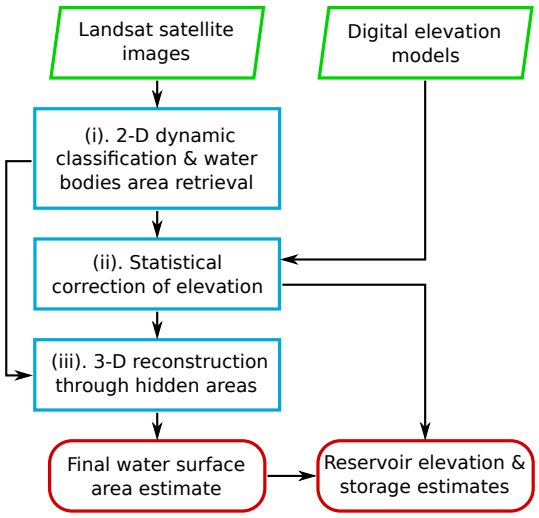

Figure 3.1: Flowchart of the reservoir storage monitoring procedure (Avisse et al., 2017).

and is appropriate for monitoring small, and often undocumented, irrigation reservoirs. The procedure works in three stages that are presented in the flowchart in Fig. 3.1. The idea behind the process is (*i*) to use Landsat bands to enhance the detection of water pixels, then (*ii*) to exploit this information to statistically correct the DEM vertical errors and characterize reservoir bathymetry, and (*iii*) to use the updated topography to reconstruct missing parts of Landsat images (e.g. pixels covered by clouds or not captured by the Landsat sensor).

Incremental natural inflows to each reservoir The rainfall–runoff hydrological model GR2M developed by Mouelhi et al. (2006) is chosen, because of its simple formulation, to estimate the natural flow at the outlet of the basin. This lump model relies on two parameters only – precipitation (see above) and evapotranspiration ETP (see below) – to produce a discharge on a monthly basis. The resulting flow is then separated between base flow and runoff. The runoff is disaggregated at each reservoir's location using a modified drainage area ratio, and the base flow is assimilated to the groundwater flow.

Rivers, pipes and canals Connections between reservoirs are obtained using DigitalGlobe and CNES/Airbus high resolution ($\sim$1 m) imagery available via Google Earth and elevation from a DEM.

Water withdrawals Irrigation water demand is calculated from remotely sensed land use maps, crop water requirements (Allen et al., 1998), precipitation (see above) and standard irrigation efficiencies.

All this data (except storage variations that are used for validating the results; see Sect. 4.2) serves as input for the MAS model that is described below. It is then retrieved on a monthly basis from 1983 onwards (period covered by PERSIANN-CDR data).

3.2 Multi-agent simulation

The PyNSim architecture (written in the object-oriented programing language Python; Knox, 2014, see Fig. 3.2) has been chosen for developing the entire Jordan Water Project MAS model (Sect. 0.1), and thus for developing the related transboundary MAS model for this Ph.D. research.

PyNSim is composed of three classes: *Component*, *Simulator*, and *Engine* (i.e. Model). The Component class (in green in the UML of Fig. 3.2) further includes the classes *Nodes*, *Links*, *Institutions*, which can form *Networks*; the Engine class (in red in the UML) includes models that are designed to solve specific problems; and the Simulator class (in blue in the UML) is eventually defined for undertaking simulations through the individual Engines for a range of time-steps. Unique agents can further be defined from these classes.

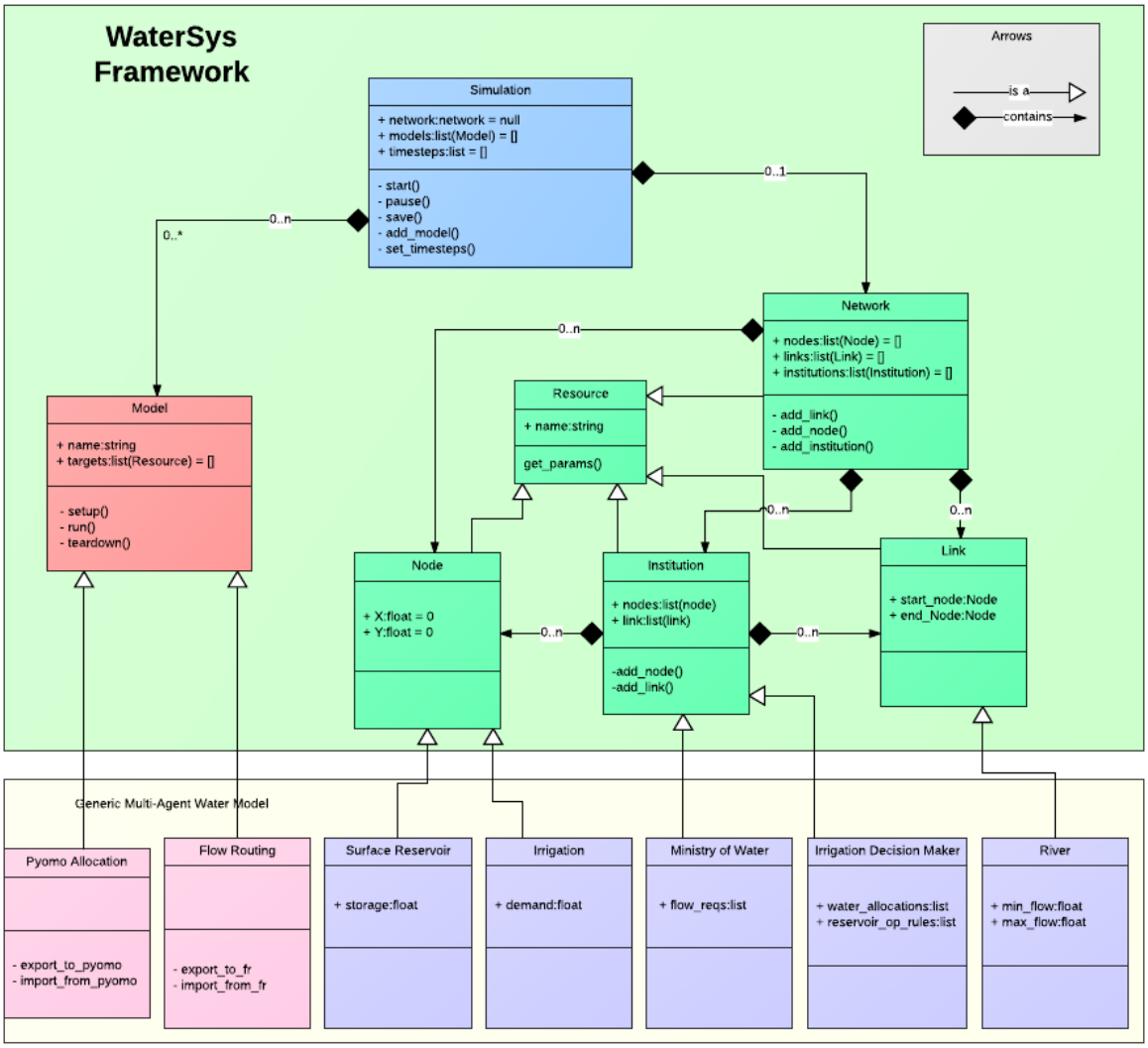

Figure 3.2: Unified modeling language (UML) diagram of PyNSim (Knox, 2014). The generic PyNSim framework is presented in the upper part ("WaterSys" refers to the previous denomination of PyNSim, but the UML remains unchanged), and the bottom part illustrates its application to the JWP.

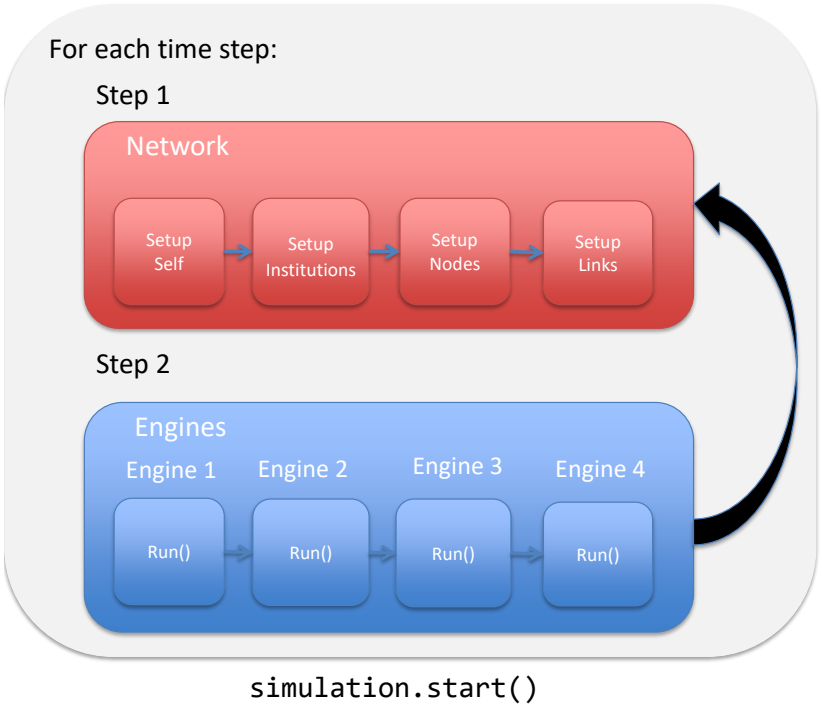

Figure 3.3: PyNSim simulation workflow. At each time-step, each resource in the network goes through a setup phase allowing it to make decisions independently. Then each engine runs, performing actions over the network as a whole (Knox, 2014).

For water resources systems, PyNSim then adopts an arc and node configuration, which is particularly useful for representing the spatially distributed organization of agents inside the same system (Harou et al., 2009, see also Sect. 1.4.2). The main asset of PyNSim, though, lies in the capacity to define different levels of agents, from individual actors who manage one site to institutions who supervise interactions within the water resources system. All these agents are integrated in a single computing framework where human and institutional decisions complement the physical processes. When a simulation is launched, the Engines are sequentially run to reach their own objectives. All agents then store and update parameters that can be either inherent to their classes, or defined by the user of the model (e.g. a capacity, storage or inflow for a reservoir agent; see the simulation workflow in Fig.3.3).

Except for the JWP modeling application, PyNSim has for instance been used to determine the optimal placement of new power plants within a network (Knox et al., 2016). It must be stressed that the PyNSim code has been developed recently, which explains why applications are for now limited.

3.3 Application to the Yarmouk River basin

Information on the inaccessible part of the YRB (i.e. Syria and the occupied Golan Heights) is retrieved using the remote sensing techniques introduced in Sect. 3.1 above and detailed in the following. The first subsection below describes the storage monitoring technique, which is used for both char-

acterizing the multi-reservoir system (i.e. locations and capacities) and further validating the MAS model (the results can be found in Sect. 4.1.3), while the next subsections describe remote sensed-input data for the MAS model.

3.3.1 Reservoir storage variations

The stages presented in the flowchart in Fig. 3.1 are applied to the YRB in order to locate reservoirs, and to monitor the storage of those with maximum storage and area larger than 1 hm^3 and 0.5 km^2 respectively for analyzing the basin. The method's prediction performance is tested against available in situ observations of reservoir storage and elevation in neighboring Jordan.

It must be stressed that this section occupies a large share of the methodology since it describes a novel protocol implemented during the Ph.D. and which has been published (see **Paper A**).

Two-dimensional dynamic classification and water body retrieval

About 300 Landsat 4, 5, 7, and 8 images for each scene – index 173/37 above a part of the YRB, 174/38 above reservoirs in Jordan, and 174/37 above parts of both in the Worldwide Reference System (WRS; see the scene frames in Fig.2.1) – are downloaded from the United States Geological Survey (USGS) EarthExplorer website (`https://earthexplorer.usgs.gov/`).

Fmask The Fmask (Function of mask) algorithm (Zhu and Woodcock, 2012; Zhu et al., 2015) is used to discriminate cloud coverage from open water. The algorithm was originally designed to separate potential cloud pixels from clear sky pixels on Landsat images using empirical thresholds on the Normalized Difference Vegetation Index (NDVI) and the near-infrared band, with an overall accuracy of 96.41% (Zhu and Woodcock, 2012). Fmask distinguishes land and water areas and produces a probability mask for clouds, which is used to manually remove images that are almost entirely covered by clouds or with obvious large errors in water body detection. After quality control, about 245 images remain per location.

Most pixels classified as water by Fmask can reasonably be considered water due to the relatively selective thresholds used in the algorithm. Hence, at this stage, the uncertainty remains with regards to pixels hidden by clouds or cloud shadows, misclassified by Fmask as land or snow, or not captured by the Landsat sensor (e.g. "N/A" – not available – stripes caused by the Landsat 7 Scan Line Corrector – SLC – failure; see Fig. 3.5a and b). The complete analysis has revealed that, on average, 24.1% of the reservoirs' pixels are misclassified as land, 8.1% are covered with clouds or cloud shadows, and 8.6% are in "N/A" areas (see **Paper A**).

Occurrence mask The frequency with which pixels are classified as water is used to distinguish actual reservoirs from small pools or misclassified land, and to delimit them. For each Landsat scene, the ∼245 satellite images are superimposed to form an image where each pixel represents the number of times it has been covered by water (see Fig. 3.4). This occurrence mask (M_{occ}) is

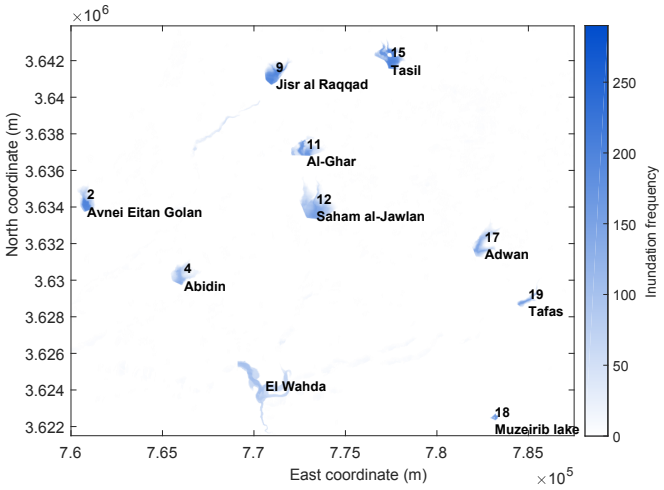

Figure 3.4: Image of the number of times each pixel has been covered by water (M_{occ}; see Avisse et al., 2017). The text in black indicates the identification number (for Syrian reservoirs) and the name of known reservoirs. Coordinates are expressed in CRS WGS 84/UTM zone 36N.

useful for filtering occasional Fmask classification errors, and for creating a water mask (M_{wat}): pixels with values greater than 5 in M_{occ} are classified as water and kept in M_{wat} while those with lower values are considered misclassified land and removed from water bodies (i.e. hidden by M_{wat}). In practice, the threshold of 5 was empirically chosen after comparing detected water bodies with Google Earth high-resolution ($\sim$1 m) imagery. The same threshold is applied to reservoirs located in the overlapping area of two Landsat images as it does not change their contours. Its small value is justified by the fact that most images with obvious mistakes have already been manually discarded at the previous step.

Aside from sporadic large wadis (intermittent rivers) that are manually removed from the mask, final water bodies in M_{wat} are deemed to be reservoirs. They are the ones depicted in blue and green dots on the map in Fig. 2.1.

Classification enhancement for each Landsat image The detection of water bodies is enhanced using NDVI and Modified Normalized Difference Water Index (MNDWI) rasters computed from Landsat imagery. A low NDVI can be attributed to both water and bare land, and a low MNDWI value can denote either water or clouds. These indices are combined and their complementary nature leveraged to detect open water.

To ensure more reliable and repeatable values for identical land use categories in different images, the two indices are computed from surface reflectance, which is estimated by applying the image-based atmospheric correction Dark Object Subtraction 1 (DOS1; Chavez, 1996) to top of atmosphere (TOA) reflectance. However, the DOS1 adjustment is not optimal because it is not based on actual atmospheric or cloud cover measurements. Moreover, the slight band variations between the various Landsat missions may affect NDVI and MNDWI, and may require different thresholds to detect water. Consequently, two supplementary water detection

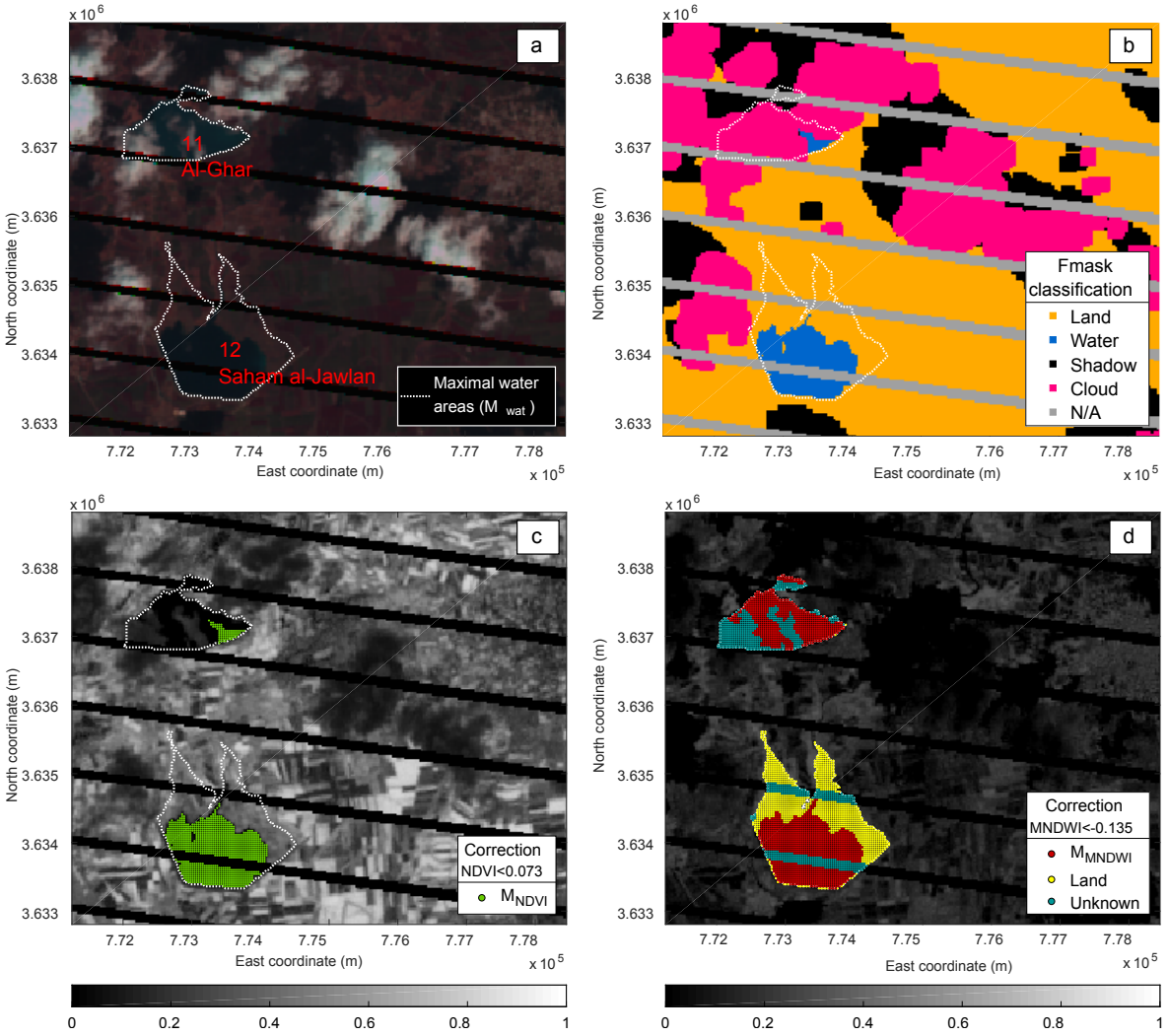

Figure 3.5: 2-D dynamic water classification over a part of a Landsat 7 image (174/37) obtained on 30 March 2010 (Avisse et al., 2017). Coordinates are expressed in CRS WGS 84/UTM zone 36N. (**a**) SWIR-R-G image. Two reservoirs can be seen by eye – even if their appearance is very similar to cloud shadow areas –, but the hedges are not easy to detect due to the cloud cover. (**b**) Results of the Fmask classification. Water areas detection is not precise enough to directly use the results for the estimation of reservoir surface area. (**c**) NDVI image. Water pixels' low NDVI here contrasts with the surrounding irrigated crops' high NDVI, as the two reservoirs are located close to cultivation areas. (**d**) MNDWI image. Red dots indicate water areas obtained after the 2-D enhancement (Sect. 3.3.1). The 3-D reconstruction is done later (Sect. 3.3.1) on the *Unknown* part.

adjustments are performed through the method presented in the flowchart in Fig. 3.6 to define a MNDWI threshold adapted to each date and climatic condition (i.e. each time t over a given scene). A NDVI mask ($M_{\mathrm{NDVI}}(t)$; Fig 3.5c) is first created to calibrate the MNDWI threshold, which is then used to build a MNDWI mask representing water areas ($M_{\mathrm{MNDWI}}(t)$; Fig. 3.5d). More detailed explanation on the definition of the thresholds and of the creation of the masks that are presented in Fig. 3.6 can be found in **Paper A**.

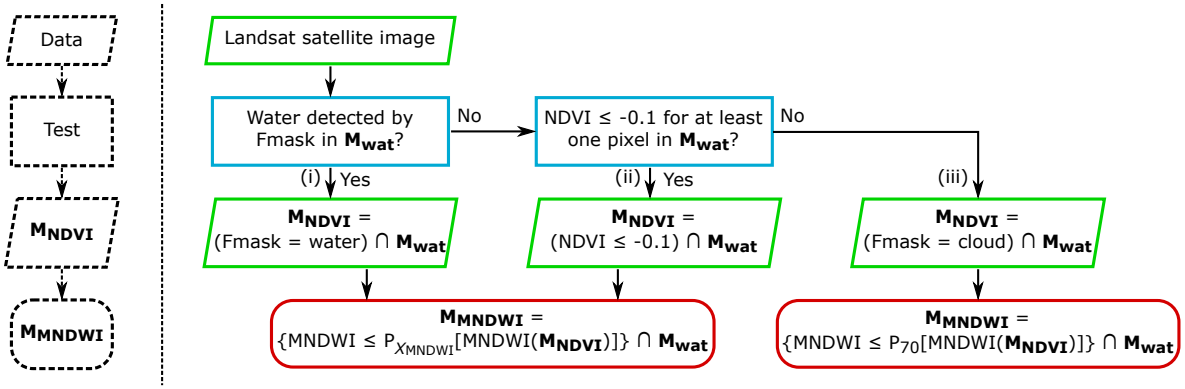

Figure 3.6: Two-dimensional dynamic classification procedure (Avisse et al., 2017).

After removing water areas smaller than 20 pixels (20×900 m^2), considered noise, the classified images have three categories: (*i*) *Water* as identified by the protocol developed above, (*ii*) *Land* according to Fmask, and if not in the category *Water*, and (*iii*) *Unknown*, which includes all other pixels (see Fig. 3.5d).

Statistical correction of elevation

Digital Elevation Models Unlike most studies (see an exhaustive review of the different approaches in **Paper A**), the proposed method does not rely on satellite altimetry to assess water bodies' elevation, but on DEMs to get the topography. It is then required that reservoirs were almost empty or not yet built when the DEM satellites passed over them, for at least one of the two sources considered: ASTER GDEM v2 and SRTM C/X. ASTER GDEM v2 data were acquired between 2001 and 2008, and SRTM-C/X data on 11–22 February 2000. All have a spatial resolution of $1''$ (approximately 30 m at the Equator), which is resampled to match Landsat images. The large coverage of these datasets is chosen over the very low precision of the measures. They indeed cover almost all of Earth's land surface (except for STM-X): from 83° N to 83° S for ASTER GDEM v2, and from 60° N to 56° S for SRTM-C; but the vertical relative precision is very low compared to satellite altimetry: objectives of 15 and 6 m for 90% of SRTM-C and SRTM-X data respectively (German Aerospace Center, 2017; Rodriguez et al., 2005), and standard deviations estimated to 3.95 and 8.68 m for SRTM-C and ASTER data respectively (ASTER GDEM Validation Team, 2011).

Elevation–area relationship To improve elevation assessment, DEMs are statistically corrected by using the information on water surface areas obtained from Landsat images. The protocol presented in Fig. 3.7 is implemented for each reservoir.

1. A water coverage quantile is computed at each pixel to determine the probability of it

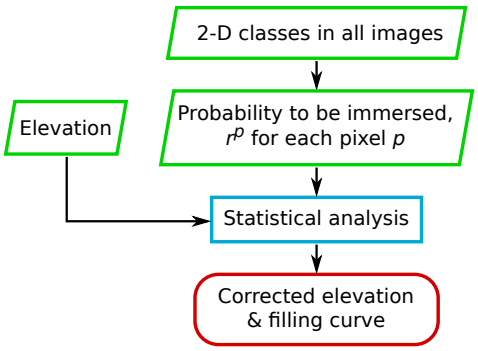

Figure 3.7: Procedure for the statistical correction of topography (Avisse et al., 2017).

being immersed. With each pixel p is associated the ratio r^{p} defined as

$$r^{\mathrm{p}} = \frac{N^{\mathrm{p}}_{\mathrm{water}}}{N^{\mathrm{p}}_{\mathrm{water}} + N^{\mathrm{p}}_{\mathrm{land}}} \tag{3.1}$$

where $N^{\mathrm{p}}_{\mathrm{water}}$ is the number of times the given pixel p is counted as Water, and $N^{\mathrm{p}}_{\mathrm{land}}$ is the number of times it is counted as Land. Images where the pixel p is classified as Unknown are ignored.

2. To illustrate the interest of this section, Fig. 3.8 shows both r^{p} and the relative elevation in the Kudnah reservoir. We can see that the two do not always match as we would expect – i.e. the lowest pixels are not always the most frequently immersed, nor are the highest pixels the most rarely immersed. The immersion frequency (r^{p}) can actually be used to correct the elevation. The former, which is estimated from the results of the 2-D classification enhancement, is indeed assumed to be more reliable than the original DEM. Hence, each pixel's elevation H^{p} is put in relation with the area A^{p}, defined as the cumulated area of all pixels q in the reservoir for which $r^{\mathrm{q}} \geq r^{\mathrm{p}}$. The examples of Fig. 3.9 confirm the observations made in Fig. 3.8: pixels' elevations are not always correlated with the number of times they are classified as water. To a certain extent the difference was expected from the DEM's low vertical precision, but some "anomalies" concerning the most often immersed pixels (i.e. lowest A^{p}) can be recurrent from one reservoir to another, due to either a strong dispersion in elevation (see the SRTM-X data in Fig. 3.9b), or a flat elevation (see the SRTM-C data in Fig. 3.9c). This irregularity is interpreted as arising from the presence of water where the satellite tried to evaluate elevation: in the case of SRTM-X, the measure over water is hampered for reasons inherent to the use of a SAR sensor; and in the case of SRTM-C, DEM pixels covered with water may have been filled during a post-treatment analysis. Either way, elevation cannot be retrieved from the given DEM for these reservoirs' most often immersed pixels.

3. To address the issue, a polynomial regression on observed land pixels ($A > A_{\mathrm{i}}$, with A_{i} the area assumed to be immersed during the satellite elevation retrieval) is used to build a "corrected elevation"–area relationship ($A \rightarrow H_{\mathrm{c}}(A)$) that best fits the data (in a least-squares

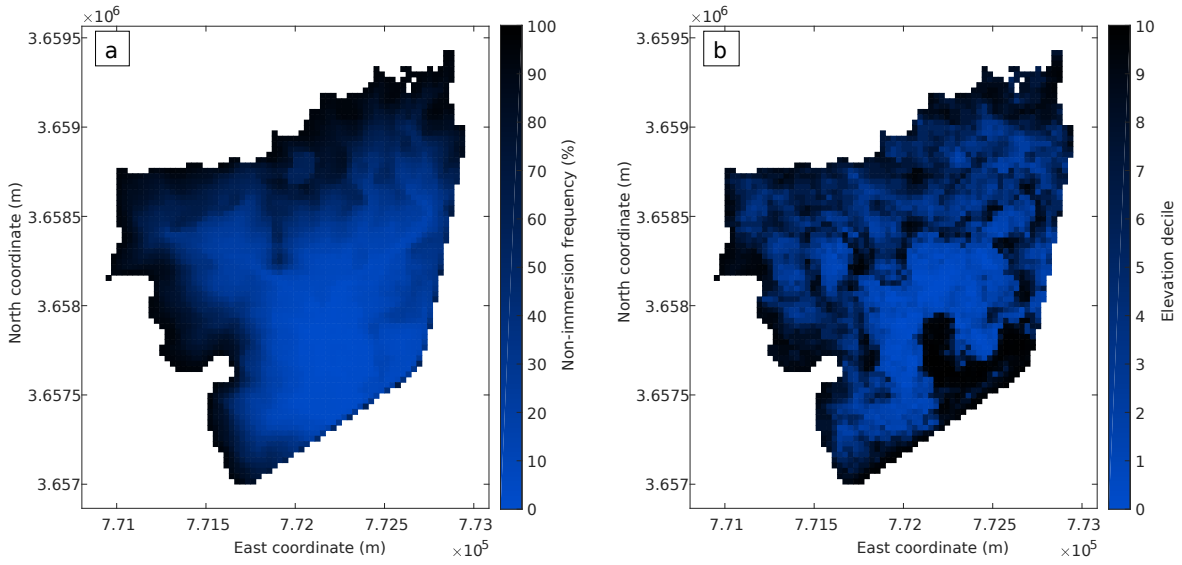

Figure 3.8: (**a**) Relative non-immersion frequency ($1 - r^{\mathrm{p}}$; from the 2-D classes) and (**b**) elevation (from the DEMs; in terms of decile) in the Kudnah reservoir (Avisse et al., 2017). Coordinates are expressed in CRS WGS 84/UTM zone 36N.

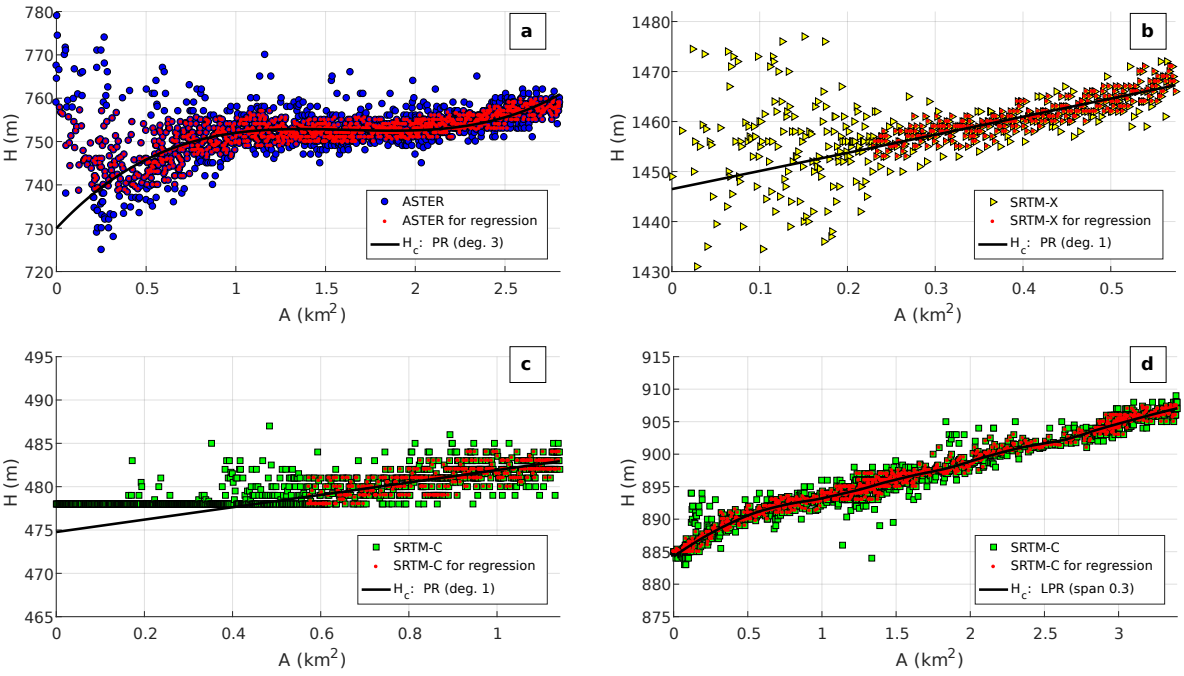

Figure 3.9: Elevation–area relationship and regression for a few reservoirs in the Yarmouk River basin: (**a**) Kudnah, (**b**) Roum, (**c**) Al Ghar, and (**d**) Qunaitera (Avisse et al., 2017). Each symbol (circle, square, or triangle, depending on the DEM) represents the information associated with 1 pixel in a reservoir. PR and LPR stand for polynomial regression and local polynomial regression respectively.

Table 3.1: Parameters and results of the elevation–area regression (Avisse et al., 2017). PR and LPR stand for polynomial regression and local polynomial regression respectively. R^2 is the coefficient of determination between the corrected elevation H_c and the elevation H for pixels taken into account by the regression (red dots in Fig.3.9).

Location	Reservoir	DEM	Visible area $1-\frac{A_i}{A_{max}}$ [%]	Regression	R^2	A_{max} [km^2]	$\Delta H_{c\,max}$ [m]	V_{max} [hm^3]
Israel-controlled	Al-Manzarah	ASTER	100	PR (deg. 2)	0.34	0.53	9.14	2.64
Golan Heights	Avnei Eitan al-Golan	ASTER	70	PR (deg. 2)	0.31	0.93	4.88	2.34
Syria	Abidin	ASTER	65	PR (deg. 1)	0.37	1.16	8.74	5.07
	Qunaitera	SRTM-C	100	LPR (span 0.3)	0.98	3.40	22.81	33.94
	Jisr al Raqqad	ASTER	30	PR (deg. 1)	0.52	1.16	16.23	9.43
	Kudnah	ASTER	100	PR (deg. 3)	0.46	2.81	30.92	29.45
	Al Ghar	SRTM-C	50	PR (deg. 1)	0.56	1.14	8.17	4.66
	Saham al-Jawlan	SRTM-C	55	PR (deg. 1)	0.84	2.48	12.93	15.99
	Ghadir al-Bustan	ASTER	50	PR (deg. 1)	0.56	1.19	15.02	8.93
	Tasil	ASTER	60	PR (deg. 1)	0.28	1.28	9.59	6.15
	Adwan	ASTER	100	PR (deg. 1)	0.33	1.31	7.92	5.17
	Ebtaa kabeer	SRTM-C	80	PR (deg. 1)	0.71	0.73	6.56	2.39
	Sheikh Miskin	SRTM-C	45	PR (deg. 1)	0.71	2.85	7.51	10.71
	Roum	SRTM-X	60	PR (deg. 1)	0.81	0.57	20.77	5.94
	Sahwat al-Khadr	SRTM-C	80	PR (deg. 3)	0.78	1.27	10.07	6.49
Border Jordan-Syria	El Wahda	SRTM-C	100	LPR (span 0.3)	0.97	2.69	53.31	66.72
Jordan	Karama	SRTM-C	85	LPR (span 0.1)	0.90	3.79	17.00	35.91
	Kafrein	SRTM-C	30	PR (deg. 1)	0.56	0.66	17.80	5.85
	Tanour	SRTM-C	85	PR (deg. 1)	0.94	0.59	36.00	10.56
	King Talal	SRTM-C	20	PR (deg. 1)	0.29	2.17	31.66	33.69
	Wala	SRTM-C	100	LPR (span 0.5)	0.85	0.61	25.86	6.37
	Mujib	SRTM-C	50	LPR (span 0.3)	0.79	1.30	44.33	30.49

sense). Values of H greater that the 80th percentile or lower than the 20th percentile are ignored to filter potential errors and smooth the data. This step is executed three times – one for each DEM – and the better quality dataset (i.e. the one with less dispersion and fewer "anomalies" as defined above) is kept. Examples are shown in Fig. 3.9.

4. A filling curve – the volume–area relationship – is finally constructed using the outcomes of the previous step.

The regression relies on the assumption that elevation estimates are correct on average by considering many pixels. Indeed, the relative error in elevation approaches zero when the number of images taken into account grows. This property has already been used by LeFavour and Alsdorf (2005) for instance, in order to estimate the slope of the Amazon River.

Parameters and results of the regression for reservoirs that fulfil the criteria mentioned at the beginning of this section (maximum storage and area larger than 1 hm^3 and 0.5 km^2 respectively) are summarized in Table 3.1.

Three-dimensional reconstruction through hidden areas

Retrieving missing parts of water bodies in the Unknown areas means dealing with Landsat drawbacks: (*i*) the 16-day repeat cycle making images regularly covered by clouds, and (*ii*) the failure

of the Landsat 7 SLC that led to large data losses for the Enhanced Thematic Mapper Plus (ETM+) sensor after May 2003 (see the grey stripes in Fig. 3.5a).

Zhang et al. (2014) developed an approach to improve significantly the estimation of a reservoir's water area. However, their method requires that only a small part of the reservoir is misclassified or hidden. This is not a problem if one works with MODIS images over very large reservoirs, but in our situation – Landsat images over small water bodies – the condition is rarely met.

An alternative algorithm has been developed to use the information from each individual pixel:

1. As the area A^{p} has been associated with each pixel p, and H_{c} has been expressed in terms of A, a corrected elevation is associated with each pixel in a reservoir.

2. Each pixel in an Unknown area adjacent to water areas is set to Water if (*i*) the pixel is in M_{wat}, and (*ii*) its corrected elevation $H_{\mathrm{c}}^{\mathrm{p}}$ is less than the $X_{H_{\mathrm{c}}}$th percentile of the corrected elevation in all adjacent water bodies. This threshold is set to 98 to ignore the highest values of H_{c}, in case they were associated with pixels misclassified as water. A sensitivity analysis has been conducted with regard to this threshold, and the results indicate that values above 98 would give similar good results considering a normalized root-mean-square error (NRMSE) criteria (see **Paper A**).

This water body reconstruction technique relies on the fact that a pixel that is often immersed likely has an elevation lower than a pixel that is rarely immersed. This is a reasonable assumption due to the large number of images analyzed. The blue dots in Fig. 3.10 show how the 3-D reconstruction complements the previous 2-D information retrieval. Finally, storage variations are obtained by combining final reconstructed areas with the previously determined filling curves.

3.3.2 Reservoir evaporation and sedimentation

Extrapolations from ground measurements in Jordan are made to estimate evaporation – which is a major water loss according to MWI/JVA (2002) – and sedimentation.

Net reservoir evaporation The net quantity of water that is evaporated (x_{e} [hm^3]) at each month t above each reservoir n is assessed by deriving reservoir area (a [10^9 m^2]) from reservoirs' simulated storage (based on storage–area relationships obtained using remote sensing as described in the section above), and by considering the weighted precipitation (P_{w} [mm]; see Sect. 3.3.5) and the same monthly reservoir evaporation (E [mm]) as the one measured by MWI/JVA (2002) above the Wahda dam (see Eq. 3.2).

$$x_{\mathrm{e_t}}^{\mathrm{n}} = (E_{\mathrm{t}} - P_{\mathrm{w_t}}^{\mathrm{n}}) \cdot a_{\mathrm{t}}^{\mathrm{n}} \tag{3.2}$$

Sedimentation 0.6 hm^3 of sediments filled the Wahda dam since the dam started to store water. From this value and the 342 hm^3 of cumulated inflows that reached the reservoir since its completion

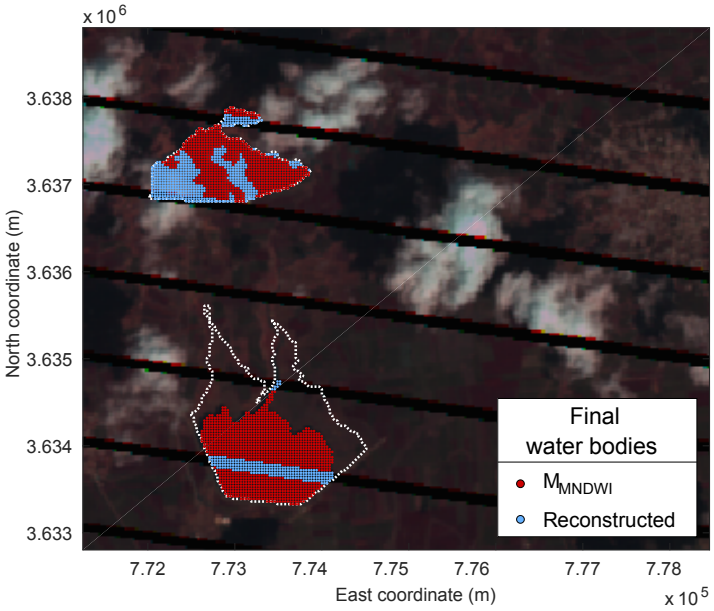

Figure 3.10: SWIR-R-G image. Final water bodies as obtained after the 2-D enhancement and the 3-D reconstruction applied to the Landsat 7 image (174/37) taken on 30 March 2010 (same as Fig. 3.5; see Avisse et al., 2017). Coordinates are expressed in CRS WGS 84/UTM zone 36N.

in 2006, we roughly get a ratio of 0.0018 cubic meter of sediments per cubic meter of water. The same ratio is used to estimate at which rate Syrian and Israeli reservoirs fill with sediments.

3.3.3 Wadis and canals

Connections between reservoirs (both wadis and canals; results are shown in Fig. 3.13) are obtained using DigitalGlobe and CNES/Airbus high resolution ($\sim$1 m) imagery available via Google Earth, and elevation from the SRTM-C DEM.

This satellite imagery analysis presents evidence of the existence of two West–East diversion systems in the YRB: one from Kudnah, and one from Ghadir al-Bustan (see Fig. 3.11). The maximal transfer capacity is calculated for each canal or pipe with the Manning-Strickler equation (Eq. 3.3).

$$Q_\mathrm{p} = K_\mathrm{s} \cdot A_\mathrm{p} \cdot {R_\mathrm{h}}^{2/3} \cdot j^{1/2} \tag{3.3}$$

where K_s [m$^{1/3}$/s] is the Strickler coefficient, A_p [m^2] the cross sectional area of flow, $R_\mathrm{h} = A_\mathrm{p}/P_\mathrm{p}$ [m] the hydraulic radius (with P_p [m] the wetted perimeter), and j [m/m] the hydraulic slope. By considering a canal in unfinished concrete (K_s = 60 m$^{1/3}$/s) and dimensions roughly determined using DigitalGlobe and CNES/Airbus imagery available via Google Earth (cross section of 1 m large and 0.5 m high, and j = 0.1%), we get $Q_\mathrm{p} \simeq 1.00$ hm^3/yr. To this discharge is applied a canal conveyance yield (0.5; World Bank, 2001; Salman and Mualla, 2008) to evaluate the quantity effectively reaching crops downstream.

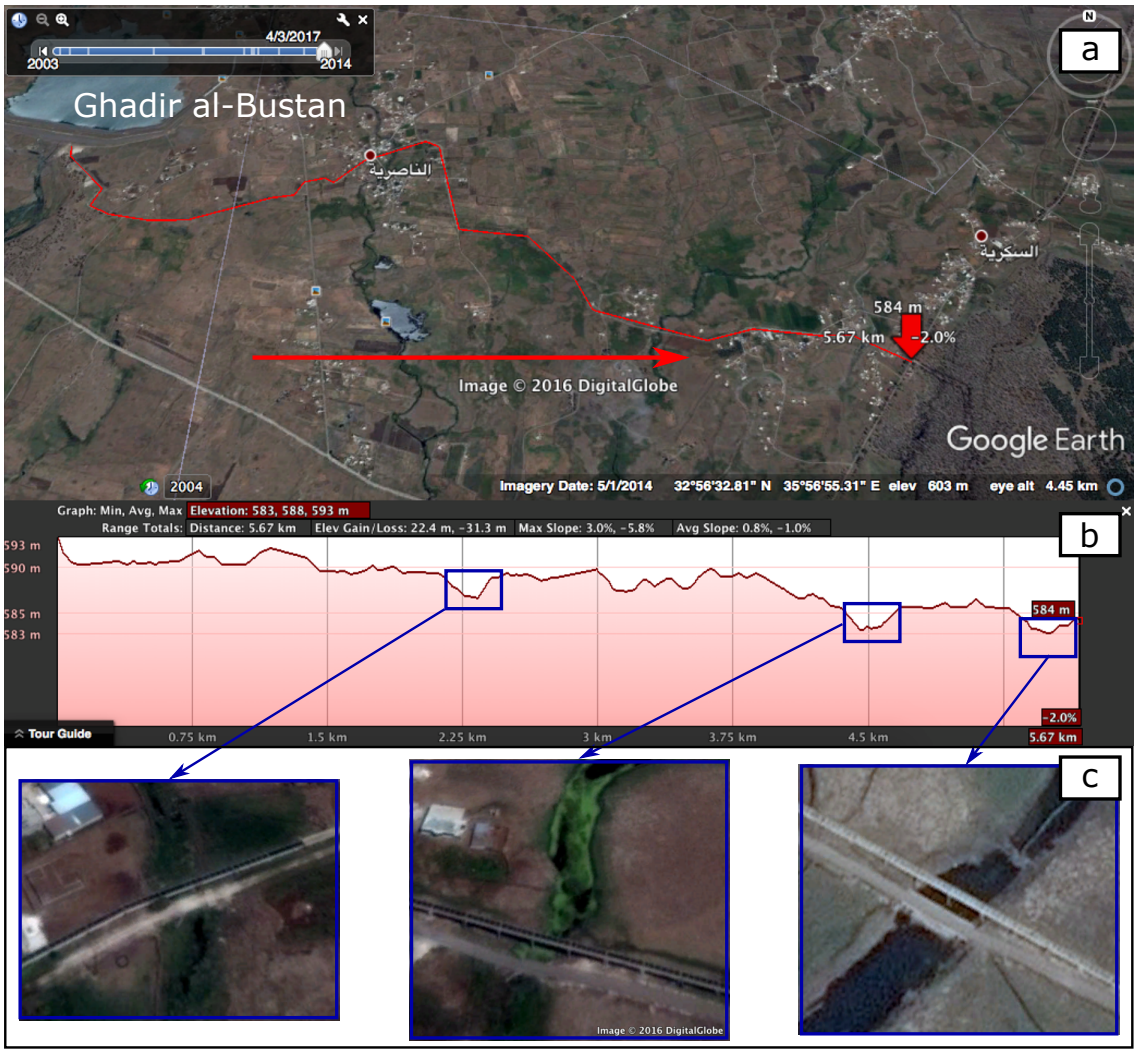

Figure 3.11: (**a**) Canals and pipes detected from Google Earth imagery, and assuring water transfers from the Ghadir al-Bustan reservoir (located in the western part of the basin) to crops in the eastern part of the basin (see Fig. 3.13). (**b**) Decreasing elevation profile along the canals and pipes, despite few obstacles along the way. (**c**) High-resolution imagery above infrastructures detected at the location of the elevation profile obstacles. The observed infrastructures may then explain elevation anomalies along the profile.

As for the wadis, 50% of losses are considered in the transmission of water releases from one reservoir to another to account for infiltration (Delannoy et al., 2016). 75% of these losses are then assumed to recharge the aquifer (Şen, 2008).

3.3.4 Water withdrawals

Agricultural usage

The focus is put on irrigation, as it accounts for 80% of water use in the Syrian part of the YRB (World Bank, 2001). This usage is also more consumptive than industrial and household usages. Irrigation

water demand is calculated from land use, crop water requirements, precipitation and an assumption on efficiency.

Al-Bakri (2015) conducted a detailed study on land use in the Jordanian part of the YRB for the year 2014. As no similar work or ground data has been found for the rest of the basin, remote sensing is relied on to create a first land use map for 2014 (see detailed protocol in Fig. 3.12; and the resulting map in Fig. 4.1.2). Landsat products are chosen because their spatial resolution (30 m) is fine enough to delineate the small irrigated crop areas cultivated by farmers in the YRB. Satellite images are gathered to cover a period of one year over the basin. NDVI is then computed from surface reflectance, which is estimated with the Dark Object Subtraction 1 (DOS1; Chavez, 1996) atmospheric correction applied to top of atmosphere (TOA) reflectance. A principal component analysis (PCA) is applied before conducting an unsupervised classification. Resulting classes are eventually associated to particular irrigated crops by using as a reference the irrigated crop areas obtained by Al-Bakri (2015), and pictures taken by local people in the YRB and available in Google Earth. Irrigated olive trees are also distinguished from rainfed ones by analyzing land surface temperature anomalies (LST anomalies; Goward et al., 2002; Wu and De Pauw, 2011) evaluated with a Split-Window algorithm developed by Du et al. (2015). Because this whole land-use map production step is quite cumbersome, and because by any means no ground data is available for years different than 2014, only two other maps are created using the same protocol – with a mask derived from the 2014 map to distinguish irrigated and rainfed olives – for key transition years between the various policy periods detailed in Sect. 2.3: 1984 and 1998. It can be noted that similar years have been considered by Ibrahim et al. (2014) to analyze the effect of agricultural policies on land use in Syria. No map is produced for the pre-development phase nor for years before 1984 because Landsat images are not available over the YRB for that period.

For each timestep and each pixel in a land use map, crop water requirements (i.e. crop evapotranspiration ET_c [mm]) are estimated using the single crop coefficient method (see Eq. 3.4).

$$ET_{c_t}^{p} = K_{c_t}^{p} \cdot ET_o^{p} \tag{3.4}$$

where K_c [-] is the crop coefficient associated to a particular crop at location p for a timestep t, and ET_o [mm] is the reference evapotranspiration at a particular pixel's location p. Both parameters are calculated using the Food and Agriculture Organisation of the United Nations (FAO) Penman-Monteith method (Allen et al., 1998). However, a correction factor calibrated with ground measurements conducted by Al-Bakri (2015) and Bastiaanssen (2015) in Jordan is applied to FAO's crop coefficient to take into account local conditions of irrigation and plant spacing.

For years between 1984, 1998, 2006 and 2014, crop water requirements are interpolated from the three land use maps and by assuming an irrigated crop area twice as large in 2006 as in 1998 (Müller et al., 2016). ET_c for 1983 and 2015 is assumed to be the same as for 1984 and 2014 respectively. A crop irrigation deficit (δ_i) is injected to consider that only 60% of the crop demand is met (average deficit in the Jordan Valley). In order to account for surface runoff and deep percolation below the root zone,

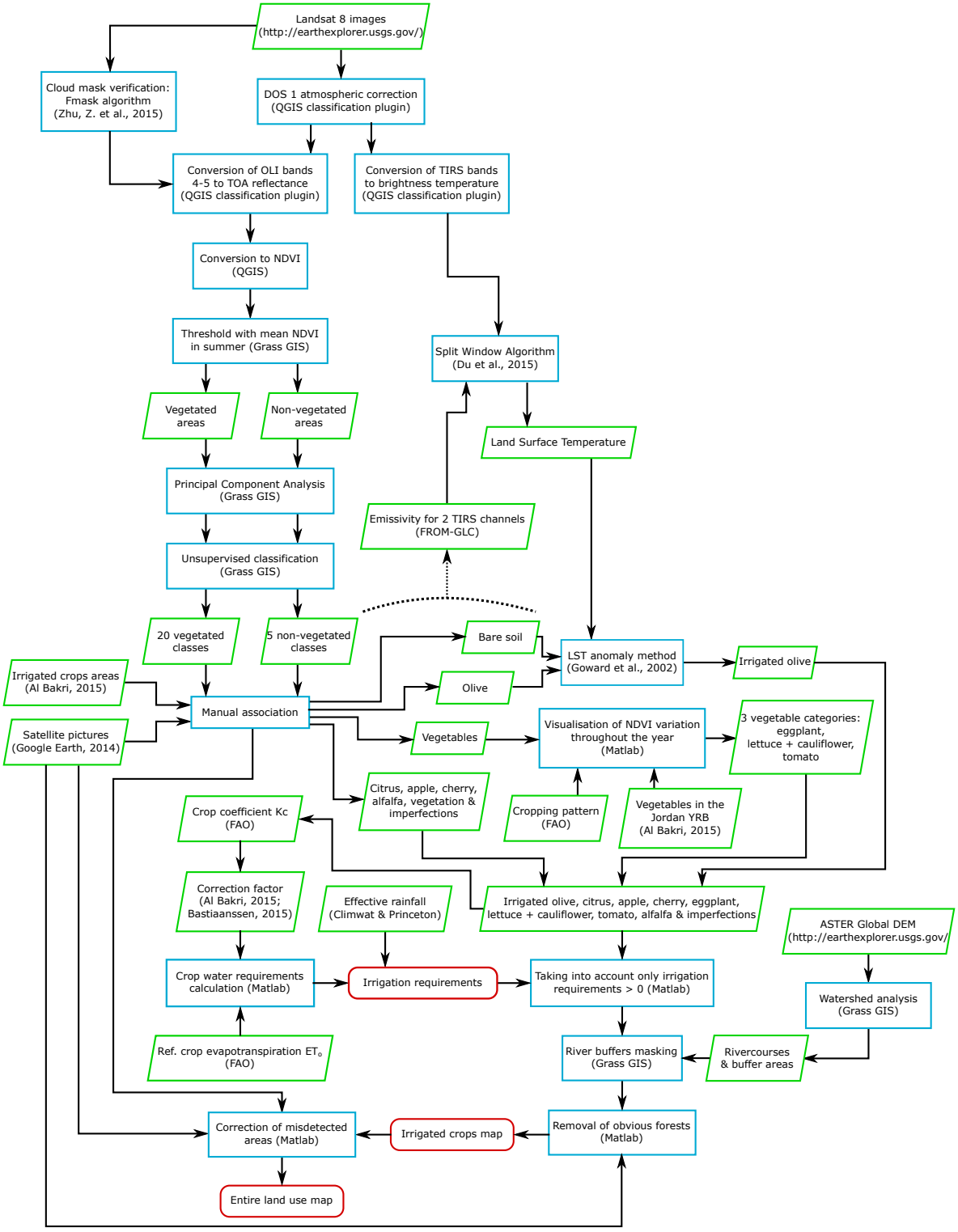

Figure 3.12: Flowchart of the protocol developed to create the land use map for 2014.

an *effective precipitation* (P_e) is computed from P_w (see Sect. 3.3.5) to estimate precipitation de facto available to crops (Dastane, 1974). Irrigation water requirements (IR [mm]) are eventually deduced for each Landsat pixel p and timestep t using Eq. 3.5.

$$IR_t^p = \max\left[(1-\delta_i)\cdot ET_{ct}^p - P_{et}^p, 0\right] \tag{3.5}$$

The quantity to be abstracted (x [hm^3]; Eq. 3.6) from a surface water source to meet these irrigation requirements for the Landsat pixel's area (a_L [10^5 ha]) is computed by considering a low irrigation efficiency (η_i = 0.5; Salman and Mualla, 2008; FAO, 2009) as most farmers in the YRB are small farmers who do not have access to modern irrigation technologies (World Bank, 2001). The same calculation is used to compute water withdrawals from a groundwater source, but with a higher irrigation efficiency (η_i = 0.7) as we assume farmers drill their own well close to their crops, limiting the loss from a conveyance system.

$$x_t^p = \frac{IR_t^p \cdot a_L}{\eta_i} \tag{3.6}$$

Return flows (f [hm^3]; Eq. 3.7) to the aquifer are then estimated to account for 30% of irrigation losses.

$$f_t^p = 0.3 \cdot (1-\eta_i) \cdot x_t^p \tag{3.7}$$

Water users are linked to water sources based on the land use maps and detailed imagery available in Google Earth. For irrigated crop areas close to the reservoirs detected using the remote sensing method presented above and built for irrigation purpose, farmers are assumed to withdraw water in reservoirs first to try to meet the demand, and then in aquifers if there is not enough water in the reservoirs (Etana Syria, 2015).

Household usage

Households near reservoirs are also considered as they are assumed to use the reservoir as their primary source of water. Water withdrawals for household consumption are then assessed using population data from the 2004 Syrian official census (CBSSYR, 2004), a 5 m^3/month/cap. consumption extrapolated from the consumption of Jordanians, and the conveyance yield of 0.5 (see Sect. 3.3.3).

3.3.5 Hydrology

Surface water

The rainfall–runoff hydrological model GR2M (Mouelhi et al., 2006) relies on two input datasets: precipitation and ETP. Precipitation directly comes from the PERSIANN-CDR satellite estimates, and ETP is calculated as the average of crop water requirements over the YRB from the land use maps that have been created, and using the single-crop coefficient method (see Sect. 3.3.4).

GR2M is calibrated with two parameters (a "production store" capacity and a percolation parameter) to minimize the sum of squared distances between simulated and "reference" naturalized water

year flows of the Yarmouk River (i.e. from October to September). This "reference" naturalized flow is generated using a proportional calculation between precipitation averaged over the YRB for each water year, and historical precipitation and discharge of 372 mm/yr and 467 hm^3/yr respectively (Salameh and Bannayan, 1993). Finally, because this thesis is principally aimed at analyzing policies in data-scarce areas, a few rare inconsistencies on simulated naturalized flows are corrected: when simulated naturalized flows are less than observed flows, the former are replaced by the latter.

The base flow is then defined as the 1st percentile of GR2M final simulated flow values at Adasiya: 9 hm^3/month. Considering the ratio between observed inflows to Adasiya and the Wahda dam location, the base flow is divided with the repartition 2 hm^3/month and 7 hm^3/month between these two stations respectively.

In order to better estimate inflows to each reservoir, the PERSIANN-CDR precipitation is corrected to represent the rainfall effectively contributing to the runoff. Indeed, while the spatial resolution of PERSIANN-CDR is already relatively fine, it is still coarse compared to the size of some reservoirs' catchment: each pixel covers more than 650 km^2, which is for example almost four times the area of Qunaitera's incremental watershed where precipitation varies a lot. Thus, PERSIANN-CDR images are resampled to match Landsat resolution, and each precipitation value is weighted inside the YRB, using a gradient derived from isohyets considered by Burdon (1954), Salameh and Bannayan (1993) and Barnes (2009), to form a *weighted precipitation* (P_w). A runoff factor is added to take into account the strong variability of infiltration inside the YRB (Burdon, 1954) and produce a *contributive precipitation* (P_c).

The naturalized runoff at Adasiya estimated with GR2M (i.e. total simulated flow minus groundwater flow) is then disaggregated to each reservoir's catchment, proportionally to the catchment's area and to the *contributive precipitation* P_c averaged over it, to get the inflows to each reservoir. Average runoffs over the historical period ($\bar{q}_{nat}$) are given in Table 3.2 below for information.

Regarding the specific cases of Ghadir al-Bustan and Kudnah, it must be stressed that their respective inflows of 1.9 and 5.4 hm^3/yr are significantly higher than the transfer capacity of their attached diversion systems (1.0 hm^3/yr; see Sect. 3.3.3). Because there are not many irrigated crops close to the two reservoirs, the low transfer capacity indicates that most of the reservoirs' outflows go to the natural route instead of the canals.

Groundwater

Courcier et al. (2005) estimated the mean annual usable recharge (R [hm^3/yr]) of the Yarmouk aquifer to be around 125 hm^3/yr. Because the base flow of the Yarmouk at Adasiya did not vary much for all the duration of Jordanian records – unlike at the Wahda dam –, and because almost all crop areas are located upstream from the Wahda dam, all groundwater abstractions are assumed to be made in the aquifer upstream from the latter station, and all return flows to eventually reach it. The water balance

of this aquifer at a given month t can then be expressed as:

$$\Delta Q_t = R/12 - \sum_p \{\bar{x}_t^p - \bar{f}_t^p\} + \sum_w \bar{i}_t^w \tag{3.8}$$

with $\bar{x}$ [hm^3] and $\bar{f}$ [hm^3] the groundwater withdrawals and return flows associated to each land use map's pixel p (see Sect. 3.3.4), and $\bar{i}$ [hm^3] the infiltration inside each wadi w (see Sect. 3.3.3), averaged over the last 24 months before t to consider a certain transit time inside the aquifer.

The base flow of the Yarmouk River at the Wahda dam location is assumed to be affected and to decrease when the water balance of the aquifer becomes negative, i.e. (by injecting Eq. 3.7 in Eq. 3.8) if:

$$X_t > \frac{R/12 + I_t}{1 - 0.3 \cdot (1 - \eta_i)} \tag{3.9}$$

with X [hm^3] and I [hm^3] the sums of all groundwater withdrawals in the YRB and infiltration inside wadis, and η_i the irrigation efficiency. Simulations have a posteriori shown infiltration to be around 1.7 hm^3/month on average over the pre-1999 stationary regime period. Consequently, based on this value and Eq. 3.9, a threshold of approximately 14.8 hm^3/month for X is obtained to characterize the level above which the aquifer lowers. In that case, the base flow at the Wahda dam location decreases by $|\Delta Q_t|$.

3.3.6 Multi-agent configuration of the Yarmouk River basin water resources system

Multi-reservoir system

37 water bodies are detected in the YRB using the water body detection and monitoring technique described in Sect. 3.3.1 above: 25 are Syrian and listed in the agreement between Syria and Jordan (1987), 1 is listed in the agreement but under Israeli control in the Golan Heights, 1 is the Wahda dam, and the remaining 10 have been unilaterally built in the basin (see Fig. 3.13). These last ones represent 34.5 hm^3 in Syria, less than 0.1 hm^3 in Jordan, and 2.9 hm^3 in the Israel-occupied Golan Heights. Many detected reservoirs are very small as they are found to have not stored more than 1 hm^3 in 30 years, and 2 dams among the 28 listed in the 1987 agreement have not been detected because they are too small or rarely filled with water.

As a trade-off between representing the entire multi-reservoir system of the YRB, and taking into account dams that can significantly affect the Yarmouk River flow, only reservoirs with a capacity larger than 1 hm^3 are considered in the model (Table 3.2).

Multi-agent simulation system

In our study area, the multi-reservoir system in the YRB and the Yarmoukeem Pool (YP)–Lake Tiberias–KAC water exchange systems make the PyNSim MAS environment (see the arcs and nodes configuration in Fig. 3.14a). The right-hand side of the system presented in Fig. 3.14a is actually a simplified version of the complex multi-reservoir system of the YRB presented in Fig. 3.13. The

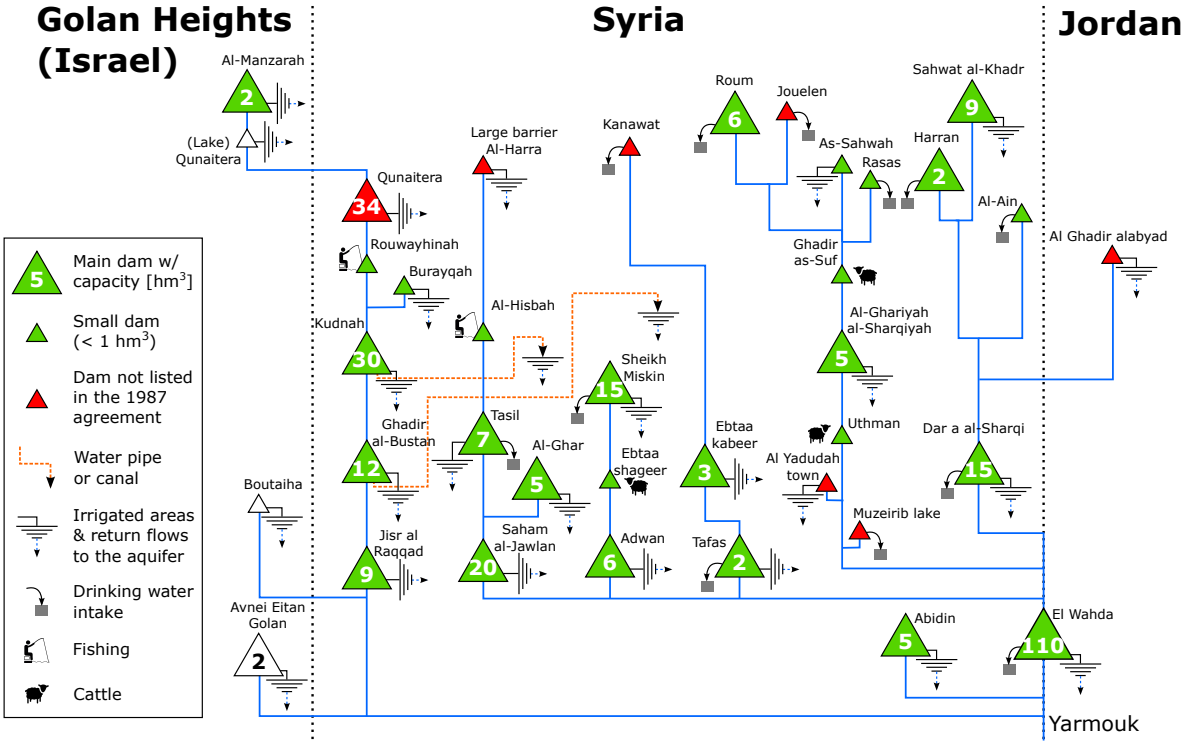

Figure 3.13: Reservoirs, usages, wadis and canals detected in the Yarmouk River basin using remote sensing.

exchange system at Adasiya separates the flow between *alpha* (diversion to the KAC) and *beta* (natural route), and the Israeli system at the Yarmoukeem Pool (3.5 km downstream from Adasiya along *beta*) sends up to 4.5 m^3/s to Lake Tiberias, essentially to satisfy the *allocation* and *concession*. This *concession* is eventually sent back to the KAC from Lake Tiberias as per the treaty between Israel and Jordan (1994). Flows above 4.5 m^3/s go to the Jordan River.

Fig. 3.14b then illustrates the multi-agent configuration of the whole system, in which main reservoirs' operators are considered as independent agents (i.e. stakeholders with their own interests in this case) storing water from the inflows, releasing water to meet certain demands (through water user agents), or spilling water in case they overflow. Indeed, local irrigation needs are assumed to be prioritized over other downstream needs in Syria (Etana Syria, 2015) and the occupied Golan Heights (no cooperation between Israel and Syria). Upstream reservoirs then release water to downstream reservoirs only when their maximal storage capacity is reached: the standard operation policy (SOP) is consequently adopted to represent the management of these reservoirs (the relevance of this choice is discussed in Sect. 4.2 below). As for the Wahda dam operator, it releases water from the reservoir only when the inflows make the simulated storage larger than the storage that has been measured on the ground by JVA. Other agents are finally defined to characterize Jordanian and Israeli controllers of the diversion systems at Adasiya and the Yarmoukeem Pool that were mentioned above. These controllers basically follow the instructions of their respective institutional supervisors, while preserving the water balance

Table 3.2: Dams considered in the modeling. Coordinates are expressed in WGS 84/UTM zone 36N.

Name	Operator's country	Listed?	Coordinates [East, North]	Completion year	Disuse year	Capacity [hm^3]	$\bar{q}_{nat}$ [hm^3/yr]
Al-Manzarah	Israel	Yes	223485, 282845	1982	-	2.3	0.3
Avnei Eitan al-Golan		-	223991, 246480	1982	-	2.3	0.5
Abidin	Syria	Yes	228895, 242487	1989	-	5.5	0.4
Qunaitera		No	231404, 280519	2006	2013	33.9	9.3
Jisr al-Raqqad		Yes	234093, 253358	1991	-	11.0	1.4
Kudnah		Yes	236056, 270196	1992	-	30.0	5.4
Al-Ghar		Yes	235663, 249285	1990	2013	5.5	0.5
Saham al-Jawlan		Yes	236335, 245880	1995	-	20.0	0.6
Ghadir al-Bustan		Yes	237999, 260863	1987	-	12.0	1.9
Tasil		Yes	240680, 253980	1984	-	6.6	7.7
Adwan		Yes	245080, 243840	1986	2013	5.7	3.0
Ebtaa kabeer		Yes	254499, 247077	1972	2013	3.5	8.9
Sheick Miskin		Yes	255463, 252644	1982	2013	15.0	30.1
Roum		Yes	305526, 237106	1977	-	6.4	0.3
Sahwat al-Khadr		Yes	277060, 218989	1986	-	8.8	0.6
Dar'a al-Sharqi		Yes	254714, 223397	1970	2013	15.0	31.1
Tafas		Yes	247434, 240864	1982	-	2.1	6.9
Al-Ghariyah al-Sharqiyah		Yes	271627, 231346	1982	2013	5.0	11.7
Harran		Yes	304324, 223335	1980	-	2.0	0.3
El Wahda	Jordan	Yes	232104, 237922	2007	-	110.0	64.4

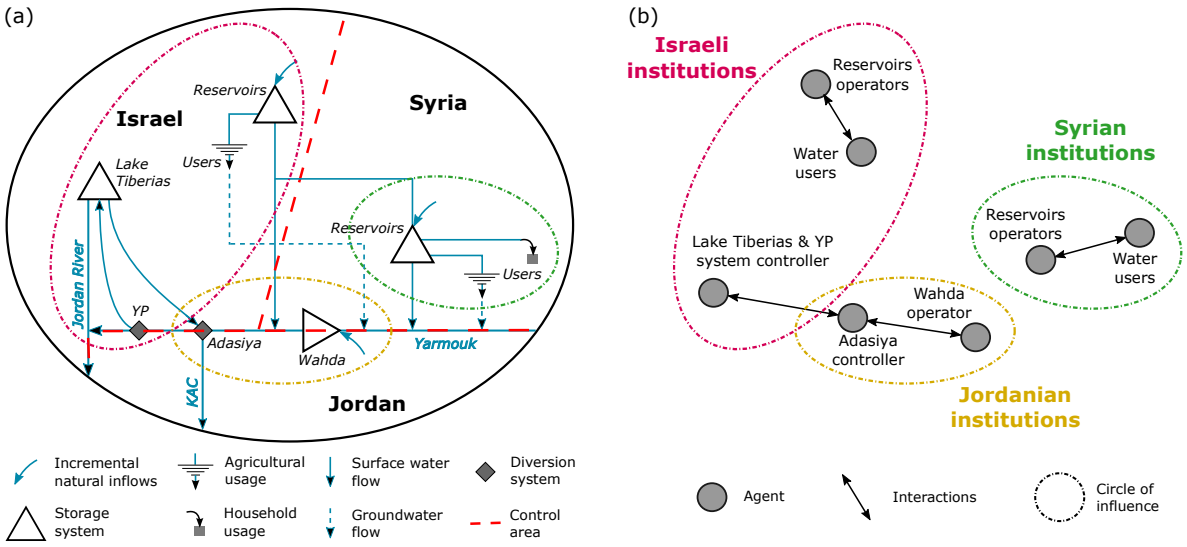

Figure 3.14: (**a**) Schematic of the water resources system considered in this study, and (**b**) associated multi-agent representation with supervising institutions from each riparian country (based on a generic MAS representation considered by Giuliani and Castelletti (2013)).

and physical constraints of each diversion system. Institutions are indeed also created in PyNSim to represent the supervising managers in each country. Since Jordan and Israel interact to transfer water as per the Treaty of Peace, the circles of influence of the two countries' institutions overlap in Fig. 3.14b. Then, it must be stressed that the circles of influence of Syrian and Jordanian institutions do not overlap because there is no effective cooperation between these two countries, despite the signature of the 1987 agreement (Hussein, 2017).

Chapter 4

Results and discussion

This chapter starts with a presentation of remote-sensed parameters and with a qualitative analysis of the potential impact of their evolution (when available) on the Yarmouk River hydrological changes since the pre-development period. Results of the remote sensing-based multi-agent simulation model are then quantitatively analyzed over the historical period and future years.

4.1 Remote sensing

4.1.1 Precipitation

Average PERSIANN-CDR precipitation for 1983–2015 over the YRB is 239 mm/yr – i.e. 64% of the average precipitation estimated by Salameh and Bannayan (1993) for the pre-development stage. The decline is consistent with the 30% rainfall drop for the second half of the 20th century compared to the pre-development period considered by the same authors, and may be responsible for a long-term decrease of the Yarmouk flows.

4.1.2 Land use

The land use map of the YRB for 2014 resulting from the procedure presented in Fig.3.12 is shown in Fig. 4.1. Irrigated crop categories are the first six ones listed in the legend of the map: olive, citrus, apple, cherry, eggplant, lettuce & cauliflower, tomato and forage.

4.1.3 Reservoir storage

Storage variations for all reservoirs in the YRB that meet the storage monitoring method criteria (i.e. maximum storage and area larger than 1 hm^3 and 0.5 km^2 respectively; see Sect. 3.3.1) are displayed in Fig. 4.2. These reservoirs are located in Syria and in the Israel-controlled Golan Heights. By qualitatively comparing our results to those obtained by Müller et al. (2016) (monitoring of Syrian reservoirs using Landsat 7 datasets but before the 2-D and 3-D corrections), we can see more coherent storage variations through the presence of annual drawdown–refill cycles – particularly for Roum and

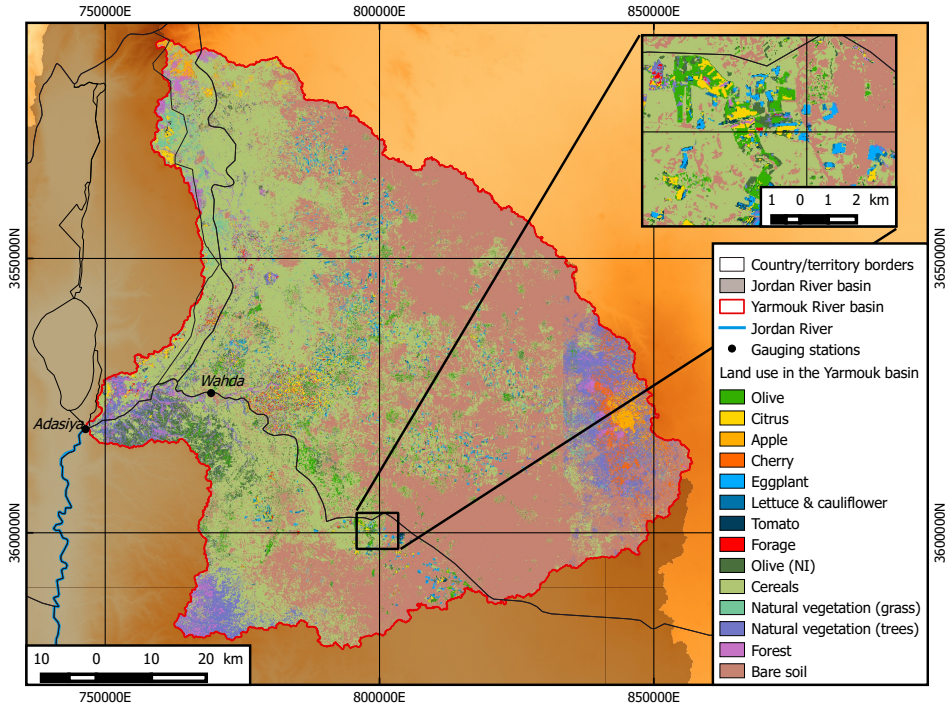

Figure 4.1: Land use map of the Yarmouk River basin for 2014. The map in the top-right corner shows irrigated crop areas that have been particularly considered for the calibration with Al-Bakri (2015). Coordinates are expressed in CRS WGS 84/UTM zone 36N, in which 1 unit equals 1 m.

Sahwat al-Khadr. This means that the 2-D enhancement and 3-D reconstruction steps have improved the detection of water and helped to overcome the low Landsat repeat cycle of 16 days.

Reservoirs managed by Jordan (i.e. green dots in Fig. 2.1) are used to validate the method by comparing our remote sensing estimates of elevation and storage with monthly in situ measurements conducted by the Jordan Valley Authority (JVA). With the exception of the King Talal dam, our results seem to follow quite accurately the historical records (see Fig. 4.3). For some reservoirs (i.e. Karama and Tanour), the method seems to have difficulties in predicting the highest storages. Indeed, if the number of high-elevation pixels is small, the uncertainty in their corrected elevation (and thus the filling curve) can potentially affect the estimate of the maximum storage. This may be a limitation of the method. In addition, we can note that elevation H and volume V may vary a lot from month to month: up to 10 m or 15 hm^3 – i.e. 50% of the maximal storage – for instance for the Mujib reservoir. Because no information is available regarding the data collection date, some of the differences between our estimates and measured data might then come from this lack of metadata.

With regard to the King Talal reservoir, we can see large errors in storage estimates (see Fig. 4.3). But they could have been expected at the end of the elevation–area relationship establishment step: the assumptions that were made to define H_c were maybe not justified in this case. Indeed, 80% of the reservoir maximal area was covered with water when the SRTM satellite passed over the dam, and the R^2 is only 0.29 for the regression applied to the remaining visible pixels (see Table 3.1). A small

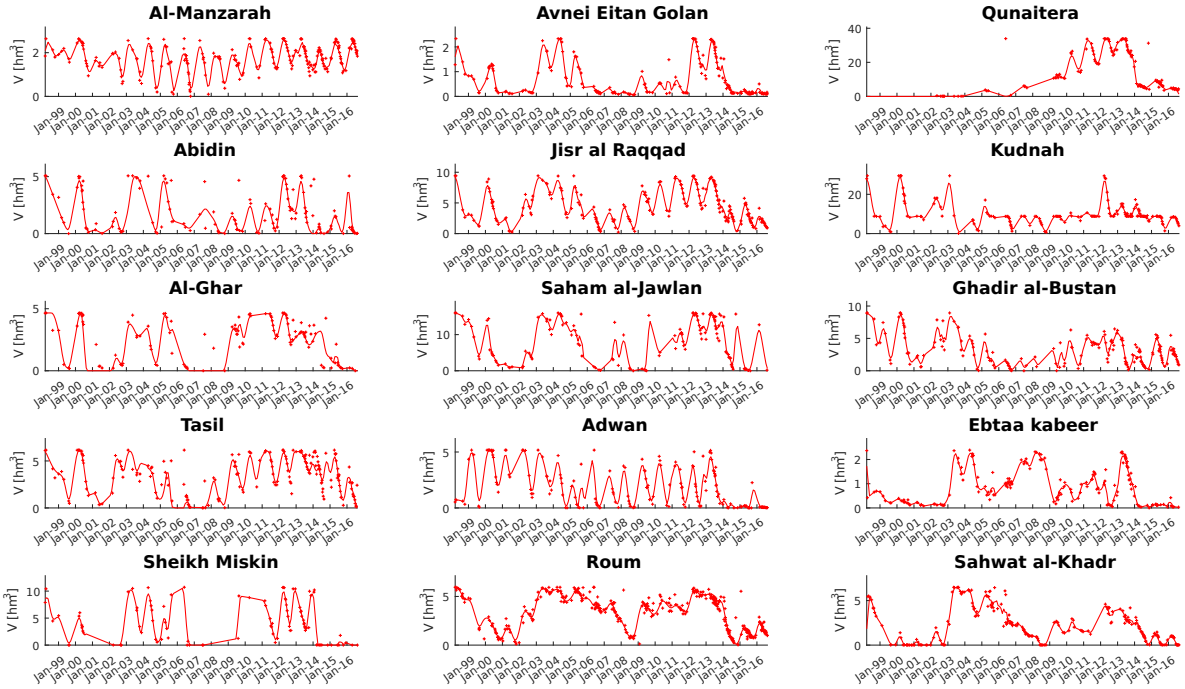

Figure 4.2: Storage variations (Avisse et al., 2017). Red crosses indicate estimates from the method developed in this thesis. Red lines are local polynomial regressions, that are plotted only with the purpose of showing storage variation trends.

visible surface area does not necessarily lead to a low-quality elevation–area relationship – see the good estimates for the Kafrein reservoir, while 70% of its maximal area was hidden when the SRTM satellite passed over it – but it certainly is a sign that results might be biased.

Errors in the estimation of elevation and storage are evaluated in terms of the coefficient of determination (R^2; Eq. 4.1) and the normalized root-mean-square error (NRMSE; Eq. 4.2):

$$R^2 = \frac{Cov(RS, Hist)^2}{\sigma^2_{\mathrm{RS}} \cdot \sigma^2_{\mathrm{Hist}}} \tag{4.1}$$

$$NRMSE = \frac{1}{Hist_{\max} - Hist_{\min}} \sqrt{\sum_{i=1}^{N} \frac{(RS_{\mathrm{i}} - Hist_{\mathrm{i}})^2}{N}} \tag{4.2}$$

where $Cov(RS, Hist)$ is the covariance between remote sensing (RS) estimates and JVA historical measurements, σ^2 the variance, and N the number of RS estimates during the period in which JVA measured storage or elevation. Results are presented in Table 4.1.

The coefficient of determination for storage ranges from 0.69 to 0.84. These high values confirm an important correlation and the similar variation trends that can be seen between the method's estimates and JVA records (see Fig. 4.3). A few high NRMSE values for both V and H_{c} though indicate that there is still some uncertainty with regard to the estimation of their absolute value at a given month. Indeed, by ignoring the King Talal dam, NRMSE ranges from 10 to 16% for storage, and reaches up

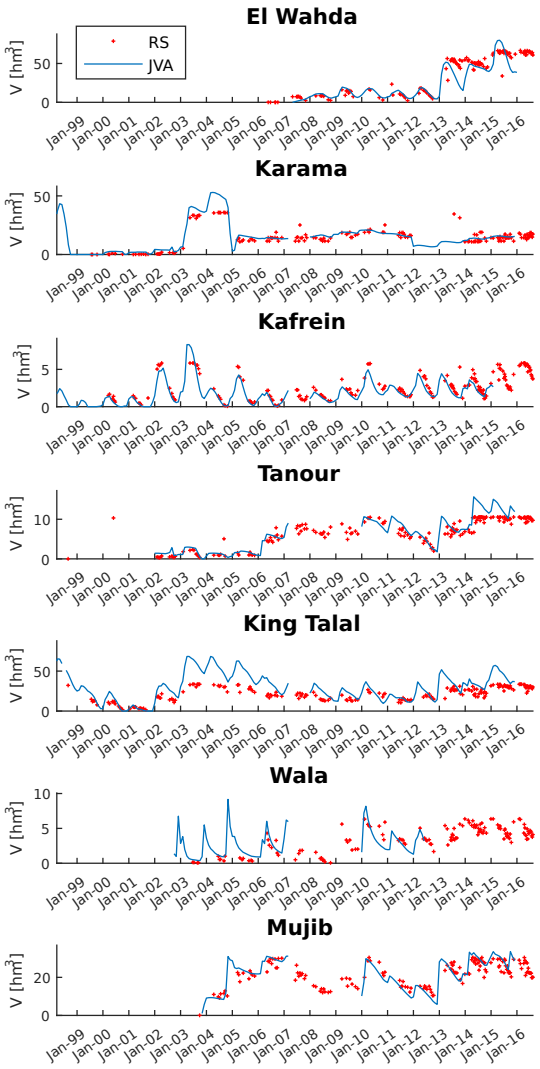

Figure 4.3: Storage variations for Jordan-managed reservoirs (Avisse et al., 2017). Red crosses indicate estimates from the method developed in this thesis. The blue lines indicate in situ data records that were made by the Jordan Valley Authority (JVA).

to 30% for elevation. These error estimates for elevation though need to be taken into account with caution due to the small number of JVA measurements available for comparison ($15 \leq N \leq 35$).

In order to better evaluate the proposed method compared to a basic fixed NDVI and near-infrared thresholds water area detection, the results presented in Table 4.2 are considered: on average, only 30.0 to 59.4% of final reservoir areas are detected by Fmask. The average additional part of final water bodies that is detected with the employment of a NDVI-based dynamic threshold for MNDWI is larger than 30% for all Jordanian reservoirs, and can reach more than 50% for the Tanour and Wala reservoirs. Similarly, the average additional part obtained through the 3-D reconstruction is larger than 3.9% (Karama reservoir), and goes beyond 16% for the more recent reservoirs Tanour, Wala, and Mujib, whose construction ended after 2002 – proportionally, more Landsat 7 images affected

Table 4.1: Errors in terms of R^2 and NRMSE for Jordanian reservoirs' H_c and V assessments (Avisse et al., 2017).

Reservoir	N		R^2		NRMSE	
	H_c	V	H_c	V	H_c	V
El Wahda	25	107	0.54	0.76	0.30	0.15
Karama	29	123	0.98	0.79	0.05	0.10
Kafrein	35	136	0.91	0.81	0.11	0.10
Tanour	16	117	0.83	0.84	0.12	0.15
King Talal	40	159	0.50	0.76	0.36	0.19
Wala	15	37	0.36	0.69	0.21	0.16
Mujib	15	104	0.73	0.75	0.15	0.15

Table 4.2: Initial Fmask classification inside the final water areas ("Other" refer to clouds, cloud shadows and snow), and stages' percentage changes that led to the classification as water ("2-D" for the 2-D classification enhancement, and "3-D" for the 3-D reconstruction; see Avisse et al., 2017).

Reservoir	Fmask classification [%]				Changes [%]	
	Water	Land	Other	N/A	2-D	3-D
El Wahda	58.6	20.8	13.1	7.5	32.2	9.2
Karama	64.1	13.3	20.9	1.7	32.0	3.9
Kafrein	58.5	15.9	17.2	8.4	31.9	9.7
Tanour	31.3	15.4	39.0	14.3	52.5	16.1
King Talal	59.4	22.1	9.7	8.8	30.8	9.8
Wala	30.0	24.4	30.0	15.7	52.6	17.5
Mujib	36.1	9.6	37.2	17.2	45.2	18.6

by "N/A" stripes were then used for them than for older dams. In light of these large shares of hidden or undetected water areas, corrections were obviously essential to consistently monitor reservoir elevation and storage.

For the reservoirs considered in the modeling but too small to apply the storage monitoring method (i.e. storage capacity larger than 1 hm^3 but maximal water area of less than 0.5 km^2: Dar'a al-Sharqi, Al-Ghariyah al-Sharqiyah, Tafas and Harran), the method's water area monitoring (i.e. stage (*i*) in Fig. 3.1) is combined to a linear storage–area relationship based on the official storage capacities (Syria and Jordan, 1987) to assess their storage.

Then, the evolution of cumulated storage capacity and cumulated water stored in reservoirs of the YRB (except Wahda) are presented in Fig. 4.4. A first qualitative analysis of the impact of the construction of dams on the discharge observed downstream (Fig. 2.2) can be drawn from these results. It is particularly interesting to notice that the pre-1995 growth of the cumulated storage capacity does not seem to have affected the hydrological regime of the river during the same period of time. However, precipitation data for years between the pre-development phase (pre-1960s) and 1983 is missing to consistently conclude on the impact of the new dams, as rainfall seems to have strongly varied during this period. On the contrary, while the cumulated storage capacity remained the same between 1999 and 2006, the runoff declined and the reservoir filling was affected. Reasons behind these changes should then be found in the late 1990s multi-year drought and/or in increasing water withdrawals. The consecutive low Yarmouk River flow and low reservoirs water storage coincide with the 2007–2008

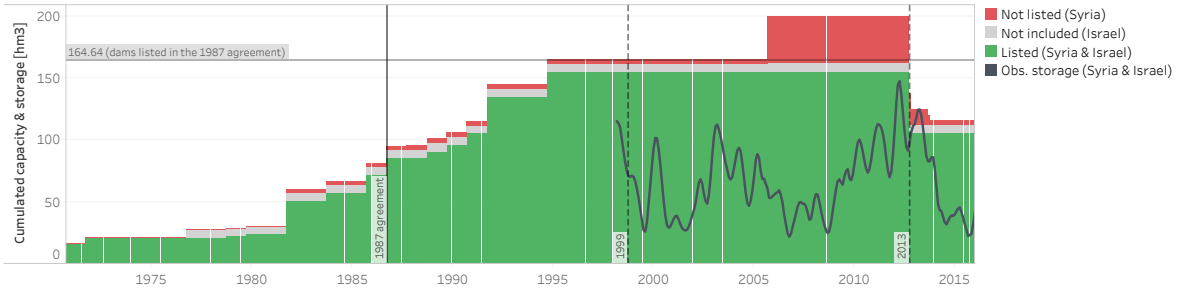

Figure 4.4: Cumulated storage capacity and variations in Syria and the Israel-occupied Golan Heights. Capacities are sorted in terms of their inclusion in the 1987 agreement. Colour codes for capacity categories are the same as in Fig. 3.13.

drought. Higher precipitation in the subsequent years (period 2009–2012), though, did not materialize in higher discharges downstream, as more water seems to have been stored in the reservoirs. Finally, it seems clear that the disuse of many reservoirs in 2013 (see also Table 3.2) led to less water stored in the YRB and to larger runoff discharges during the following years.

Scenarios are defined and tested further below to quantitatively complement these qualitative results deduced from remote sensing observations; but the model first need to be validated with historical measurements.

4.2 Historical flows

The PyNSim MAS simulation model is first run to recreate the observed flows at the Wahda dam and Adasiya over the historical period, so that the validity of the MAS modeling can be attested. Results are presented in Fig. 4.5.

Qualitatively, the model reproduces well the seasonality of the Yarmouk River flow. More importantly with regard to the objective of this study, it replicates well the three periods initially identified at the Wahda dam station: (*i*) the stationary period before 1999, (*ii*) the subsequent collapse of both the base flow and the runoff, and (*iii*) the return of the runoff in 2013. The fact that the simulated base flow collapses in 1999, at the exact same time as in the observations, also validates the reasoning behind the definition of a threshold on groundwater abstractions (Sect. 3.3.5). The slight difference in the rate of the base flow reduction may be explained either by errors on irrigation requirements estimates (or a change in irrigation efficiency), or by the simplistic representation of the aquifer's dynamics in the modeling. The contrasted quality of the results for certain years (e.g. 1990, 2004, 2014 at Wahda, or 1993 at Adasiya) may be caused by errors in PERSIANN-CDR data, by the difficulty to locally calibrate this precipitation dataset (or the GR2M model), or by a few temporary changes in the Syrian reservoirs' operation.

The remote sensing storage monitoring (Sect. 3.3.1) is used to discuss the validity of the SOP. By comparing the simulated monthly cumulated storage in Syria and the occupied Golan Heights to

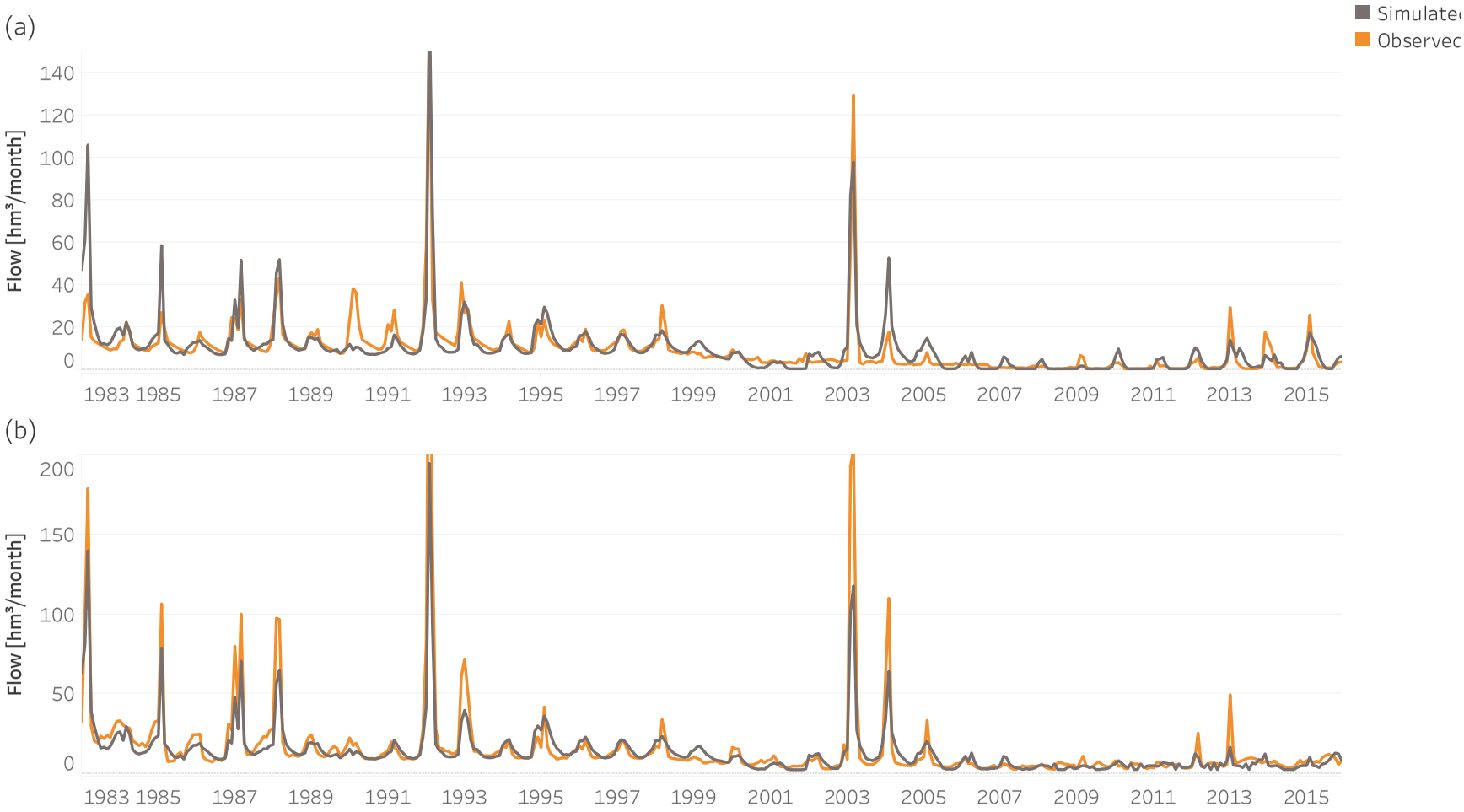

Figure 4.5: Measured flows and simulation results of the historical run at (**a**) Wahda and (**b**) Adasiya stations.

remote sensing observations, we obtain a correlation coefficient of 0.67. This means that the simulated human decisions concerning reservoir operation are significantly correlated with the decisions that reservoir managers actually took between 1998 and 2015. Differences between model estimates and remote-sensed values are potentially influenced by errors on the assessment of natural inflows, land use, irrigation requirements, crop–water source association, reservoir operation, or just remote-sensed storage estimates.

As for the results at the outlet of the YRB, the modified Kling-Gupta efficiency-statistic (KGE' in Eq. 4.3; Gupta et al., 2009; Kling et al., 2012) is chosen to take into account the strong variability of the Yarmouk River discharge, and to measure the quality of the simulated flows:

$$KGE' = 1 - \sqrt{(r-1)^2 + (\beta-1)^2 + (\gamma-1)^2} \tag{4.3}$$

where r is the correlation coefficient between simulated and observed flows, $\beta = \mu_s/\mu_o$ is the bias ratio with μ the mean discharge, $\gamma = CV_s/CV_o = (\sigma_s/\mu_s)/(\sigma_o/\mu_o)$ is the variability ratio with CV the coefficient of variation and σ the standard deviation, and s and o indices stand for *simulated* and *observed* data respectively.

KGE' values of 0.64 and 0.90 are then respectively obtained for discharges at Adasiya and the Wahda dam. These high values confirm the validity of the modeling, subsequently enabling to test alternative situations by modifying parts of the MAS model.

4.3 Scenarios over the historical period

In this section, scenarios are developed to represent alternative theories (either narratives from the riparian countries, or complementary ideas that have never been fully explored) on the hydrological changes of the Yarmouk River flow. The goal is to test the validity of these theories and to identify impacts on Jordan and Israel, considering water diversions downstream from the YRB as per the 1994 Treaty of Peace. Five counterfactual scenarios are quantitatively analyzed.

No precipitation decline A higher precipitation is considered to produce the 422 hm^3/yr natural flow at Adasiya that was expected by MWI/JVA (2002) in the feasibility study of the Wahda dam. This scenario addresses a Syrian narrative.

Listed dams only Only dams listed in the 1987 agreement (all dams except Qunaitera and Avnei Eitan al-Golan; see Table 3.2) are taken into account in the model. This scenario addresses a Jordanian narrative.

No groundwater pumping development Crop water requirements in areas located far from reservoirs remain unchanged after the signature of the agreement between Syria and Jordan (1987). The goal of this scenario is to assess the impact of increasing groundwater withdrawals, which is hardly mentioned by Jordanian authorities, although it is explained in several qualitative studies (see Sect. 2.3).

All dams active 2013–present This scenario assumes all dams continue to operate in 2011 as in prior years (as though the Syrian civil war did not occur).

Aggregate effects Combination of the four prior scenarios with increased precipitation, no groundwater development, only dams listed in the agreement between Syria and Jordan (1987), and continued operation of those dams in 2011.

4.3.1 Impact on the Yarmouk River flow

Because most reservoirs and irrigated crops in the YRB are located upstream from the Wahda dam, and because the flow at Adasiya mainly depends on the operation of Wahda, the scenarios analysis focuses on the flow simulated at the Wahda station.

Results are presented in Fig. 4.6a, with the simulated *historical* flow for comparison. It is particularly interesting to notice that the base flow still sharply decreases in 1999 with the *no climate change* and *listed dams only* scenarios. It means that neither the reduced precipitation nor the unlisted dams caused that major hydrological change. On the contrary, with the *no groundwater development* scenario – and a fortiori the *aggregate effects* –, the base flow remains unchanged after 1999. This stationary state confirms that the growth of groundwater abstractions, which was probably fostered by the Syrian policies to subsidize irrigation from the aquifer (see Sect. 2.3), strongly impacted the Yarmouk River flow. If groundwater pumping had not developed since the signature of the bilateral agreement, the groundwater table would have remained at the same level and the base flow would not have been affected.

The difference between water year flows for each scenario and the simulated *historical* flow is presented in Fig. 4.6b to better visualize the impact of each past change on the Yarmouk discharge. Until 1999, for instance, the simulations show that no anthropogenic activity affected the Yarmouk River flows. The only difference between the *historical* and *aggregated effects* flows lies in the precipitation decline. From 2000 onwards however, as mentioned above, the impact of human activities through growing groundwater withdrawals is particularly clear as the gap between the simulated *historical* and *no groundwater development* scenarios keeps increasing until the complete disappearance of the base flow in 2006. In 2013, our modeling shows that the destruction/disuse of Syrian dams led to an increase of the runoff by 25.3 hm^3/yr on average over the period 2013–2015. This value is consistent with the $\sim$25 hm^3/yr estimate from Müller et al. (2016). It must be stressed that such additional inflows did not alleviate water scarcity in Jordan though, as more than 500,000 Syrian refugees entered the country during the same period of time (UNHCR, 2017). Another aspect revealed by the simulation of the *listed dams only* scenario is that the impact of the unilateral construction of dams by Syria and Israel is marginal over the whole 1983–2015 historical period.

Moreover, it is interesting to note that even with the uncoordinated construction of reservoirs upstream from Jordan, and with the significant decline in precipitation over the YRB, Jordan would still have got a discharge close to the 117.6 hm^3/yr it expected to fill the Wahda reservoir (see Sect. 2.2) if ground-

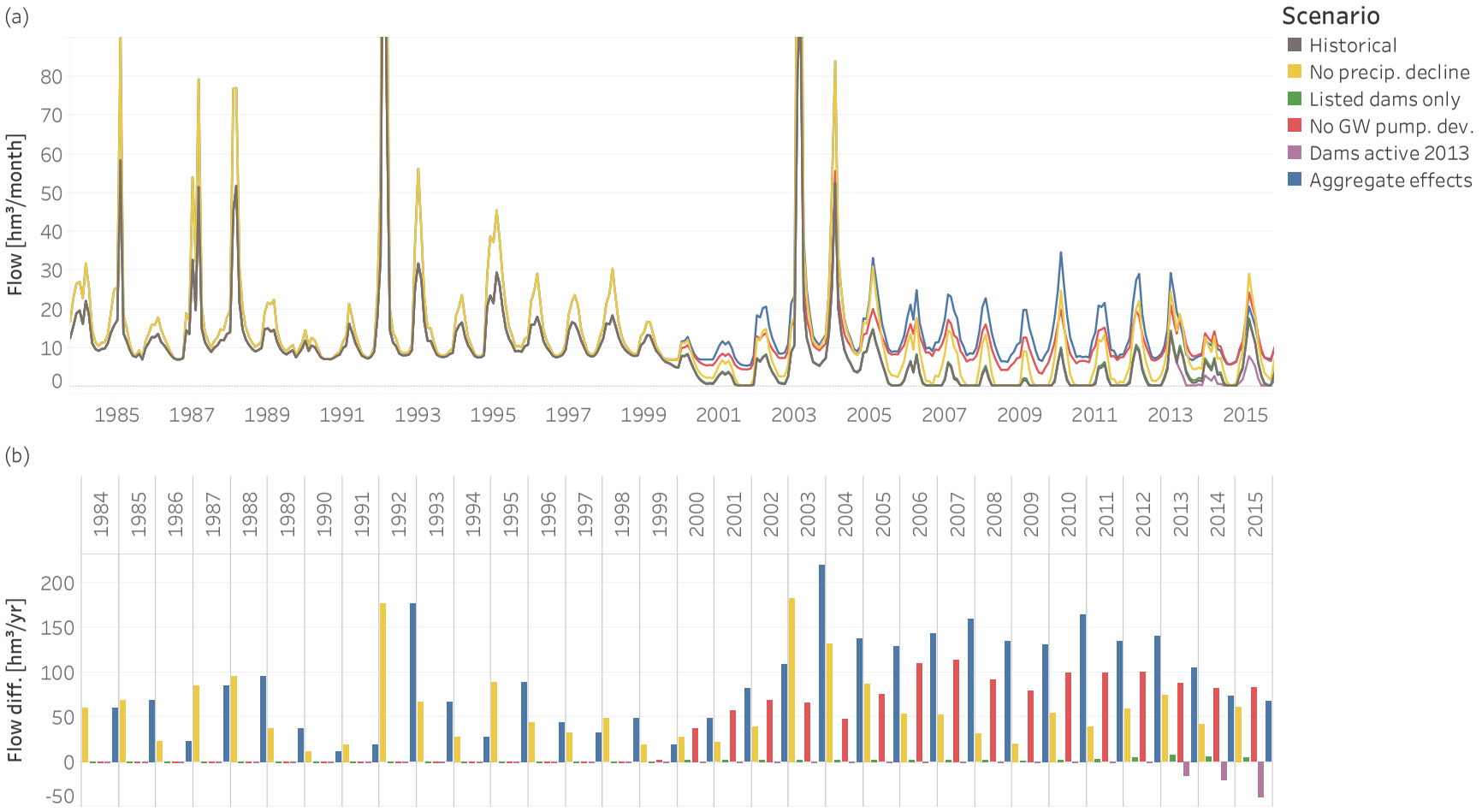

Figure 4.6: (**a**) Simulation results at the Wahda dam location for the proposed scenarios, and (**b**) water year flow difference with the historical run.

Table 4.3: Consequences of each scenario on the transfers as per the 1994 Treaty of Peace between Israel and Jordan (1994). μ and Diff. respectively are the average flow and the difference with the simulated historical flow for the period 1994–2015.

Beneficiary's share		Historical	No precip. decline	List. dams only	No GW pump. dev.	Aggregate effects
Jordan	μ [hm^3·y^{-1}]	118.5	134.8	119.9	146.4	150.5
	Diff. [%]	-	+13.8	+1.2	+23.6	+27.0
Israel	μ [hm^3·y^{-1}]	39.7	54.9	40.2	56.7	67.7
	Diff. [%]	-	+38.3	+1.3	+42.9	+70.7
Jordan River	μ [hm^3·y^{-1}]	17.2	49.7	17.6	26.4	64.1
	Diff. [%]	-	+188.6	+2.4	+53.5	+272.8

water abstractions had remained at the 1987 level. Indeed, with the simulation of the *no groundwater pumping development* scenario, the flow reaching Wahda during the period 2006–2012, for instance, remains close to 100 hm^3/yr above the $\sim$15 hm^3/yr measured by MWI/JVA during this period.

4.3.2 Consequences on the water transfers as per the 1994 Treaty of Peace

In this section, the focus is on the effects that past hydrological changes and human development/ management policies have had on the sharing of the flows at Adasiya (Fig. 3.14b) as per the treaty that Israel and Jordan (1994) signed. Because the situation changes with each scenario, operating policies of the Wahda dam from the *historical* run are updated to release more water in case the outflow was not sufficient to satisfy the *allocation*.

The following analysis describes and compares flows over the 1994–2015 time period. All scenarios defined in the previous sections are considered but the *all dams active* one, because it only has effects on the Yarmouk streamflow after 2013. Results are presented in Table 4.3, in terms of discharges eventually available for Jordan (through the KAC after the *concession* is sent back by Israel), for Israel (share pumped to Lake Tiberias and remaining after the *concession* is sent back to Jordan), and for the Jordan River (JR; overflow from Yarmoukeem Pool).

We can see that the increase of groundwater abstractions is the change that most affected Jordan and Israel (+23.6 and +42.9% respectively). By looking at average flows, we can also notice that Jordan would have received more additional water than Israel with any scenario. This assessment is consistent with the water rights' definition in the Treaty of Peace: Jordan is the one that bears the hydrological risk (Israel and Jordan, 1994), and thus the one that has been more affected by the decline of the Yarmouk flows. As for the uncoordinated construction of dams, Jordan is estimated to have lost 1.4 hm^3/yr, while Israel has lost only 0.5 hm^3/yr – loss even more marginal that the cumulated storage in the Golan Heights it controls is 5.2 hm^3. With regard to the flow reaching the Jordan River, it seems to significantly increase with the two main scenarios: +188.6% with *no climate change* and +53.5% with *no groundwater development* because of recurrent Yarmoukeem Pool overflows.

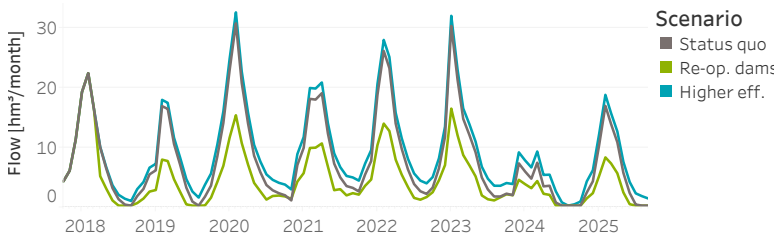

Figure 4.7: Simulation results at the Wahda dam location for future scenarios.

4.4 Scenarios for the future

We examine three future scenarios for the years 2016–2015 with the aim to identify (*i*) potential water flows of the Yarmouk as the Syrian civil war winds down, and (*ii*) how Jordan can support the post-war recovery to simultaneously assist Syrians and promote Jordan's own hydrological interests. Each scenario assumes precipitation is the same as for 2006–2015 (236 mm/yr on average, similar to the historical 239 mm/yr average). We recognize that future conditions (social, hydrological, and other) are highly uncertain in conflict areas such as the Yarmouk basin in Syria; and the precision of results critically depends on scenario assumptions. The main value of these future scenarios is to compare results across conditions that may manifest in the post-war period and help basin states see what role, if any, they could play in recovery efforts.

Status quo The water resources system configuration remains the same as in 2015 (7 dams in disuse because of the Syrian civil war; see Table 3.2).

Re-operate dams Starting in 2018, Syrian independently rebuild and re-operate dams that fell into disuse to their prior capacities.

Higher irrigation efficiency Donor organizations promote and support Syrian farmers to rebuild and redevelop their irrigation systems to increase efficiency by 0.1 to reach 0.6 and 0.8 from surface water and groundwater sources respectively from 2018 onwards.

By taking as a reference the *status quo* scenario, we can see in Fig. 4.7 that the inflow to the Wahda dam would slightly increase with a *higher irrigation efficiency* in Syria. According to our simulations, Jordan and Syria would respectively receive 2.1 and 4.9 hm^3/yr more water with this scenario. Moreover, just as Jordan regularly buys water from Israel (430,000 USD/hm^3 in 2016) through a Lake Tiberias–KAC transfer, it could be economically interesting at some point for Jordan to contribute to the upgrading of the Syrian farmers irrigation network system. As for the scenario that considers to *re-operate dams*, it must be stressed that if these dams are re-operated and unilaterally managed by Syria as before 2013, Jordan can expect the Yarmouk River to significantly decrease to return to the 2010 low flow state. In this case, the simulations show that Jordan and Israel would then respectively lose 18.7 and 6.8 hm^3/yr on average.

Conclusions

Due to the difficulty to access reliable data in non-cooperatively managed, institutionally complex, over-built, international basins, most studies have remained qualitative or conceptual to analyze this kind of basins. This Ph.D. research presents the successful development of a modeling framework to quantitatively analyze hydrological changes in such basins. By taking the Yarmouk basin as a case study, the contributions of natural and anthropogenic factors to the collapse of the Yarmouk flows are identified and assessed using remote sensing, multi-agent simulation, and scenario analysis.

While some studies have already used remote sensing for hydrological modeling, the technique remains challenging for water system modeling applications as it requires extensive on-the-ground observations and interactions with water resources managers. The scope of most modeling techniques is also limited by their inability to handle the multiplicity of institutions dealing with water. The approach developed in this Ph.D. thesis brings about a paradigm shift in the access to, and processing of, information related to human decisions in transboundary basins, as such access would not depend on the level of cooperation between countries anymore. With information on human activities freely available to riparian parties, data secrecy becomes obsolete, and issues hampering any equitable sharing of the water resources can better be identified, and contested claims or political narratives be independently assessed.

Limitations of the modeling framework reside in the limitations of the individual remote sensing techniques used to retrieve specific parameters. The main limitation of the storage monitoring method is its inapplicability to reservoirs that were significantly "covered" with water when the DEM satellites passed over them. Fortunately, this information can be readily obtained from remote sensing data and used to determine the applicability of the method a priori. As detailed in the thesis, producing land use maps in inaccessible areas is a cumbersome method and requires at least calibration data in neighboring areas. This step is however only necessary for reservoirs whose first usage is to provide water for irrigation purpose.

Finally, the algorithms used in the methodology are based on datasets available over the whole continental surface (for land use, dams characterization method, precipitation, and thus hydrological and system modeling). The storage monitoring method automatically detect water bodies, define the water area retrieval parameters, build filling curves, and assess reservoir storage. This protocol is comparable to the one developed by Zhu and Woodcock (2014) for the Continuous Change Detection and

Classification (CCDC) of land cover. Therefore, by using such near real-time updates on both water bodies storage and land cover and precipitation forecast, one could further use the modeling framework presented in this thesis to get a near-real time modeling of a water resources system.

An example of operational research application

Potential operational applications of the method include, for instance, the anticipation of future water supplies in transboundary river basins using land-data assimilation and hydro-economic modeling. We have indeed imagined such a modeling framework in the Tekezze-Atbara River basin shared between Ethiopia and Sudan: the latter is relying on the releases of the Tekezze reservoir (whose purpose is the production of hydro-electricity) that is located in the former. Used by Sudan, the remote sensing-based storage monitoring method has the potential to provide an assessment of water availability upstream from its part of the basin, and a decentralized hydro-economic modeling could provide water allocation policies in Ethiopia.

Applications of decentralized hydro-economic modeling to mimic water allocation policies in a river basin's sub-region like a riparian country, or a sub-basin, can be found in Jeuland et al. (2014) and in Arjoon et al. (2014). When dealing with multi-reservoir systems, the release policies at a given time of the year are usually a function of both the storage level and the inflow during that period. Consequently, any information on upstream reservoir storage has the potential to reduce the hydrological risk exposure of the downstream riparian. Remote sensing estimates of storage in the Tekezze reservoir can actually be included as an exogenous state variable in an optimization model of the Sudanese reservoirs system – such modeling is indeed well suited to address reservoir systems' stochasticity and complexity (Labadie, 2004). Goor et al. (2010) and Arjoon et al. (2014) for instance applied optimization modeling on multi-purpose multi-reservoir systems on the Eastern Nile River basin. They used Stochastic Dual Dynamic Programing (SDDP) to determine the optimal allocation policies for various cooperation scenarios. The proposed project relies on these works and aims at incorporating estimates of upstream reservoir inflows and storage within the SDDP modeling framework in order to anticipate future water supplies and optimal allocation water policies in Sudan.

Technically, the protocol for assessing this "alternative no-cooperation" scenario is divided in two steps: (*i*) estimating storage levels with the method developed in this thesis, and (*ii*) incorporating the storage levels as an exogenous state variable into the SDDP hydro-economic model of the Sudanese multi-purpose multi-reservoir system. The validation of remote sensing measurements of the storage in the Tekezze reservoir starts with the use of the hydrological model GR2M (Mouelhi et al., 2006) to reproduce the natural flow of the Tekezze-Atbara river flow at the border between the two countries. As the construction started in 1999 and ended in 2009, information on both the natural flow of the river and the flow impacted by the Tekezze dam can be found in in situ measurements of the flow – assuming that they started before 1999. The natural flow would be used to calibrate the GR2M model, and the one impacted by the dam would be employed to validate remote sensing storage estimates, by making a simple water balance calculation on the reservoir. Once the storage estimates are validated,

they would be incorporated as an exogenous state variable in a SDDP model following the method developed by Piña et al. (2017). The benefits of this additional data on allocation policies could consequently be assessed.

Bibliography

Ababsa, M.: Agrarian Counter-Reform in Syria, in: Agriculture and Reform in Syria, Raymond Hinnebusch, Lynne Rienner Publishers and University of St Andrews Centre for Syrian Studies, Boulder, USA, 2010.

Ababsa, M.: Crise agraire, crise foncière et sécheresse en Syrie (2000-2011), Maghreb - Machrek, 215, 101–122, doi:10.3917/machr.215.0101, 2013.

Al-Bakri, J. T.: Mapping Irrigated Crops and Their Water Consumption in Yarmouk Basin. A report for Regional Coordination on Improved Water Resources Management and Capacity Building, Tech. rep., Ministry of Water and Irrigation, 2015.

Allen, R. G., Pereira, L. S., Raes, D., and Smith, M.: Crop evapotranspiration: Guidelines for computing crop water requirements, no. 56 in FAO Irrigation and drainage paper, Food and Agriculture Organization, Rome, Italy, 1998.

Alsdorf, D. E., Rodríguez, E., and Lettenmaier, D. P.: Measuring surface water from space, Reviews of Geophysics, 45, doi:10.1029/2006RG000197, rG2002, 2007.

Arjoon, D., Mohamed, Y., Goor, Q., and Tilmant, A.: Hydro-economic risk assessment in the eastern Nile River basin, Water Resources and Economics, 8, 16–31, doi:10.1016/j.wre.2014.10.004, 2014.

Arjoon, D., Tilmant, A., and Herrmann, M.: Sharing water and benefits in transboundary river basins, Hydrology and Earth System Sciences, 20, 2135–2150, doi:10.5194/hess-20-2135-2016, 2016.

Ashton, P. J.: Disputes and conflicts over water in Africa, in: Mambo N. (Ed.), Violent Conflicts, Fragile Peace: Perspectives on Africa's Security, pp. 1–11, Adonis and Abbey, London, 2007.

ASTER GDEM Validation Team: ASTER Global Digital Elevation Model Version 2 - Summary of Validation Results, Tech. rep., NASA LPDAAC-Japan-US ASTER Science Team, URL https://lpdaacaster.cr.usgs.gov/GDEM/Summary_GDEM2_validation_report_final.pdf, 2011.

Avisse, N., Tilmant, A., Müller, M. F., and Zhang, H.: Monitoring small reservoirs' storage with satellite remote sensing in inaccessible areas, Hydrology and Earth System Sciences, 21, 6445–6459, doi:10.5194/hess-21-6445-2017, 2017.

Aw-Hassan, A., Rida, F., Telleria, R., and Bruggeman, A.: The impact of food and agricultural policies on groundwater use in Syria, Journal of Hydrology, 513, 204–215, doi:10.1016/j.jhydrol.2014.03.043, 2014.

Barnaud, C., Le Page, C., Dumrongrojwatthana, P., and Trébuil, G.: Spatial representations are not neutral: Lessons from a participatory agent-based modelling process in a land-use conflict, Environmental Modelling & Software, 45, 150–159, doi:10.1016/j.envsoft.2011.11.016, 2013.

Barnes, J.: Managing the Waters of Ba'th Country: The Politics of Water Scarcity in Syria, Geopolitics, 14, 510–530, doi:10.1080/14650040802694117, 2009.

Bastiaanssen, W.: Satellite-based estimation of evapotranspiration, soil moisture and biomass production for two irrigated areas in Jordan, Report for the Ministry of Water and Irrigation, MWI, 2015.

Beaumont, P.: Dividing the Waters of the River Jordan: An Analysis of the 1994 Israel–Jordan Peace Treaty, International Journal of Water Resources Development, 13, 415–424, doi:10.1080/07900629749764, 1997.

Becu, N., Perez, P., Walker, A., Barreteau, O., and Le Page, C.: Agent based simulation of a small catchment water management in northern Thailand, Ecological Modelling, 170, 319–331, doi:10.1016/S0304-3800(03)00236-9, 2003.

Berger, T. and Ringler, C.: Tradeoffs efficiency gains and technical change - Modeling water management and land use within a multiple-agent framework, Quaterly Journal of International Agriculture, 41 (1/2), 119–144, 2002.

Berger, T., Birner, R., McCarthy, N., Díaz, J., and Wittmer, H.: Capturing the complexity of water uses and water users within a multi-agent framework, Water Resources Management, 21, 129–148, doi:10.1007/s11269-006-9045-z, 2007.

Bousquet, F. and Le Page, C.: Multi-agent simulations and ecosystem management: a review, Ecological Modelling, 176, 313–332, doi:10.1016/j.ecolmodel.2004.01.011, 2004.

Burdon, D. J.: Infiltration rates in the Yarmouk basin of Syria-Jordan, Association Internationale d'Hydrologie Scientifique, 2, 343–355, 1954.

Cai, X., McKinney, D. C., and Lasdon, L. S.: Integrated Hydrologic-Agronomic-Economic Model for River Basin Management, Journal of Water Resources Planning and Management, 129, 4–17, doi:10.1061/(ASCE)0733-9496(2003)129:1(4), 2003.

CBSSYR: 2004 Census, Official document, Central Bureau of Statistics Syria, URL https://web.archive.org/web/20130310211017/http://www.cbssyr.org/General%20census/census%202004/pop-man.pdf, 2004.

Chavez, P.: Image-based atmospheric corrections revisited and improved, Photogrammetric Engineering & Remote Sensing, 62, 1025–1036, 1996.

Chenoweth, J. L. and Feitelson, E.: Analysis of Factors Influencing Data and Information Exchange in International River Basins, Water International, 26, 499–512, doi:10.1080/02508060108686951, 2001.

Conradt, T., Wechsung, F., and Bronstert, A.: Three perceptions of the evapotranspiration landscape: comparing spatial patterns from a distributed hydrological model, remotely sensed surface temperatures, and sub-basin water balances, Hydrology and Earth System Sciences, 17, 2947–2966, doi:10.5194/hess-17-2947-2013, 2013.

Courcier, R., Vénot, J.-P., and Molle, F.: Historical transformations of the lower Jordan river basin (in Jordan): Changes in water use and projections (1950-2025), in: Comprehensive Assessment Research Report 9, Comprehensive Assessment Secretariat, Colombo, Sri Lanka, 2005.

Crétaux, J.-F., Biancamaria, S., Arsen, A., Bergé-Nguyen, M., and Becker, M.: Global surveys of reservoirs and lakes from satellites and regional application to the Syrdarya river basin, Environ. Res. Lett., 10, doi:10.1088/1748-9326/10/1/015002, 2015.

Dastane, N. G.: Effective rainfall in irrigated agriculture, no. 25 in FAO Irrigation and drainage paper, Food and Agriculture Organization, Rome, Italy, 1974.

Delannoy, J.-J., Madeline, P., and Lhenaff, R.: Géographie physique: Aspects et dynamique du géosystème terrestre, Vuibert, Paris, France, 2016.

Dellapenna, J. W.: Rivers as Legal Sttructures: The Examples of the Jordan and the Nile, Natural Resources Journal, 36, 217, 1996.

Dinar, A. and Wolf, A.: Economic potential and political considerations of regional water trade: The Western Middle East example, Resource and Energy Economics, 16, 335–356, doi:10.1016/0928-7655(94)90025-6, 1994.

Dinar, A., Dinar, S., McCaffrey, S., and McKinney, D.: Bridges over water: Understanding transboundary water conflict, negotiation and cooperation, vol. 3 of *World Scientific Series on Energy and Resources Economics*, World Scientific Publishing Co. Pte. Ltd., Singapore, 2007.

Ding, N., Erfani, R., Mokhtar, H., and Erfani, T.: Agent Based Modelling for Water Resource Allocation in the Transboundary Nile River, Water, 8, doi:10.3390/w8040139, 2016.

Döll, P., Fiedler, K., and Zhang, J.: Global-scale analysis of river flow alterations due to water withdrawals and reservoirs, Hydrology and Earth System Sciences, 13, 2413–2432, doi:10.5194/hess-13-2413-2009, 2009.

Dombrowsky, I.: Conflict, cooperation and institutions in international water management: An economic approach, Edward Elgar Publishing, Cheltenham, UK, 2007.

Du, C., Ren, H., Qin, Q., Meng, J., and Zhao, S.: A Practical Split-Window Algorithm for Estimating Land Surface Temperature from Landsat 8 Data, Remote Sensing, 7, 647–665, doi: 10.3390/rs70100647, 2015.

Duan, Z. and Bastiaanssen, W.: Estimating water volume variations in lakes and reservoirs from four operational satellite altimetry databases and satellite imagery data, Remote Sensing of Environment, 134, 403–416, doi:10.1016/j.rse.2013.03.010, 2013.

Dufournaud, C. M.: On the mutually beneficial cooperative scheme: Dynamic change in the payoff matrix of international river basin schemes, Water Resources Research, 18, 764–772, doi:10.1029/WR018i004p00764, 1982.

Elimam, L., Rheinheimer, D., Connell, C., and Madani, K.: An ancient struggle: a game theory approach to resolving the nile conflict, in: Babcock, R. W., Walton, R. (Eds.), Proceeding of the 2008 World Environmental and Water Resources Congress, pp. 1–10, Honolulu, Hawaii, 2008.

Etana Syria: The Yarmouk Basin: Between Conflict and Development, Tech. rep., Etana Syria, URL http://www.etanasyria.org/uploads/files/7202_Etana%20files-The%20Yarmouk%20Basin%20-11%20En%20-%20final.pdf, 2015.

Falkenmark, M.: The massive water scarcity now threatening Africa: why isn't it being addressed?, Ambio, 18 (2), 112–118, 1989.

FAO: Irrigation in the Middle East region in figures: AQUASTAT survey - 2008, no. 34 in FAO Water Reports, Food and Agriculture Organization, Rome, Italy, 2009.

Feuillette, S., Bousquet, F., and Goulven, P. L.: SINUSE: a multi-agent model to negotiate water demand management on a free access water table, Environmental Modelling & Software, 18, 413–427, doi:10.1016/S1364-8152(03)00006-9, 2003.

Food and Agriculture Organization: Coping with water scarcity: An action framework for agriculture and food security, no. 38 in FAO Water Reports, FAO, Rome, 2012.

Gao, H., Birkett, C., and Lettenmaier, D. P.: Global monitoring of large reservoir storage from satellite remote sensing, Water Resources Research, 48, doi:10.1029/2012WR012063, w09504, 2012.

Geressu, R. T. and Harou, J. J.: Screening reservoir systems by considering the efficient trade-offs—informing infrastructure investment decisions on the Blue Nile, Environmental Research Letters, 10, 125 008, 2015.

German Aerospace Center: SRTM Products, available at: http://www.dlr.de/eoc/en/Portaldata/60/Resources/dokumente/7_sat_miss/srtm_products_en.pdf, (last access: 11 January 2017), 2017.

Giuliani, M. and Castelletti, A.: Assessing the value of cooperation and information exchange in large water resources systems by agent-based optimization, Water Resources Research, 49, 3912–3926, doi:10.1002/wrcr.20287, 2013.

Giuliani, M., Castelletti, A., Amigoni, F., and Cai, X.: Multiagent Systems and Distributed Constraint Reasoning for Regulatory Mechanism Design in Water Management, Journal of Water Resources Planning and Management, 141, 04014 068, doi:10.1061/(ASCE)WR.1943-5452.0000463, 2015.

Goor, Q., Halleux, C., Mohamed, Y., and Tilmant, A.: Optimal operation of a multipurpose multireservoir system in the Eastern Nile River Basin, Hydrology and Earth System Sciences, 14, 1895–1908, doi:10.5194/hess-14-1895-2010, 2010.

Goward, S. N., Xue, Y., and Czajkowski, K. P.: Evaluating land surface moisture conditions from the remotely sensed temperature/vegetation index measurements. An exploration with the simplified simple biosphere model, Remote Sensing of Environment, 79, 225–242, doi:10.1016/S0034-4257(01)00275-9, 2002.

Gül, A., Rida, F., Aw-Hassan, A., and Büyükalaca, O.: Economic analysis of energy use in groundwater irrigation of dry areas: a case study in Syria, Applied Energy, 82, 285–299, doi:10.1016/j.apenergy.2004.09.013, 2005.

Gupta, H. V., Kling, H., Yilmaz, K. K., and Martinez, G. F.: Decomposition of the mean squared error and NSE performance criteria: Implications for improving hydrological modelling, Journal of Hydrology, 377, 80–91, doi:10.1016/j.jhydrol.2009.08.003, 2009.

Hanasaki, N., Kanae, S., and Oki, T.: A reservoir operation scheme for global river routing models, Journal of Hydrology, 327, 22–41, doi:10.1016/j.jhydrol.2005.11.011, 2006.

Hardin, G.: The tragedy of the commons, Science, 162 (3859), 1243–1248, 1968.

Harou, J. J., Pulido-Velazquez, M., Rosenberg, D. E., Medellín-Azuara, J., Lund, J. R., and Howitt, R. E.: Hydro-economic models: Concepts, design, applications, and future prospects, Journal of Hydrology, 375, 627–643, doi:10.1016/j.jhydrol.2009.06.037, 2009.

Helm, C. and Sprinz, D.: Measuring the Effectiveness of International Environmental Regimes, Journal of Conflict Resolution, 44, 630–652, doi:10.1177/0022002700044005004, 2000.

Heywood, S.: Diverting the flow: Cooperation over international water resources, Quaker United Nations Office, Geneva, 2012.

Hof, F. C.: Dividing the Yarmouk's waters: Jordan's treaties with Syria and Israel, Water Policy, 1, 81–94, doi:10.1016/S1366-7017(98)00008-7, 1998.

Hussein, H.: Whose 'reality'? Discourses and hydropolitics along the Yarmouk River, Contemporary Levant, 0, 1–13, doi:10.1080/20581831.2017.1379493, 2017.

Ibrahim, W. Y., Batzli, S., and Menzel, W. P.: Agricultural policy effects on land cover and land use over 30 years in Tartous, Syria, as seen in Landsat imagery, Journal of Applied Remote Sensing, 8, 083 506, doi:10.1117/1.JRS.8.083506, 2014.

International Conference on Water and the Environment: International Conference on Water and the Environment: Development issues for the 21st century, 1992.

International Law Association: The Helsinki rules on the uses of the waters of international rivers, 1966.

Israel and Jordan: Treaty of peace between the State of Israel and the Hashemite Kingdom of Jordan, 1994.

Jennings, N. R., Sycara, K., and Wooldridge, M.: A Roadmap of Agent Research and Development, Autonomous Agents and Multi-Agent Systems, 1, 7–38, doi:10.1023/A:1010090405266, 1998.

Jeuland, M., Baker, J., Bartlett, R., and Lacombe, G.: The costs of uncoordinated infrastructure management in multi-reservoir river basins, Environmental Research Letters, 9, doi:10.1088/1748-9326/9/10/105006, 2014.

Jordan and Saudi Arabia: Agreement between the Government of the Hashemite Kingdom of Jordan and the Government of the Kingdom of Saudi Arabia for the Management and Utilization of the Ground Waters in the Al-Sag/Al-Disi Layer, 2015.

Kaisi, A. and Yasser, M.: Participatory management of water resources for agricultural purposes in Syrian Arab Republic, in: Participatory water saving management and water cultural heritage, pp. 243–253, Hamdy A. (ed.), Tüzün M. (ed.), Lamaddalena N. (ed.), Todorovic M. (ed.), Bogliotti C. (ed.), URL http://om.ciheam.org/om/pdf/b48/05002298.pdf, options Méditerranéennes : Série B. Études et Recherches; n. 48, 2004.

Kelley, C. P., Mohtadi, S., Cane, M. A., Seager, R., and Kushnir, Y.: Climate change in the Fertile Crescent and implications of the recent Syrian drought, Proceedings of the National Academy of Sciences, 112, 3241–3246, doi:10.1073/pnas.1421533112, 2015.

Kling, H., Fuchs, M., and Paulin, M.: Runoff conditions in the upper Danube basin under an ensemble of climate change scenarios, Journal of Hydrology, 424, 264–277, doi:10.1016/j.jhydrol.2012.01.011, 2012.

Kliot, N., Shmueli, D., and Shamir, U.: Institutions for management of transboundary water resources: their nature, characteristics and shortcomings, Water Policy, 3, 229–255, doi:10.1016/S1366-7017(01)00008-3, 2001.

Knox, S.: PyNSim's documentation, URL http://umwrg.github.io/pynsim/, 2014.

Knox, S., Meier, P., Yoon, J., Selby, P., Klassert, C., Harou, J., Lachaut, T., Avisse, N., Tilmant, A., and Gorelick, S.: Pynsim: An Open-Source Software Framework for Building Simulation Models of Multi-Actor Resource Networks, in: Sauvage S.,Sánchez-Pérez J.-M., Rizzoli A. (Eds.), International Environmental Modelling and Software Society (iEMSs) 8th International Congress on Environmental Modelling and Software, Toulouse, France, 2016.

Kucukmehmetoglu, M. and Guldmann, J.-M.: International Water Resources Allocation and Conflicts: The Case of the Euphrates and Tigris, Environment and Planning A, 36, 783–801, doi: 10.1068/a3670, 2004.

Labadie, J. W.: Optimal Operation of Multireservoir Systems: State-of-the-Art Review, Journal of Water Resources Planning and Management, 130, 93–111, doi:10.1061/(ASCE)0733-9496(2004) 130:2(93), 2004.

Lakshmi, V.: The role of satellite remote sensing in the Prediction of Ungauged Basins, Hydrological Processes, 18, 1029–1034, doi:10.1002/hyp.5520, 2004.

Le, Q. B., Seidl, R., and Scholz, R. W.: Feedback loops and types of adaptation in the modelling of land-use decisions in an agent-based simulation, Environmental Modelling & Software, 27-28, 83–96, 2012.

LeFavour, G. and Alsdorf, D.: Water slope and discharge in the Amazon River estimated using the shuttle radar topography mission digital elevation model, Geophysical Research Letters, 32, doi: 10.1029/2005GL023836, L17404, 2005.

Lehner, B., Liermann, C. R., Revenga, C., Vörösmarty, C., Fekete, B., Crouzet, P., Döll, P., Endejan, M., Frenken, K., Magome, J., Nilsson, C., Robertson, J. C., Rödel, R., Sindorf, N., and Wisser, D.: High-resolution mapping of the world's reservoirs and dams for sustainable river-flow management, Frontiers in Ecology and the Environment, 9, 494–502, doi:10.1890/100125, 2011.

Lettenmaier, D. P., Alsdorf, D., Dozier, J., Huffman, G. J., Pan, M., and Wood, E. F.: Inroads of remote sensing into hydrologic science during the WRR era, Water Resources Research, 51, 7309–7342, doi:10.1002/2015WR017616, 2015.

Liebe, J. R., van de Giesen, N., Andreini, M., Walter, M. T., and Steenhuis, T. S.: Determining watershed response in data poor environments with remotely sensed small reservoirs as runoff gauges, Water Resources Research, 45, doi:10.1029/2008WR007369, w07410, 2009.

Madani, K.: Game theory and water resources, Journal of Hydrology, 381, 225–238, doi:10.1016/j. jhydrol.2009.11.045, 2010.

Madani, K. and Hipel, K. W.: Strategic insights into the Jordan River conflict, in: Kabbes K. C. (Ed.), Proceeding of the 2007 World Environmental and Water Resources Congress, American Society of Civil Engineers, Tampa, Florida, 2007.

Madani, K. and Hipel, K. W.: Non-Cooperative Stability Definitions for Strategic Analysis of Generic Water Resources Conflicts, Water Resources Management, 25, 1949–1977, doi:10.1007/s11269-011-9783-4, 2011.

Madani, K., Rouhani, O. M., Mirchi, A., and Gholizadeh, S.: A negotiation support system for resolving an international trans-boundary natural resource conflict, Environmental Modelling & Software, 51, 240–249, doi:10.1016/j.envsoft.2013.09.029, 2014.

Marty, F.: Managing international rivers: Problems, politics and institutions, Peter Lang, Bern, Switzerland, 2001.

McKinney, D. C. and Teasley, R. L.: Cooperative game theory for transboundary river basins: The Syr Darya Basin. World Environmental and Water Resources Congress 2007: Restoring Our Natural Habitat, 2007.

Mendiguren, G., Koch, J., and Stisen, S.: Spatial pattern evaluation of a calibrated national hydrological model – a remote-sensing-based diagnostic approach, Hydrology and Earth System Sciences, 21, 5987–6005, doi:10.5194/hess-21-5987-2017, 2017.

Messerschmid, C. and Selby, J.: Misrepresenting the Jordan River Basin, Water Alternatives, 8, 258–279, 2015.

Mianabadi, H., Mostert, E., Pande, S., and van de Giesen, N.: Weighted Bankruptcy Rules and Transboundary Water Resources Allocation, Water Resources Management, 29, 2303–2321, doi:10.1007/s11269-015-0942-x, 2015.

Molden, D., Frenken, K., Barker, R., de Fraiture, C., Mati, B., Svendsen, M., Sadoff, C. W., Finlayson, M., Atapattu, S., Giordano, M., Inocencio, A., Lannerstad, M., Manning, N., Molle, F., Smedema, B., and Vallée, D.: Trends in water and agricultural development, in: Molden, David (Ed.). Water for food, water for life: a Comprehensive Assessment of Water Management in Agriculture. International Water Management Institute (IWMI), pp. 57–89, Colombo, Sri Lanka, 2007.

Mouelhi, S., Michel, C., Perrin, C., and Andréassian, V.: Stepwise development of a two-parameter monthly water balance model, Journal of Hydrology, 318, 200–214, doi:10.1016/j.jhydrol.2005.06.014, 2006.

Müller, M. F., Yoon, J., Gorelick, S. M., Avisse, N., and Tilmant, A.: Impact of the Syrian refugee crisis on land use and transboundary freshwater resources, Proceedings of the National Academy of Sciences, 113, 14 932–14 937, doi:10.1073/pnas.1614342113, 2016.

MWI/JVA: Al-Wehdah dam project: Updated feasibility, Tech. rep., The Hashemite Kingdom of Jordan, Ministry of Water and Irrigation/Jordan Valley Authority, Amman, Jordan, 2002.

Ostrom, E.: Governing the commons: The evolution of institutions for collective actions, Cambridge University Press, Cambridge, UK, 1990.

Parker, D. C., Manson, S. M., Janssen, M. A., Hoffmann, M. J., and Deadman, P.: Multi-Agent Systems for the Simulation of Land-Use and Land-Cover Change: A Review, Annals of the Association of American Geographers, 93, 314–337, 2003.

Parrachino, I., Dinar, A., and Patrone, F.: Cooperative game theory and its application to natural, environmental and water resources issues: 3. Application to water resources, World bank policy research paper 4074, World Bank, 2006.

Pereira-Cardenal, S. J., Riegels, N. D., Berry, P. A. M., Smith, R. G., Yakovlev, A., Siegfried, T. U., and Bauer-Gottwein, P.: Real-time remote sensing driven river basin modeling using radar altimetry, Hydrology and Earth System Sciences, 15, 241–254, doi:10.5194/hess-15-241-2011, 2011.

Piña, J., Tilmant, A., and Côté, P.: Optimizing Multireservoir System Operating Policies Using Exogenous Hydrologic Variables, Water Resources Research, 53, 9845–9859, doi:10.1002/2017WR021701, 2017.

Reynolds, C. W.: Flocks, herds, and schools: A distributed behavioral model, Computer Graphics, 21 (4), 25–34, 1987.

Ringler, C., von Braun, J., and Rosegrant, M. W.: Water Policy Analysis for the Mekong River Basin, Water International, 29, 30–42, doi:10.1080/02508060408691746, 2004.

Rodrigues, L. N., Sano, E. E., Steenhuis, T. S., and Passo, D. P.: Estimation of Small Reservoir Storage Capacities with Remote Sensing in the Brazilian Savannah Region, Water Resources Management, 26, 873–882, doi:10.1007/s11269-011-9941-8, 2012.

Rodriguez, E., Morris, C., Belz, J., Chapin, E., Martin, J., Daffer, W., and Hensley, S.: An assessment of the SRTM topographic products, Technical Report JPL D-31639, Jet Propulsion Laboratory, Pasadena, California, 2005.

Rogers, P.: A Game Theory Approach to the Problems of International River Basins, Water Resources Research, 5, 749–760, doi:10.1029/WR005i004p00749, 1969.

Rosegrant, M., Ringler, C., McKinney, D., Cai, X., Keller, A., and Donoso, G.: Integrated economic-hydrologic water modeling at the basin scale: the Maipo river basin, Agricultural Economics, 24, 33–46, doi:10.1111/j.1574-0862.2000.tb00091.x, 2000.

Rosenberg, D. E.: The Yarmouk River Agreements: Jordan-Syrian transboundary water management, 1953 - 2004, Arab World Geographer, 9, 23–39, 2006.

Salameh, E. and Bannayan, H.: Water resources of Jordan: present status and future potentials, Friedrich Ebert Stiftung, Amman, Jordan, 1993.

Salman, M. and Mualla, W.: Water demand management in Syria: centralized and decentralized views, Water Policy, 10, 549–562, doi:10.2166/wp.2008.065, 2008.

Sawunyama, T., Senzanje, A., and Mhizha, A.: Estimation of small reservoir storage capacities in Limpopo River Basin using geographical information systems (GIS) and remotely sensed surface areas: Case of Mzingwane catchment, Physics and Chemistry of the Earth, Parts A/B/C, 31, 935–943, doi:10.1016/j.pce.2006.08.008, 2006.

Selby, J.: Cooperation, Domination and Colonisation: The Israeli-Palestinian Joint Water Committee, Water Alternatives, 6, 1–24, doi:10.2166/wp.2008.065, 2013.

Şen, Z.: Wadi hydrology, Taylor & Francis, Boca Raton, USA, 2008.

Sheikhmohammady, M. and Madani, K.: Sharing a multi-national resource through bankruptcy procedures, in: Babcock, R. W., Walton, R. (Eds.), Proceeding of the 2008 World Environmental and Water Resources Congress, American Society of Civil Engineers, Honolulu, Hawaii, 2008.

Sheikhmohammady, M., Kilgour, D. M., and Hipel, K. W.: Modeling the Caspian Sea Negotiations, Group Decision and Negotiation, 19, 149–168, doi:10.1007/s10726-008-9121-2, 2010.

Shiklomanov, I. A. and Rodda, J. C.: World water resources at the beginning of the twenty-first century, International hydrology series, Cambridge University Press, New York, 2003.

Shoham, Y. and Leyton-Brown, K.: Multiagent systems: Algorithmic, game-theoretic, and logical foundations, Cambridge University Press, New York, USA, 2009.

Siegfried, T. and Bernauer, T.: Estimating the performance of international regulatory regimes: Methodology and empirical application to international water management in the Naryn/Syr Darya basin, Water Resources Research, 43, 1–14, doi:10.1029/2006WR005738, w11406, 2007.

Solander, K. C., Reager, J. T., and Famiglietti, J. S.: How well will the Surface Water and Ocean Topography (SWOT) mission observe global reservoirs?, Water Resources Research, 52, 2123–2140, doi:10.1002/2015WR017952, 2016.

Song, C., Huang, B., and Ke, L.: Modeling and analysis of lake water storage changes on the Tibetan Plateau using multi-mission satellite data, Remote Sensing of Environment, 135, 25–35, doi:10.1016/j.rse.2013.03.013, 2013.

Stisen, S., Jensen, K. H., Sandholt, I., and Grimes, D. I.: A remote sensing driven distributed hydrological model of the Senegal River basin, Journal of Hydrology, 354, 131–148, doi:10.1016/j.jhydrol.2008.03.006, 2008.

Syria and Jordan: Agreement between the Republic of Syria and the Hashemite Kingdom of Jordan concerning the utilization of the Yarmuk waters, 1953.

Syria and Jordan: Agreement between the Syrian Arab Republic and the Hashemite Kingdom of Jordan concerning the utilization of the Yarmuk waters, 1987.

Teasley, R. L. and McKinney, D. C.: Calculating the Benefits of Transboundary River Basin Cooperation: Syr Darya Basin, Journal of Water Resources Planning and Management, 137, 481–490, doi:10.1061/(ASCE)WR.1943-5452.0000141, 2011.

Tilmant, A. and Kinzelbach, W.: The cost of noncooperation in international river basins, Water Resources Research, 48, doi:10.1029/2011WR011034, w01503, 2012.

UN-ESCWA and BGR: Inventory of shared water resources in Western Asia, Tech. rep., United Nations Economic and Social Commission for Western Asia and Bundesanstalt für Geowissenschaften und Rohstoffe, Beirut, Lebanon, 2013.

Underdal, A.: The Concept of Regime 'Effectiveness', Cooperation and Conflict, 27, 227–240, doi:10.1177/0010836792027003001, 1992.

UNDP: Beyond scarcity: Power, poverty and the global water crisis, Human development report, United Nations Development Programme, New York, USA, 2006.

UNEP: Atlas of international freshwater agreements, United Nations Environment Programme, Nairobi, Kenya, 2002.

UNHCR: Syria Regional Refugee Response: Inter-agency Information Sharing Portal, URL http://data.unhcr.org/syrianrefugees/country.php?id=107, 2017.

United Nations: Convention on the Law of the Non-navigational Uses of International Watercourses, 1997.

Vörösmarty, C., Askew, A., Grabs, W., Barry, R. G., Birkett, C., Döll, P., Goodison, B., Hall, A., Jenne, R., Kitaev, L., Landwehr, J., Keeler, M., Leavesley, G., Schaake, J., Strzepek, K., Sundarvel, S. S., Takeuchi, K., and Webster, F.: Global water data: A newly endangered species, Eos, Transactions American Geophysical Union, 82, 54–58, doi:10.1029/01EO00031, 2001.

Vörösmarty, C. J., Sharma, K. P., Fekete, B. M., Copeland, A. H., Holden, J., Marble, J., and Lough, J. A.: The Storage and Aging of Continental Runoff in Large Reservoir Systems of the World, Ambio, 26, 210–219, 1997.

Wanders, N., Bierkens, M. F. P., de Jong, S. M., de Roo, A., and Karssenberg, D.: The benefits of using remotely sensed soil moisture in parameter identification of large-scale hydrological models, Water Resources Research, 50, 6874–6891, doi:10.1002/2013WR014639, 2014.

Wolf, A. T.: Sharing water, sharing benefits: Working towards effective transboundary water resources management, UNESCO and World Bank, Paris, France, 2010.

Wolf, A. T., Yoffe, S. B., and Giordano, M.: International waters: identifying basins at risk, Water Policy, 5, 29–60, 2003.

World Bank: Syrian Arab Republic Irrigation Sector Report, Report No. 22602-SYR, World Bank, Rural Development, Water and Environment Group, Middle East and North Africa Region, 2001.

Wu, W. and De Pauw, E.: A Simple Algorithm to Identify Irrigated Croplands by Remote Sensing, Tech. rep., GISU/ICARDA, URL http://www.isprs.org/proceedings/2011/ISRSE-34/211104015Final00930.pdf, 2011.

Wu, X. and Whittington, D.: Incentive compatibility and conflict resolution in international river basins: A case study of the Nile Basin, Water Resources Research, 42, doi:10.1029/2005WR004238, w02417, 2006.

Yang, Y.-C. E., Cai, X., and Stipanović, D. M.: A decentralized optimization algorithm for multiagent system-based watershed management, Water Resources Research, 45, doi:10.1029/2008WR007634, w08430, 2009.

Yang, Y.-C. E., Zhao, J., and Cai, X.: Decentralized Optimization Method for Water Allocation Management in the Yellow River Basin, Journal of Water Resources Planning and Management, 138, 313–325, doi:10.1061/(ASCE)WR.1943-5452.0000199, 2012.

Yoon, Y. and Beighley, E.: Simulating streamflow on regulated rivers using characteristic reservoir storage patterns derived from synthetic remote sensing data, Hydrological Processes, 29, 2014–2026, doi:10.1002/hyp.10342, 2015.

Yorke, V.: Jordan's Shadow State and Water Management: Prospects for Water Security Will Depend on Politics and Regional Cooperation, pp. 227–251, Springer International Publishing, Cham, doi:10.1007/978-3-319-18971-0_15, 2016.

Zeitoun, M. and Mirumachi, N.: Transboundary water interaction I: reconsidering conflict and cooperation, International Environmental Agreements: Politics, Law and Economics, 8, 297–316, doi:10.1007/s10784-008-9083-5, 2008.

Zeitoun, M. and Warner, J.: Hydro-hegemony – a framework for analysis of trans-boundary water conflicts, Water Policy, 8, 435–460, doi:10.2166/wp.2006.054, 2006.

Zhang, H., Gorelick, S. M., Avisse, N., Tilmant, A., Rajsekhar, D., and Yoon, J.: A New Temperature-Vegetation Triangle Algorithm with Variable Edges (TAVE) for Satellite-Based Actual Evapotranspiration Estimation, Remote Sensing, 8, doi:10.3390/rs8090735, 2016.

Zhang, S., Gao, H., and Naz, B. S.: Monitoring reservoir storage in South Asia from multisatellite remote sensing, Water Resources Research, 50, 8927–8943, doi:10.1002/2014WR015829, 2014.

Zhu, Z. and Woodcock, C. E.: Object-based cloud and cloud shadow detection in Landsat imagery, Remote Sensing of Environment, 118, 83–94, doi:10.1016/j.rse.2011.10.028, 2012.

Zhu, Z. and Woodcock, C. E.: Continuous change detection and classification of land cover using all available Landsat data, Remote Sensing of Environment, 144, 152–171, doi:10.1016/j.rse.2014.01.011, 2014.

Zhu, Z., Wang, S., and Woodcock, C. E.: Improvement and expansion of the Fmask algorithm: cloud, cloud shadow, and snow detection for Landsats 4-7, 8, and Sentinel 2 images, Remote Sensing of Environment, 159, 269–277, doi:10.1016/j.rse.2014.12.014, 2015.

Appendix A

Monitoring small reservoirs' storage with satellite remote sensing in inaccessible areas

Résumé

Dans les bassins versants disposant de systèmes de retenue d'eau, la mise à disposition de données régulièrement mises à jour sur le niveau et le stockage est fondamentale pour une gestion efficace de ces installations. Cependant, pour la plupart des réservoirs à travers le monde, soit les niveaux de stockage ne sont pas mesurés, soit ils ne sont pas facilement disponibles pour des raisons financières, politiques ou légales. Ce papier propose une nouvelle approche utilisant les images Landsat et des modèles numériques de terrain (MNT) pour récupérer des informations sur les variations des retenues d'eau dans des régions inaccessibles. Contrairement aux approches déjà existantes, cette méthode ne requiert aucune mesure sur le terrain et est adaptée pour faire le suivi de petits barrages, dont l'usage premier est souvent l'irrigation, et pour lesquels aucune information n'est généralement disponible. Elle consiste en trois étapes de reconstitution de l'information : (i) une classification dynamique 2-D de l'information issue des bandes spectrales Landsat pour quantifier la surface de l'étendue d'eau, (ii) une correction statistique des données du MNT afin de caractériser la topographie de chaque réservoir, et (iii) une reconstruction 3-D pour corriger les erreurs dues à la présence de nuages et à la panne du Scan Line Corrector à bord du Landsat 7. La méthode est utilisée pour quantifier la quantité d'eau dans les barrages du bassin du Yarmouk au sud de la Syrie; bassin à l'intérieur duquel les mesures terrain sont impossibles du fait de la guerre civile actuelle. Elle est validée à partir de données locales sur des barrages jordaniens à proximité. Le coefficient de détermination varie de 0,69 à 0,84, et l'erreur quadratique moyenne normalisée de 10 à 16 % sur les estimations de stockage de six barrages jordaniens dont la superficie de la retenue d'eau varie entre 0,59 et 3,79 km^2.

Hydrol. Earth Syst. Sci., 21, 6445–6459, 2017
https://doi.org/10.5194/hess-21-6445-2017

Hydrology and Earth System Sciences
Open Access
EGU

Monitoring small reservoirs' storage with satellite remote sensing in inaccessible areas

Nicolas Avisse[1], Amaury Tilmant[1], Marc François Müller[2], and Hua Zhang[3]

[1]Department of Civil Engineering and Water Engineering, Université Laval, Québec, QC G1V 0A6, Canada
[2]Department of Civil & Environmental Engineering & Earth Science, University of Notre Dame, Notre Dame, IN 46556, USA
[3]Department of Engineering, School of Engineering and Computing Sciences, Texas A & M University – Corpus Christi, Corpus Christi, TX 78412, USA

Correspondence: Nicolas Avisse (nicolas.avisse@gmail.com)

Received: 28 June 2017 – Discussion started: 19 July 2017
Revised: 7 November 2017 – Accepted: 12 November 2017 – Published: 18 December 2017

Abstract. In river basins with water storage facilities, the availability of regularly updated information on reservoir level and capacity is of paramount importance for the effective management of those systems. However, for the vast majority of reservoirs around the world, storage levels are either not measured or not readily available due to financial, political, or legal considerations. This paper proposes a novel approach using Landsat imagery and digital elevation models (DEMs) to retrieve information on storage variations in any inaccessible region. Unlike existing approaches, the method does not require any in situ measurement and is appropriate for monitoring small, and often undocumented, irrigation reservoirs. It consists of three recovery steps: (i) a 2-D dynamic classification of Landsat spectral band information to quantify the surface area of water, (ii) a statistical correction of DEM data to characterize the topography of each reservoir, and (iii) a 3-D reconstruction algorithm to correct for clouds and Landsat 7 Scan Line Corrector failure. The method is applied to quantify reservoir storage in the Yarmouk basin in southern Syria, where ground monitoring is impeded by the ongoing civil war. It is validated against available in situ measurements in neighbouring Jordanian reservoirs. Coefficients of determination range from 0.69 to 0.84, and the normalized root-mean-square error from 10 to 16 % for storage estimations on six Jordanian reservoirs with maximal water surface areas ranging from 0.59 to 3.79 km^2.

1 Introduction

Reservoirs are essential for the development and management of a river basin's water resources, no matter their size (Liebe et al., 2005; Leemhuis et al., 2009). By increasing the availability of water during low-flow periods (International Commission On Large Dams, 2016), dams often play a key role in water supply, irrigated agriculture, hydropower generation, navigation, cattle breeding, fisheries, etc.

Despite these valuable applications, there is a scarcity of monitoring data as many countries cannot financially afford to build gauging stations (Solander et al., 2016). And even when monitoring systems do exist, there may not be institutions to collect the data, or legal means to disseminate them, as they are often considered sensitive data (Alsdorf et al., 2007; Dombrowsky, 2007; Duan and Bastiaanssen, 2013). Yet this information is essential to conduct hydrological studies in committed basins, from defining reservoir operation rules in simulation models (Yoon and Beighley, 2015) to assessing the impact of multi-reservoir systems on downstream river discharge (Vörösmarty et al., 1997; Hanasaki et al., 2006; Döll et al., 2009).

In that context, remote sensing is a promising tool to overcome the difficulty in accessing reliable information on a reservoir. This technique has also been applied to characterize a range of continental water bodies such as large lakes (Birkett, 1995; Ponchaut and Cazenave, 1998; Mercier et al., 2002), paddy rice fields (Islam et al., 2010), or tidal floods (Yan et al., 2010). The general procedure to monitor storage consists in associating water surface elevation and area after evaluating them independently (e.g. Frappart et al., 2006).

Satellite radar and laser altimetry are the predominant approaches to estimating the elevation of open water bodies (e.g. Morris and Gill, 1994; Crétaux and Birkett, 2006; Calmant et al., 2008; Gao et al., 2012; Wang et al., 2013), or their bathymetry (Arsen et al., 2014). Orbit repeat periods of radar altimeters such as Topex/Poseidon (T/P), GFO, Jason-1 and 2, or Envisat range from 10 to 35 days. They have a high vertical accuracy with root-mean-square errors of the order of centimetres to tens of centimetres, depending on the altimeter and the size of the water body (Calmant et al., 2008; Crétaux et al., 2016). However, the above-mentioned sensors are affected by important drawbacks, including nadir viewing, narrow swath, coarse cross-track spacing (a few hundred kilometres), long along-track path length (about 1 km), and large elevation differences around some water areas that impede their application to more than a few hundred large lakes and reservoirs on the planet (i.e. area $> 100\,km^2$ and width $> 500\,m$) (Crétaux and Birkett, 2006; Alsdorf et al., 2007; Gao et al., 2012). More recent satellites such as Cryostat-2 or Sentinel-3 present significant improvements in terms of along-track resolution ($\sim 300\,m$). However, their respective inter-tracks of 7 and 52 km (Donlon et al., 2012; Crétaux et al., 2016) still place many reservoirs out of the trajectory of their nadir-viewing sensors onboard. The small inter-track of Cryosat is also realized at the expense of a long revisit cycle (369 days) that impedes any monitoring of small reservoirs on a monthly basis. Alternatively, the Geoscience Laser Altimeter System onboard the Ice, Cloud, and Elevation Satellite (ICESat/GLAS) measured land surface elevations between 2003 and 2009 with a much finer spatial resolution (footprint size between 50 and 105 m every 170 m along the track), a vertical accuracy close to 10 cm (Zhang et al., 2011; Duan and Bastiaanssen, 2013), and a finer cross-track resolution (15 km maximum at the Equator, Zwally et al., 2002). There was however no continuous elevation retrieval: ICESat/GLAS gathered data only during designated campaigns, with a long ground-track repeat cycle for almost all of it (183 days). Furthermore, unlike radar altimeters that can be used under all weather conditions (Birkett and Beckley, 2010), laser measurements are affected by the presence of thin clouds (Duan and Bastiaanssen, 2013). Many existing studies consequently used ICESat/GLAS data to get a trend on pre-determined large lake variations over several years (e.g. Zhang et al., 2011; Duan and Bastiaanssen, 2013; Song et al., 2013), or to calibrate area–elevation relationships for a limited number of water bodies large enough for the satellite to take sufficient elevation measurements per track (Zhang et al., 2014).

Water surface areas are commonly determined from optical satellite imagery such as MODerate Resolution Imaging Spectroradiometer (MODIS) and Landsat products (Xiao et al., 2006; Gao et al., 2012), or synthetic aperture radar (SAR) sensors (e.g. RADARSAT, JERS-1, ERS, or Sentinel-1) (Annor et al., 2009; Duan and Bastiaanssen, 2013; Amitrano et al., 2014). The latter has however been less used due to the difficulty in getting consistent results, as the required condition of a significantly lower phase coherence of water areas than of the surrounding land surface is not always met, with orbital repeat cycles of more than a few days, or with wind or rain (Alsdorf et al., 2007; Eilander et al., 2014). Therefore, existing approaches have used either MODIS or Landsat, depending on their emphasis on spatial or temporal resolution (Solander et al., 2016; Zhang et al., 2016). Images acquired during the various Landsat missions have a much finer spatial resolution (30 m) than MODIS' (250 m for the red band, 500 m for infrared), but they are taken on a repeat cycle of 16 days compared to the daily MODIS products. The higher revisit frequency of MODIS satellites allows MODIS-based approaches to better address clouds and smoke artifacts in optical images. However, MODIS missions cover a much shorter period (July 2000 to present) than Landsat missions (July 1982 to present). The potential of the recent two Sentinel-2 satellites can also be mentioned for post-2015 studies. Launched in June 2015 (Sentinel-2A) and March 2017 (Sentinel-2B), they provide spectral bands at a resolution of 10 m for visible and NIR bands, and at 20 m for SWIR bands. They also have a repeat cycle of 5 days by combining the two (European Space Agency, 2013; Yang et al., 2017).

The common protocol to separate water areas from other land use categories is to apply a threshold to indices such as the Normalized Difference Vegetation Index (NDVI) (e.g. Frappart et al., 2006; Gao et al., 2012), or the Modified Normalized Difference Water Index (MNDWI) proposed by Xu (2006) (e.g. Crétaux et al., 2015; Müller et al., 2016). But determining an adequate value for a multi-temporal analysis can be challenging because such a threshold is known to be case-dependent (Liu et al., 2012; Coltin et al., 2016). Furthermore, separating water from land or vegetation may be difficult due to subpixel land-cover components (Ji et al., 2009) or water quality that can vary throughout a water body (Gao et al., 2012). To address these issues, decision tree defined thresholds have successfully been applied with various vegetation indices (e.g. Xiao et al., 2006; Islam et al., 2010; Yan et al., 2010), but remain case-dependent. Coltin et al. (2016) then advocated the implementation of automatic thresholds as they developed a supervised learning approach to improve flood mapping. Other methods like unsupervised classification (Wang et al., 2008), or direct elevation–area relationships from a digital elevation model (DEM, Wang et al., 2005), have also been tested, but did not prove to be more precise. Gao et al. (2012) recently developed a method to combine both an index analysis and an unsupervised classification to improve the accuracy of the delineation of water areas. The approach was refined by Zhang et al. (2014), who enhanced the storage assessment with a novel surface area retrieval algorithm.

While promising, these approaches generally fail to systematically combine remote sensing surface area and elevation due to the different timing in orbital repeat cycles

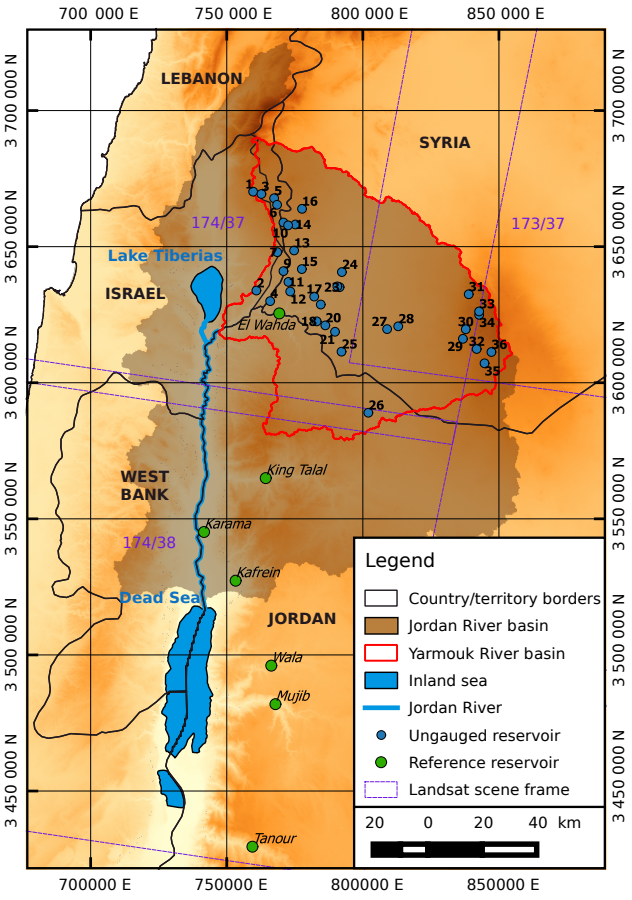

Figure 1. Reservoirs identified in Jordan and the Yarmouk River basin using the method developed in this paper. Because in situ measurements are accessible for those managed by Jordan, they are used to validate the method. Coordinates are expressed in the Coordinate Reference System (CRS) WGS 84/UTM zone 36N (EPSG:32636), in which 1 unit equals 1 m.

of different satellites. Elevation–area relationships are then deduced from remote sensing data that are available at the same time (e.g. through linear or polynomial regressions, Gao et al., 2012; Duan and Bastiaanssen, 2013; Song et al., 2013), so that reservoir storage can be computed with either remote sensing elevation or area only. Even then, existing methods estimate storage in relative terms, either from the already known elevation, area and storage at capacity (Zhang et al., 2014), or from the lowest water level detected (Duan and Bastiaanssen, 2013).

Furthermore, these approaches have only been applied to reservoirs larger than 100 km^2, which are estimated to represent only 0.54 % of reservoirs larger than 0.1 km^2 in the world (Lehner et al., 2011). Studies that analysed small reservoirs delineated water surface with Landsat optical sensors (e.g. Liebe et al., 2005; Sawunyama et al., 2006; Rodrigues et al., 2012) or radar images to address the cloud cover issue (Annor et al., 2009; Liebe et al., 2009), and could only get an estimation of storage capacities by conducting bathymetrical

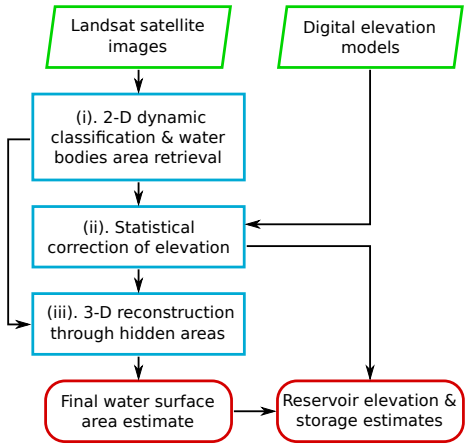

Figure 2. Flowchart of the whole procedure.

surveys. Due to their reliance on in situ observations, these methods are inapplicable to remote, ungauged, or conflict-torn areas.

This paper introduces a new method to monitor reservoir storage based on remote sensing data exclusively. The method is applied to small reservoirs – capacities and water surface areas starting from 1 hm^3 (million cubic metres) and 0.5 km^2 respectively – in the Yarmouk River basin (YRB; see Fig. 1) in southern Syria during the ongoing civil war and the decade before it started. Its prediction performance is tested against available in situ observations of reservoir storage and elevation in neighbouring Jordan.

The document is organized as follows: Sect. 2 presents the method and algorithms developed for the monitoring of reservoir storage, Sect. 3 reviews results, error measurements, and sensitivity analysis, and Sect. 4 concludes the study.

2 Methodology

The procedure is based on two types of data: Landsat images for water area estimation, and DEM for topography. It works in three stages that are presented in the flowchart in Fig. 2. The idea behind the process is (i) to use Landsat bands to enhance the detection of water pixels, then (ii) to exploit this information to statistically correct the DEM vertical errors and characterize reservoir bathymetry, and (iii) to use the updated topography to reconstruct missing parts of Landsat images (e.g. pixels covered by clouds or not captured by the Landsat sensor).

2.1 Two-dimensional dynamic classification and water body area retrieval

Landsat images are chosen because they are freely available with a spatial resolution fine enough (30 m) to detect variations in the area of small reservoirs. The spatial resolution of MODIS images is indeed too coarse to assign to any small reservoir a proper range of area and elevation (1 km^2 is covered by 16 MODIS image 250 m pixels only). Thus, about 300 Landsat 4, 5, 7, and 8 images for each scene – index 173/37 above a part of the YRB, 174/38 above reservoirs in Jordan, and 174/37 above parts of both in the Worldwide Reference System (WRS; see the scene frames in Fig. 1) – are downloaded from the United States Geological Survey (USGS) EarthExplorer website (https://earthexplorer.usgs.gov/).

2.1.1 Fmask

We use the Fmask (Function of mask) algorithm (Zhu and Woodcock, 2012; Zhu et al., 2015) to discriminate cloud coverage from open water. The algorithm was originally designed to separate potential cloud pixels from clear sky pixels on Landsat images using empirical thresholds on the NDVI and the near-infrared band, with an overall accuracy of 96.41 % (Zhu and Woodcock, 2012). Fmask distinguishes land and water areas and produces a probability mask for clouds, which we use to manually remove images that are almost entirely covered by clouds or with obvious large errors in water body detection. After quality control, about 245 images remain per location.

Most pixels classified as water by Fmask can reasonably be considered water due to the relatively selective thresholds used in the algorithm. Hence, at this stage, the uncertainty remains with regards to pixels hidden by clouds or cloud shadows, misclassified by Fmask as land or snow, or not captured by the Landsat sensor (e.g. "N/A" – not available – stripes caused by the Landsat 7 Scan Line Corrector – SLC – failure; see Fig. 4a and b). Our analysis reveals that, on average, 24.1 % of the reservoirs' pixels are misclassified as land, 8.1 % are covered with clouds or cloud shadows, and 8.6 % are in "N/A" areas (see Sect. 3.1).

2.1.2 Occurrence mask

We use the frequency with which pixels are classified as water to distinguish actual reservoirs from small pools or misclassified land, and to delimit them. For each Landsat scene, the ∼245 satellite images are superimposed to form an image where each pixel represents the number of times it has been covered by water (see Fig. 3). This occurrence mask (M_{occ}) is useful for filtering occasional Fmask classification errors, and for creating a water mask (M_{wat}): pixels with values greater than 5 in M_{occ} are classified as water and kept in M_{wat}, while those with lower values are considered misclassified land and removed from water bodies (i.e. hidden by M_{wat}). In practice, the threshold of 5 was empirically chosen after comparing detected water bodies with Google Earth high-resolution (∼ 1 m) imagery. The same threshold is applied to reservoirs located in the overlapping area of two Landsat images as it does not change their contours. Its small value is justified by the fact that most images with obvious mistakes have already been manually discarded at the previous step.

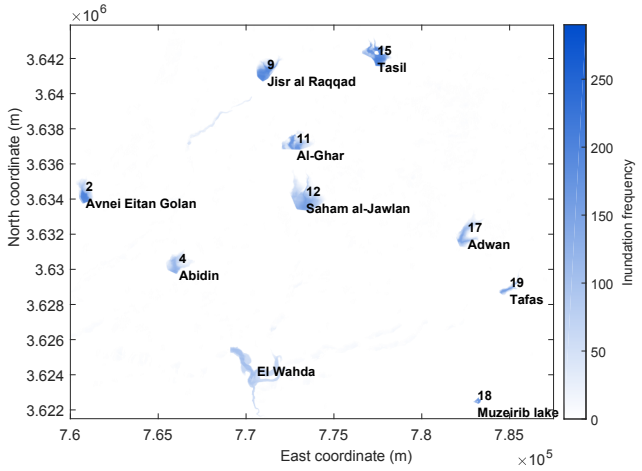

Figure 3. Image of the number of times each pixel has been covered by water (M_{occ}). The text in black indicates the identification number (for Syrian reservoirs) and the name of known reservoirs. Coordinates are expressed in CRS WGS 84/UTM zone 36N.

Aside from sporadic large wadis (intermittent rivers) that are manually removed from the mask, final water bodies in M_{wat} are deemed to be reservoirs. They are the ones depicted in blue and green dots on the map in Fig. 1.

2.1.3 Classification enhancement for each Landsat image

The detection of water bodies is enhanced using NDVI and MNDWI rasters computed from Landsat imagery. A low NDVI can be attributed to both water and bare land, and a low MNDWI value can denote either water or clouds. We combine these indices and leverage their complementary nature to detect open water.

To ensure more reliable and repeatable values for identical land use categories in different images, the two indices are computed from surface reflectance, which is estimated by applying the image-based atmospheric correction Dark Object Subtraction 1 (DOS1, Chavez, 1996) to top of atmosphere (TOA) reflectance. However, the DOS1 adjustment is not optimal because it is not based on actual atmospheric or cloud cover measurements. Moreover, the slight band variations between the various Landsat missions may affect NDVI and MNDWI, and may require different thresholds to detect water. Consequently, two supplementary water detection ad-

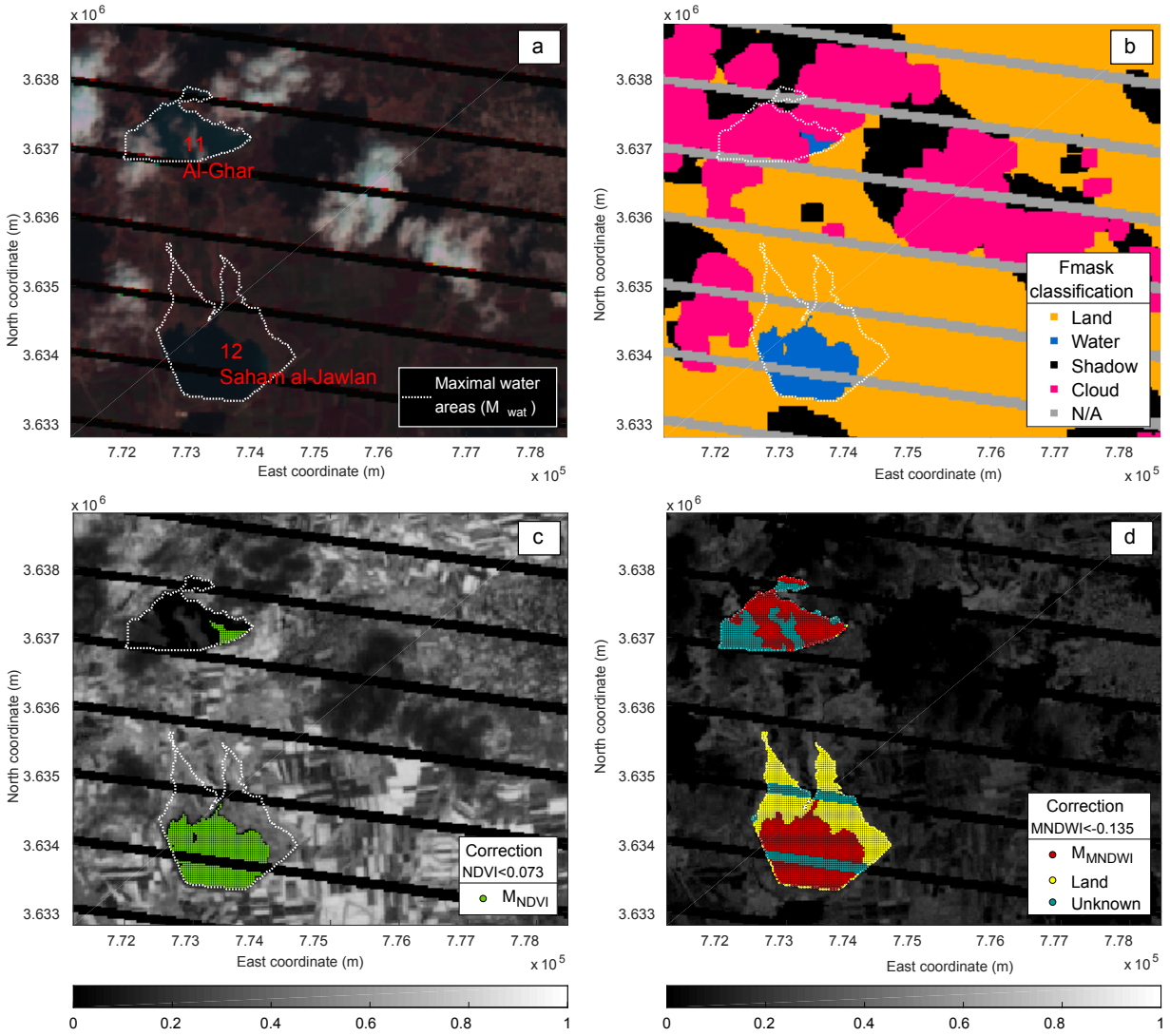

Figure 4. Two-dimensional dynamic water classification over a part of a Landsat 7 image (174/37) obtained on 30 March 2010. Coordinates are expressed in CRS WGS 84/UTM zone 36N. **(a)** SWIR-R-G image. Two reservoirs can be seen by eye – even if their appearance is very similar to cloud shadow areas – but the hedges are not easy to detect due to the cloud cover. **(b)** Results of the Fmask classification. Water area detection is not precise enough to directly use the results for the estimation of reservoir surface area. **(c)** NDVI image. Water pixels' low NDVI here contrasts with the surrounding irrigated crops' high NDVI, as the two reservoirs are located close to cultivation areas. **(d)** MNDWI image. Red dots indicate water areas obtained after the 2-D enhancement (Sect. 2.1). The 3-D reconstruction is done later (Sect. 2.3) on the *Unknown* part.

justments are performed through the method presented in the flowchart in Fig. 5 to define a MNDWI threshold adapted to each date and climatic condition (i.e. each time t over a given scene). A NDVI mask ($M_{\mathrm{NDVI}}(t)$) is first created to calibrate the MNDWI threshold, which is then used to build a MNDWI mask representing water areas ($M_{\mathrm{MNDWI}}(t)$).

1. The goal of $M_{\mathrm{NDVI}}(t)$ is to find with the NDVI all pixels where there could potentially be water. Depending on the results of the Fmask classification in M_{wat}, three situations can arise.

   i. If water is already detected by Fmask in M_{wat} reservoirs, $M_{\mathrm{NDVI}}(t)$ is formed from those ones (see the green dots in the Fig. 4c example).

   ii. Where water is not detected by Fmask, we impose a threshold on the NDVI. Pixels with a NDVI of less than -0.1 in M_{wat} are used to form $M_{\mathrm{NDVI}}(t)$. The lowest values are indeed generally typical of water. This condition has been added to take into account images where thin clouds cover reservoirs.

   iii. In ~ 1 % of all images, no pixel meets the previous conditions, even if water can be seen by eye on the

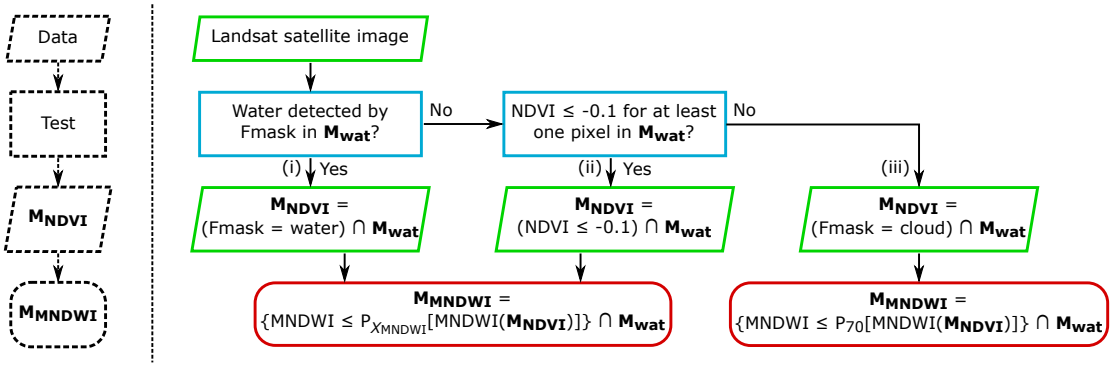

Figure 5. Two-dimensional dynamic classification procedure.

original spectral bands. We have indeed noticed that for these few cases, Fmask associates water bodies with clouds. $M_{\mathrm{NDVI}}(t)$ is thus built on pixels classified as cloud in M_{wat}.

2. The detection of water bodies is further enhanced by imposing a threshold on MNDWI images. The threshold is defined automatically so as to optimally distinguish water bodies from clouds. For the two first situations, the threshold is set to the X_{MNDWI}th percentile ($P_{X_{\mathrm{MNDWI}}}$) of MNDWI values in $M_{\mathrm{NDVI}}(t)$. X_{MNDWI} is set to the maximum, 100, in order to avoid over-constraining the classification. The sensitivity of the method to the choice of this parameter is presented in Sect. 3.2 below. For the third case, the threshold is set to the 70th percentile (P_{70}) of MNDWI values in $M_{\mathrm{NDVI}}(t)$.

   Finally, the water mask – or MNDWI mask – $M_{\mathrm{MNDWI}}(t)$ is formed by including only areas with a MNDWI of less than the MNDWI threshold in M_{wat}. This last step allows us to incorporate most water pixels left out by Fmask and undetectable with NDVI (see the red dots in Fig. 4d).

After removing water areas smaller than 20 pixels ($20 \times 900\,\mathrm{m}^2$), considered noise, the classified images have three categories: (i) *Water* as identified by the protocol developed above, (ii) *Land* according to Fmask, and if not in the category *Water*, and (iii) *Unknown*, which includes all other pixels (see Fig. 4d).

2.2 Statistical correction of elevation

2.2.1 Digital elevation models

Unlike most studies, the proposed method does not rely on satellite altimetry to assess water bodies' elevation, but on DEMs to get the topography. It is then required that reservoirs were almost empty or not yet built when the DEM satellites passed over them, for at least one of the two sources considered: ASTER GDEM v2 and SRTM-C/X. ASTER GDEM v2 data were acquired between 2001 and 2008, and SRTM-C/X data on 11–22 February 2000. All have a spatial resolution of 1″ (approximately 30 m at the Equator), which we resample to match Landsat images. The large coverage of these datasets is chosen over the very low precision of the measures. They indeed cover almost all of the Earth's land surface (except for SRTM-X): from 83° N to 83° S for ASTER GDEM v2, and from 60° N to 56° S for SRTM-C; but the vertical relative precision is very low compared to satellite altimetry: objectives of 15 and 6 m for 90 % of SRTM-C and SRTM-X data respectively (German Aerospace Center, 2017; Rodriguez et al., 2005), and standard deviations estimated to 3.95 and 8.68 m for SRTM-C and ASTER data respectively (ASTER GDEM Validation Team, 2011).

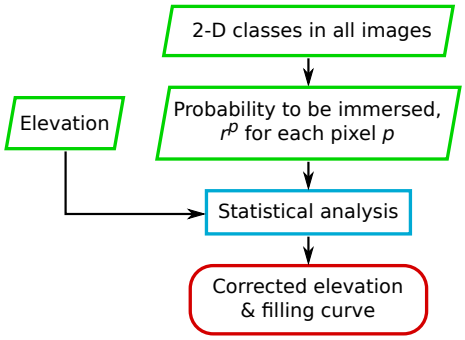

Figure 6. Procedure for the statistical correction of topography.

2.2.2 Elevation–area relationship

To improve elevation assessment, DEMs are statistically corrected by using the information on water surface areas obtained from Landsat images. The protocol presented in Fig. 6 is implemented for each reservoir.

1. a water coverage quantile is computed at each pixel to determine the probability of it being immersed. With each pixel p is associated the ratio r^{p} defined as

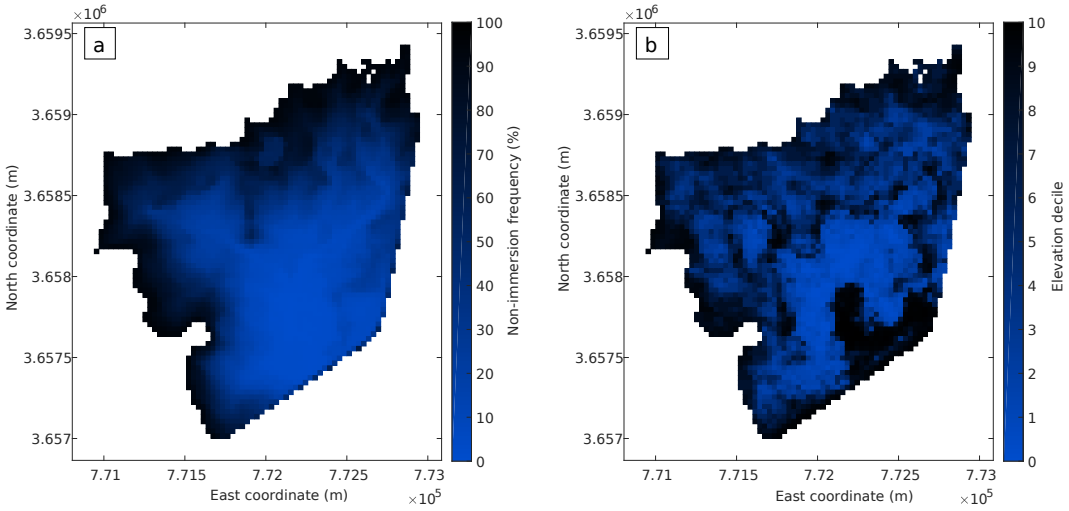

Figure 7. (a) Relative non-immersion frequency ($1 - r^p$, from the 2-D classes) and **(b)** elevation (from the DEMs, in terms of decile) in the Kudnah reservoir. Coordinates are expressed in CRS WGS 84/UTM zone 36N.

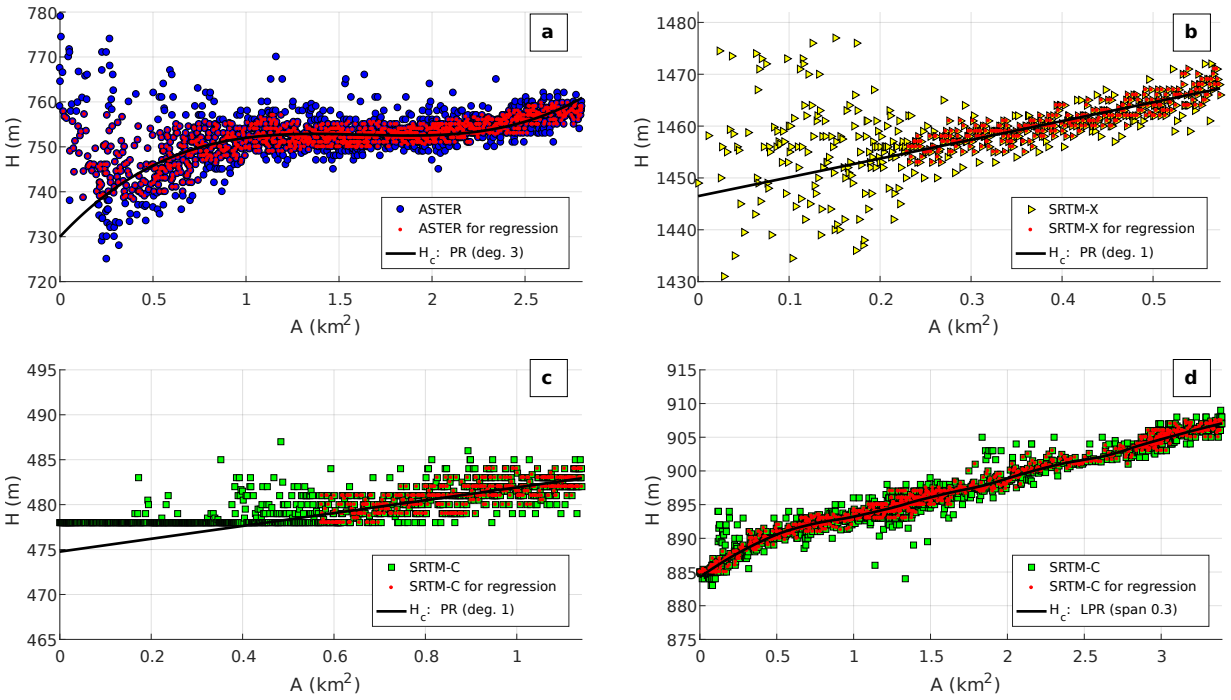

Figure 8. Elevation–area relationship and regression for a few reservoirs in the Yarmouk River basin: **(a)** Kudnah, **(b)** Roum, **(c)** Al Ghar, and **(d)** Qunaitera. Each symbol (circle, square, or triangle, depending on the DEM) represents the information associated with 1 pixel in a reservoir. PR and LPR stand for polynomial regression and local polynomial regression respectively.

$$r^{\mathrm{p}} = \frac{N^{\mathrm{p}}_{\mathrm{water}}}{N^{\mathrm{p}}_{\mathrm{water}} + N^{\mathrm{p}}_{\mathrm{land}}}, \quad (1)$$

where $N^{\mathrm{p}}_{\mathrm{water}}$ is the number of times the given pixel p is counted as Water, and $N^{\mathrm{p}}_{\mathrm{land}}$ is the number of times it is counted as Land. We ignore the images where the pixel p is classified as Unknown.

2. To illustrate the interest of this section, Fig. 7 shows both r^{p} and the relative elevation in the Kudnah reservoir. We can see that the two do not always match as we would expect – i.e. the lowest pixels are not always the most frequently immersed, nor are the highest pixels the most rarely immersed. The immersion frequency (r^{p}) can actually be used to correct the elevation. The former, which is estimated from the results of the 2-D clas-

sification enhancement, is indeed assumed to be more reliable than the original DEM. Hence, each pixel's elevation H^p is put in relation with the area A^p, defined as the cumulated area of all pixels q in the reservoir for which $r^q \geq r^p$. The examples of Fig. 8 confirm the observations made in Fig. 7: pixels' elevations are not always correlated with the number of times they are classified as water. To a certain extent the difference was expected from the DEM's low vertical precision, but some "anomalies" concerning the most often immersed pixels (i.e. lowest A^p) can be recurrent from one reservoir to another, due to either a strong dispersion in elevation (see the SRTM-X data in Fig. 8b), or a flat elevation (see the SRTM-C data in Fig. 8c). We interpret this irregularity as arising from the presence of water where the satellite tried to evaluate elevation: in the case of SRTM-X, the measure over water is hampered for reasons inherent to the use of a SAR sensor; and in the case of SRTM-C, DEM pixels covered with water may have been filled during a post-treatment analysis. Either way, elevation cannot be retrieved from the given DEM for these reservoirs' most often immersed pixels.

3. To address the issue, a polynomial regression on observed land pixels ($A > A_i$, with A_i the area assumed to be immersed during the satellite elevation retrieval) is used to build a "corrected elevation"–area relationship ($A \rightarrow H_c(A)$) that best fits the data (in a least-squares sense). Values of H greater than the 80th percentile or lower than the 20th percentile are ignored to filter potential errors and smooth the data. This step is executed three times – one for each DEM – and the better quality dataset (i.e. the one with less dispersion and fewer "anomalies" as defined above) is kept. Examples are shown in Fig. 8.

4. A filling curve – the volume–area relationship – is finally constructed using the outcomes of the previous step.

The regression relies on the assumption that elevation estimates are correct on average by considering many pixels. Indeed, the relative error in elevation approaches zero when the number of images taken into account grows. This property has already been used by LeFavour and Alsdorf (2005) for instance, in order to estimate the slope of the Amazon River.

Parameters and results of the regression for reservoirs that fulfil the criteria mentioned at the beginning of this article – maximum storage and area larger than 1 hm^3 and 0.5 km^2 respectively – are summarized in Table 1.

2.3 Three-dimensional reconstruction through hidden areas

Retrieving missing parts of water bodies in the Unknown areas means dealing with Landsat drawbacks: (i) the 16-day repeat cycle making images regularly covered by clouds, and (ii) the failure of the Landsat 7 SLC that led to large data losses for the Enhanced Thematic Mapper Plus (ETM+) sensor after May 2003 (see the grey stripes in Fig. 4b).

Zhang et al. (2014) developed an approach to improve quite significantly the estimation of a reservoir's water area. However, their method requires that only a small part of the reservoir is misclassified or hidden. This is not a problem if one works with MODIS images over very large reservoirs, but in our situation – Landsat images over small water bodies – the condition is rarely met.

We developed an alternative algorithm to use the information from each individual pixel.

1. As the area A^p has been associated with each pixel p, and H_c has been expressed in terms of A, a corrected elevation is associated with each pixel in a reservoir.

2. Each pixel in an Unknown area adjacent to water areas is set to Water if (i) the pixel is in M_{wat}, and (ii) its corrected elevation H_c^p is less than the X_{H_c}th percentile of the corrected elevation in all adjacent water bodies. This threshold is set to 98 to ignore the highest values of H_c, in case they were associated with pixels misclassified as water. A sensitivity analysis has been conducted with regard to this threshold, and the results are available in Sect. 3.2 below.

This water body reconstruction technique relies on the fact that a pixel that is often immersed likely has an elevation lower than a pixel that is rarely immersed. This is a reasonable assumption due to the large number of images analysed. The blue dots in Fig. 9 show how the 3-D reconstruction complements the previous 2-D information retrieval. Finally, storage variations are obtained by combining final reconstructed areas with the previously determined filling curves.

3 Results

3.1 Storage variations: validation and discussion

Storage variations estimated by remote sensing for all reservoirs that cannot be gauged in the YRB are displayed in Fig. 10. These reservoirs are located in Syria and in the Israel-controlled Golan Heights. By qualitatively comparing our results to those obtained by Müller et al. (2016) (monitoring of Syrian reservoirs using Landsat 7 datasets but before the 2-D and 3-D corrections), we can see more coherent storage variations through the presence of annual drawdown–refill cycles – particularly for Roum and Sahwat al-Khadr. This means that the 2-D enhancement and 3-D reconstruction steps have improved the detection of water and helped to overcome the low Landsat repeat cycle of 16 days.

Reservoirs managed by Jordan are used to validate the method by comparing our remote sensing estimates of elevation and storage with monthly in situ measurements con-

Table 1. Parameters and results of the elevation–area regression. PR and LPR stand for polynomial regression and local polynomial regression respectively. R^2 is the coefficient of determination between the corrected elevation H_c and the elevation H for pixels taken into account by the regression (red dots in Fig. 8).

Location	Reservoir	DEM	Visible area $1-\frac{A_i}{A_{max}}$ (%)	Regression	R^2	A_{max} (km^2)	$\Delta H_{c_{max}}$ (m)	V_{max} (hm^3)
Israel-controlled	Al Manzarah	ASTER	100	PR (deg. 2)	0.34	0.53	9.14	2.64
Golan Heights	Avnei Eitan Golan	ASTER	70	PR (deg. 2)	0.31	0.93	4.88	2.34
Syria	Abidin	ASTER	65	PR (deg. 1)	0.37	1.16	8.74	5.07
	Qunaitera	SRTM-C	100	LPR (span 0.3)	0.98	3.40	22.81	33.94
	Jisr al Raqqad	ASTER	30	PR (deg. 1)	0.52	1.16	16.23	9.43
	Kudnah	ASTER	100	PR (deg. 3)	0.46	2.81	30.92	29.45
	Al Ghar	SRTM-C	50	PR (deg. 1)	0.56	1.14	8.17	4.66
	Saham al-Jawlan	SRTM-C	55	PR (deg. 1)	0.84	2.48	12.93	15.99
	Ghadir al-Bustan	ASTER	50	PR (deg. 1)	0.56	1.19	15.02	8.93
	Tasil	ASTER	60	PR (deg. 1)	0.28	1.28	9.59	6.15
	Adwan	ASTER	100	PR (deg. 1)	0.33	1.31	7.92	5.17
	Ebtaa kabeer	SRTM-C	80	PR (deg. 1)	0.71	0.73	6.56	2.39
	Sheikh Miskin	SRTM-C	45	PR (deg. 1)	0.71	2.85	7.51	10.71
	Roum	SRTM-X	60	PR (deg. 1)	0.81	0.57	20.77	5.94
	Sahwat al-Khadr	SRTM-C	80	PR (deg. 3)	0.78	1.27	10.07	6.49
Border Jordan–Syria	El Wahda	SRTM-C	100	LPR (span 0.3)	0.97	2.69	53.31	66.72
Jordan	Karama	SRTM-C	85	LPR (span 0.1)	0.90	3.79	17.00	35.91
	Kafrein	SRTM-C	30	PR (deg. 1)	0.56	0.66	17.80	5.85
	Tanour	SRTM-C	85	PR (deg. 1)	0.94	0.59	36.00	10.56
	King Talal	SRTM-C	20	PR (deg. 1)	0.29	2.17	31.66	33.69
	Wala	SRTM-C	100	LPR (span 0.5)	0.85	0.61	25.86	6.37
	Mujib	SRTM-C	50	LPR (span 0.3)	0.79	1.30	44.33	30.49

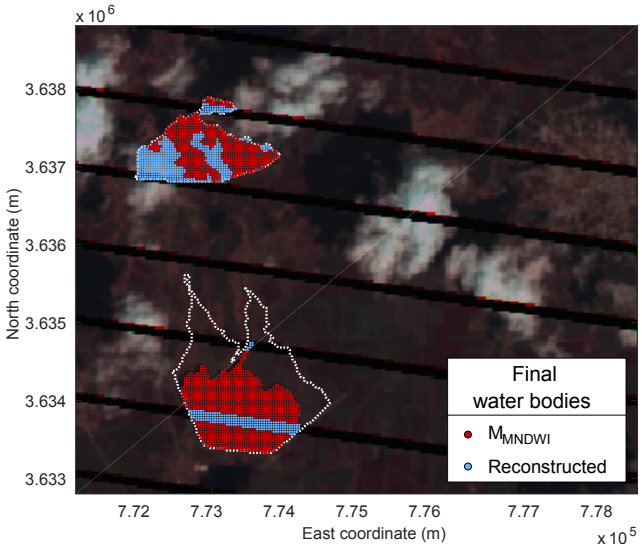

Figure 9. SWIR-R-G image. Final water bodies as obtained after the 2-D enhancement and the 3-D reconstruction applied to the Landsat 7 image (174/37) taken on 30 March 2010 (same as Fig. 4). Coordinates are expressed in CRS WGS 84/UTM zone 36N.

ducted by the Jordan Valley Authority (JVA). With the exception of the King Talal dam, our results seem to follow quite accurately the historical records (see Fig. 11). For some reservoirs (i.e. Karama and Tanour), the method seems to have difficulties in predicting the highest storages. Indeed, if the number of high-elevation pixels is small, the uncertainty in their corrected elevation (and thus the filling curve) can potentially affect the estimate of the maximum storage. This may be a limitation of the method. In addition, we can note that elevation H and volume V may vary a lot from month to month: up to 10 m or 15 hm^3 – i.e. 50 % of the maximal storage – for instance for the Mujib reservoir. Because no information is available regarding the data collection date, some of the differences between our estimates and measured data might then come from this lack of metadata.

With regard to the King Talal reservoir, we can see large errors in storage estimates (see Fig. 11). But they could have been expected at the end of the elevation–area relationship establishment step: the assumptions that were made to define H_c were maybe not justified in this case. Indeed, 80 % of the reservoir maximal area was covered with water when the SRTM satellite passed over the dam, and the R^2 is only 0.29 for the regression applied to the remaining visible pixels (see Table 1). A small visible surface area does not necessar-

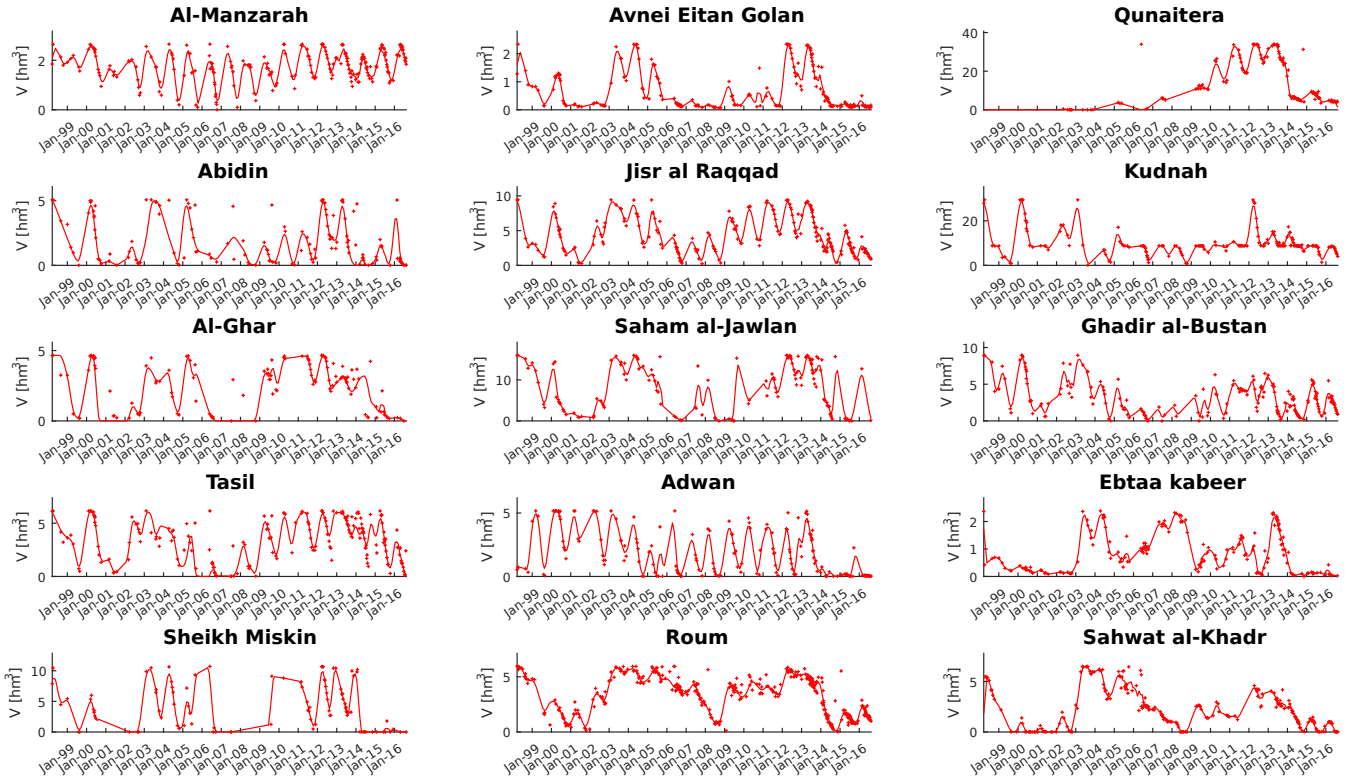

Figure 10. Storage variations. Red crosses indicate estimates from the method developed in this paper. Red lines are local polynomial regressions that are plotted only with the purpose of showing storage variation trends.

ily lead to a low-quality elevation–area relationship – see the good estimates for the Kafrein reservoir, while 70 % of its maximal area was hidden when the SRTM satellite passed over it – but it certainly is a sign that results might be biased.

Errors in the estimation of elevation and storage are evaluated in terms of the coefficient of determination (R^2, Eq. 2) and the normalized root-mean-square error (NRMSE, Eq. 3):

$$R^2 = \frac{\mathrm{Cov}(\mathrm{RS}, \mathrm{Hist})^2}{\sigma^2_{\mathrm{RS}} \cdot \sigma^2_{\mathrm{Hist}}}, \quad (2)$$

$$\mathrm{NRMSE} = \frac{1}{\mathrm{Hist}_{\max} - \mathrm{Hist}_{\min}} \sqrt{\sum_{i=1}^{N} \frac{(\mathrm{RS}_i - \mathrm{Hist}_i)^2}{N}}, \quad (3)$$

where Cov(RS, Hist) is the covariance between remote sensing (RS) estimates and JVA historical measurements, σ^2 the variance, and N the number of RS estimates during the period in which JVA measured storage or elevation. Results are presented in Table 2.

The coefficient of determination for storage ranges from 0.69 to 0.84. These high values confirm an important correlation and the similar variation trends that can be seen between the method's estimates and JVA records (see Fig. 11). A few high NRMSE values for both V and H_c though indicate that there is still some uncertainty with regard to the estimation of their absolute value at a given month. Indeed, by ignoring the King Talal dam, NRMSE ranges from 10 to 16 % for storage, and reaches up to 30 % for elevation. These error estimates for elevation though need to be taken into account with caution due to the small number of JVA measurements available for comparison ($15 \leq N \leq 35$).

Table 2. Errors in terms of R^2 and NRMSE for Jordanian reservoirs' H_c and V assessments.

Reservoir	N		R^2		NRMSE	
	H_c	V	H_c	V	H_c	V
El Wahda	25	107	0.54	0.76	0.30	0.15
Karama	29	123	0.98	0.79	0.05	0.10
Kafrein	35	136	0.91	0.81	0.11	0.10
Tanour	16	117	0.83	0.84	0.12	0.15
King Talal	40	159	0.50	0.76	0.36	0.19
Wala	15	37	0.36	0.69	0.21	0.16
Mujib	15	104	0.73	0.75	0.15	0.15

In order to better evaluate the proposed method compared to a basic fixed NDVI and near-infrared thresholds water area detection, we consider the results presented in Table 3: on average, only 30.0 to 59.4 % of final reservoir areas are detected by Fmask. The average additional part of final wa-

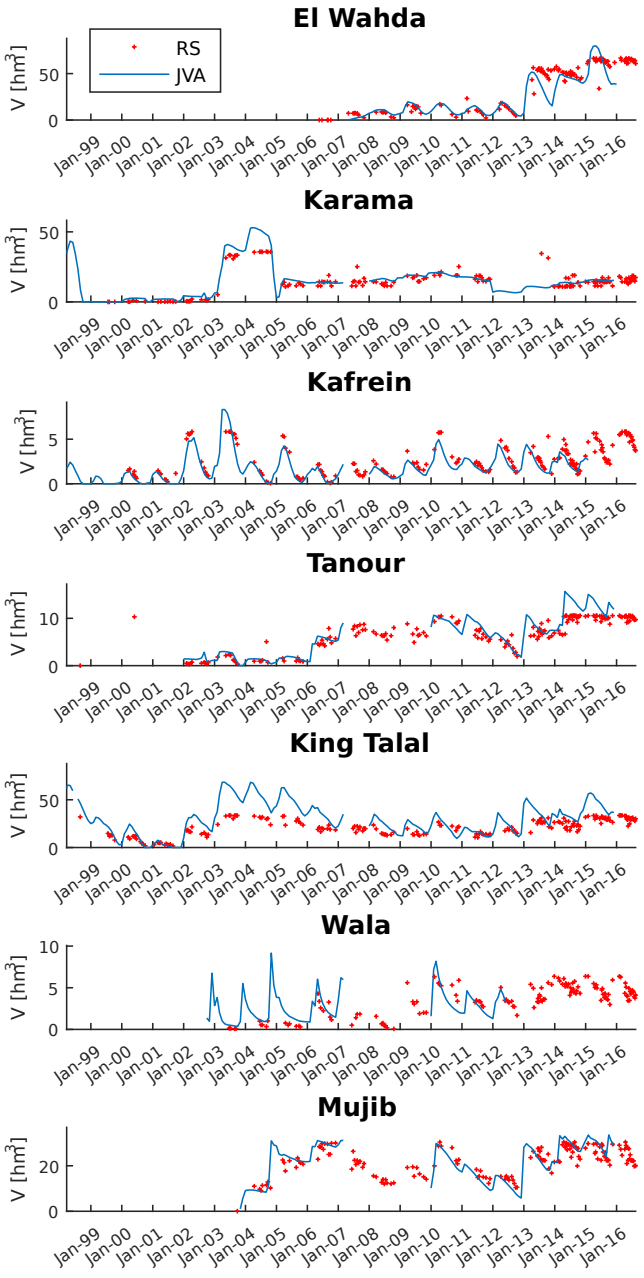

Figure 11. Storage variations for Jordan managed reservoirs. Red crosses indicate estimates from the method developed in this paper. The blue lines indicate in situ data records that were made by the Jordan Valley Authority (JVA).

ter bodies that is detected with the employment of a NDVI-based dynamic threshold for MNDWI is larger than 30 % for all Jordanian reservoirs, and can reach more than 50 % for the Tanour and Wala reservoirs. Similarly, the average additional part obtained through the 3-D reconstruction is larger than 3.9 % (Karama reservoir), and goes beyond 16 % for the more recent reservoirs Tanour, Wala, and Mujib, whose construction ended after 2002 – proportionally, more Landsat 7 images affected by "N/A" stripes were then used for them than for older dams. In light of these large shares of hidden or undetected water areas, corrections were obviously essential to consistently monitor reservoir elevation and storage.

Table 3. Initial Fmask classification inside the final water areas ("Other" refers to clouds, cloud shadows, and snow), and stages' percentage changes that led to the classification as water ("2-D" for the 2-D classification enhancement, and "3-D" for the 3-D reconstruction). "N/A" means not available.

Reservoir	Fmask classification (%)				Changes (%)	
	Water	Land	Other	N/A	2-D	3-D
El Wahda	58.6	20.8	13.1	7.5	32.2	9.2
Karama	64.1	13.3	20.9	1.7	32.0	3.9
Kafrein	58.5	15.9	17.2	8.4	31.9	9.7
Tanour	31.3	15.4	39.0	14.3	52.5	16.1
King Talal	59.4	22.1	9.7	8.8	30.8	9.8
Wala	30.0	24.4	30.0	15.7	52.6	17.5
Mujib	36.1	9.6	37.2	17.2	45.2	18.6

3.2 Sensitivity analysis

The two algorithms used to improve the estimation of reservoir area rely on one empirical threshold each: the classification enhancement is performed through the definition of a MNDWI percentile threshold (X_{MNDWI}) to build a mask dynamically adapted to each Landsat image, and the reconstruction is achieved with the choice of a percentile for H_{c} values ($X_{H_{\mathrm{c}}}$), which is set to avoid water area overestimation.

The sensitivity of the whole method to these two parameters is tested in terms of the above defined indices: R^2 and NRMSE, which are averaged for all reservoirs in Jordan (King Talal excluded). The sensitivity analysis is conducted by making the percentile thresholds vary between 90 and 100 with a step of 1. Results are presented for both storage and elevation in Fig. 12.

The coefficient of determination reaches its maximum with X_{MNDWI} values around 98 for storage and 93 or 95 for elevation. However, R^2 does not quantitatively assess the accuracy of the method, and as it remains fairly high (above 0.78 for storage, or 0.74 for elevation) in the whole 90–100 range for both parameters, it is not considered to select the threshold percentiles.

NRMSE decreases as X_{MNDWI} and $X_{H_{\mathrm{c}}}$ increase. The method does not detect an excessive number of water pixels – see the retrieval over the large missing parts detailed in Table 3 – but rather obtains estimates for elevation and storage closer to the measurements conducted by JVA. Two conclusions can be drawn from these observations. First, the success in the 2-D enhancement means that there is enough information in Landsat bands to better detect water areas. And second, the precision of the 3-D reconstruction implies that enough Landsat images are available for most reservoirs

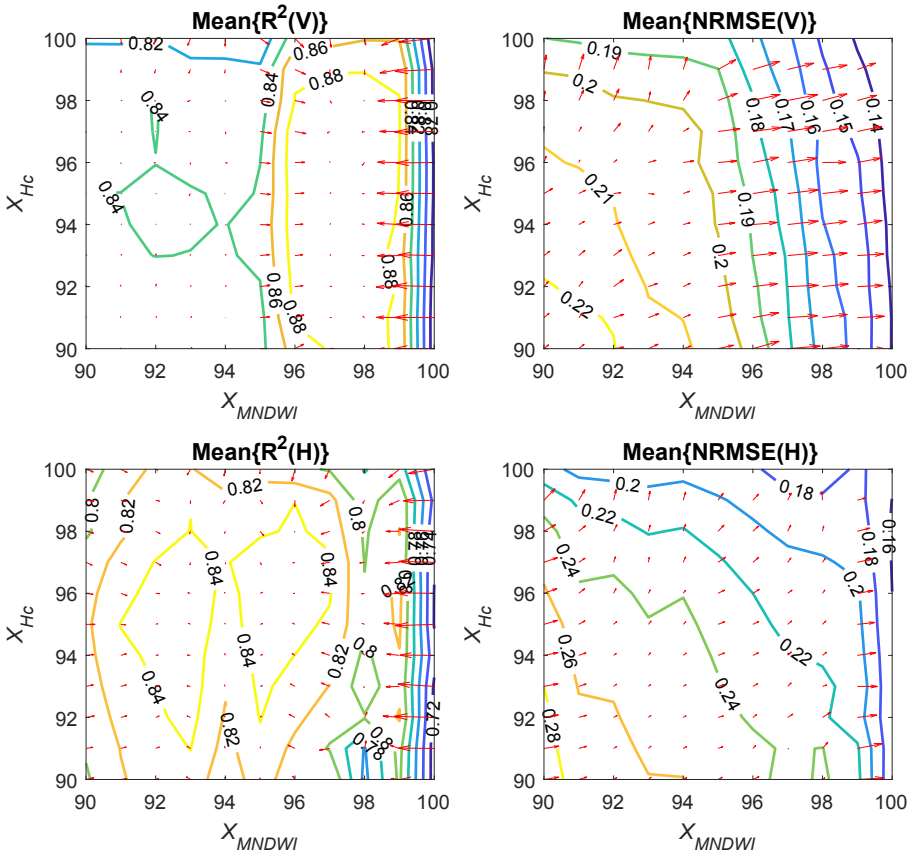

Figure 12. Sensitivity analysis of the two thresholds used to improve water body surface area estimates. Indices are averaged for all Jordanian reservoirs (except King Talal). Arrows point towards larger R^2, or lower NRMSE, and lengths are proportional to the gradient.

to statistically improve the detection of water bodies when clouds or "N/A" stripes hide land.

However, the H_c upper limit for the reconstruction has a decreasing impact on NRMSE as the MNDWI threshold increases: fewer missing water pixels lead to fewer pixels available to "fill with water" during the subsequent reconstruction. For lower X_{MNDWI} values, the decrease in NRMSE for high X_{H_c} values is clearer. It shows that the reconstruction algorithm addresses well the Fmask and dynamic threshold method limitations, even if it cannot entirely balance the errors. The fact that NRMSE is on average lower for maximal X_{H_c} values than for maximal X_{MNDWI} values could however be expected as the reconstruction relies on the reservoir's elevation–area relationship, which is established from the elevation of the pixels that are detected in the first stage.

In the end, the percentiles that we chose in this study – respectively 100 and 98 for X_{MNDWI} and X_{H_c} – enable a trade-off between the options of lowering NRMSE for both storage and elevation. Also, with these percentiles, R^2 is still sufficiently high to ensure a strong correlation. It should be noted that the thresholds do not depend on the location, nor the date on which the Landsat images were taken. Therefore, the sensitivity analysis reveals that the highest values for both X_{MNDWI} and X_{H_c} could be used to apply the method to any other region in the world.

4 Conclusions

Although information on small reservoirs' storage is crucial for water management in a river basin, it is most of the time not freely available in remote, ungauged, or conflict-torn areas. A remote sensing method is proposed in this paper to monitor small water bodies (capacities and water surface areas starting from 1 hm^3 and 0.5 km^2 respectively). The method is based only on DEMs for elevation, and Landsat satellite images for water surface area, to quantitatively estimate storage variations.

The method is applied to reservoirs in Syria and the Israel-controlled Golan Heights in the Yarmouk River basin, and an uncertainty analysis is conducted with neighbouring Jordan reservoirs for which in situ measurements are available. The NRMSE is relatively low compared to the size of the studied reservoirs and the precision of the datasets that are used.

The main limitation of the approach is its inapplicability to reservoirs that were significantly "covered" with water when the DEM satellites passed over them. Fortunately, this infor-

mation can be readily obtained from remote sensing data and used to determine the applicability of the method a priori.

For all "uncovered" small or large reservoirs, the uses of datasets available over the whole continental surface make this method a valuable complement to satellite altimetry to increase the number of reservoirs observable anywhere in the world. The thresholds dynamically defined for both the 2-D enhancement and the 3-D reconstruction also make the method potentially suitable to monitor reservoirs in truly inaccessible areas. Moreover, the precision of the filling curve and the 3-D reconstruction algorithm increases with the number of pixels taken into account. Applying the method to large "uncovered" reservoirs could then potentially lead to better results. The sensitivity analysis also shows that choosing maximum thresholds in both water area retrieval stages gives the best reservoir storage estimates.

The recent two Sentinel-2 satellites also promise a great improvement of the method for post-2015 studies, as they produce images with spatial and temporal resolutions finer than Landsat (up to 10 m and 5 days). Combining Landsat and Sentinel-2 satellites would then reduce the already short revisit cycle of water bodies and would provide near real-time updates on water body storage.

Furthermore, the algorithms used in the method automatically detect water bodies, define the water area retrieval parameters, build filling curves, and assess reservoir storage. Such algorithmic tools can then be dynamically updated with each new image from Sentinel-2 and Landsat satellites, giving the model the potential to learn by itself and correct previous storage estimates while generating new ones. This approach is somehow comparable to the continuous change detection proposed by Zhu and Woodcock (2014).

Code and data availability. The source code of the algorithm is available at https://drive.google.com/open?id=0B54cRCK06X-9RUdqaTZmWkdsOXc. Underlying research data are not publicly accessible. Remote sensing data access for this study is explained in Sect. 2. JVA data records are not publicly available.

Competing interests. The authors declare that they have no conflict of interest.

Acknowledgements. Jordanian reservoirs' monitoring data were provided by Jordan's Ministry of Water and Irrigation, and the Jordan Valley Authority. Landsat satellite images were obtained through the United States Geological Survey (USGS) EarthExplorer (https://earthexplorer.usgs.gov/). ASTER GDEM is a product of METI and NASA, and was found on EarthExplorer. SRTM (C-band) data were released by NASA, and are available at the US Geological Survey's EROS Data Center (https://eros.usgs.gov/). SRTM/X-SAR were operated by the German Aerospace Center (DLR) with participation of the Italian Space Agency (ASI), and obtained through EOWEB (http://eoweb.dlr.de:8080/index.html). This work was conducted as part of the Belmont Forum water security theme for which coordination was supported by the National Science Foundation under grant GEO/OAD-1342869 to Stanford University. Any opinions, findings, and conclusions or recommendations expressed in this material are those of the authors and do not necessarily reflect the views of the National Science Foundation. The authors acknowledge the financial support of NSERC through grant G8PJ-437384-2012. The authors also thank T. Francke, W. Gumindoga and an anonymous referee for their constructive comments and suggestions.

Edited by: Dominic Mazvimavi
Reviewed by: Webster Gumindoga and one anonymous referee

References

Alsdorf, D. E., Rodríguez, E., and Lettenmaier, D. P.: Measuring surface water from space, Rev. Geophys., 45, rG2002, https://doi.org/10.1029/2006RG000197, 2007.

Amitrano, D., Martino, G. D., Iodice, A., Mitidieri, F., Papa, M. N., Riccio, D., and Ruello, G.: Sentinel-1 for Monitoring Reservoirs: A Performance Analysis, Remote Sensing, 6, 10676–10693, https://doi.org/10.3390/rs61110676, 2014.

Annor, F., van de Giesen, N., Liebe, J., van de Zaag, P., Tilmant, A., and Odai, S.: Delineation of small reservoirs using radar imagery in a semi-arid environment: A case study in the upper east region of Ghana, Phys. Chem. Earth Pt. A/B/C, 34, 309–315, https://doi.org/10.1016/j.pce.2008.08.005, 2009.

Arsen, A., Crétaux, J.-F., Berge-Nguyen, M., and del Rio, R. A.: Remote Sensing-Derived Bathymetry of Lake Poopó, Remote Sensing, 6, 407–420, https://doi.org/10.3390/rs6010407, 2014.

ASTER GDEM Validation Team: ASTER Global Digital Elevation Model Version 2 – Summary of Validation Results, Tech. rep., NASA LPDAAC-Japan-US ASTER Science Team, https://lpdaacaster.cr.usgs.gov/GDEM/Summary_GDEM2_validation_report_final.pdf (last access: 13 December 2017), 2011.

Birkett, C. M.: The contribution of TOPEX/POSEIDON to the global monitoring of climatically sensitive lakes, J. Geophys. Res.-Oceans, 100, 25179–25204, https://doi.org/10.1029/95JC02125, 1995.

Birkett, C. M. and Beckley, B.: Investigating the Performance of the Jason-2/OSTM Radar Altimeter over Lakes and Reservoirs, Mar. Geodesy, 33, 204–238, https://doi.org/10.1080/01490419.2010.488983, 2010.

Calmant, S., Seyler, F., and Crétaux, J. F.: Monitoring Continental Surface Waters by Satellite Altimetry, Surv. Geophys., 29, 247–269, https://doi.org/10.1007/s10712-008-9051-1, 2008.

Chavez, P.: Image-based atmospheric corrections revisited and improved, Photogram. Eng. Remote Sens., 62, 1025–1036, 1996.

Coltin, B., McMichael, S., Smith, T., and Fong, T.: Automatic boosted flood mapping from satellite data, Int. J. Remote Sens., 37, 993–1015, https://doi.org/10.1080/01431161.2016.1145366, 2016.

Crétaux, J.-F. and Birkett, C.: Lake studies from satellite radar altimetry, Comptes Rendus Geoscience, 338, 1098–1112, https://doi.org/10.1016/j.crte.2006.08.002, 2006.

Crétaux, J.-F., Biancamaria, S., Arsen, A., Bergé-Nguyen, M., and Becker, M.: Global surveys of reservoirs and lakes from satellites and regional application to the Syrdarya river basin, Environ. Res. Lett., 10, 015002, https://doi.org/10.1088/1748-9326/10/1/015002, 2015.

Crétaux, J.-F., Abarca-del Río, R., Bergé-Nguyen, M., Arsen, A., Drolon, V., Clos, G., and Maisongrande, P.: Lake Volume Monitoring from Space, Surv. Geophys., 37, 269–305, https://doi.org/10.1007/s10712-016-9362-6, 2016.

Döll, P., Fiedler, K., and Zhang, J.: Global-scale analysis of river flow alterations due to water withdrawals and reservoirs, Hydrol. Earth Syst. Sci., 13, 2413–2432, https://doi.org/10.5194/hess-13-2413-2009, 2009.

Dombrowsky, I.: Conflict, cooperation and institutions in international water management: An economic approach, Edward Elgar Publishing, Cheltenham, 2007.

Donlon, C., Berruti, B., Buongiorno, A., Ferreira, M.-H., Féménias, P., Frerick, J., Goryl, P., Klein, U., Laur, H., Mavrocordatos, C., Nieke, J., Rebhan, H., Seitz, B., Stroede, J., and Sciarra, R.: The Global Monitoring for Environment and Security (GMES) Sentinel-3 mission, Remote Sens. Environ., 120, 37–57, https://doi.org/10.1016/j.rse.2011.07.024, 2012.

Duan, Z. and Bastiaanssen, W.: Estimating water volume variations in lakes and reservoirs from four operational satellite altimetry databases and satellite imagery data, Remote Sens. Environ., 134, 403–416, https://doi.org/10.1016/j.rse.2013.03.010, 2013.

Eilander, D., Annor, F. O., Iannini, L., and van de Giesen, N.: Remotely Sensed Monitoring of Small Reservoir Dynamics: A Bayesian Approach, Remote Sensing, 6, 1191, https://doi.org/10.3390/rs6021191, 2014.

European Space Agency: Sentinel-2 Mission Details, available at: https://earth.esa.int/web/guest/missions/esa-operational-eo-missions/sentinel-2 (last access: 15 October 2017), 2013.

Frappart, F., Minh, K. D., L'Hermitte, J., Cazenave, A., Ramillien, G., Le Toan, T., and Mognard-Campbell, N.: Water volume change in the lower Mekong from satellite altimetry and imagery data, Geophys. J. Int., 167, 570–584, https://doi.org/10.1111/j.1365-246X.2006.03184.x, 2006.

Gao, H., Birkett, C., and Lettenmaier, D. P.: Global monitoring of large reservoir storage from satellite remote sensing, Water Resour. Res., 48, w09504, https://doi.org/10.1029/2012WR012063, 2012.

German Aerospace Center (DLR): SRTM Products, available at: http://www.dlr.de/eoc/en/Portaldata/60/Resources/dokumente/7_sat_miss/srtm_products_en.pdf, last access: 11 January 2017.

Hanasaki, N., Kanae, S., and Oki, T.: A reservoir operation scheme for global river routing models, J. Hydrol., 327, 22–41, https://doi.org/10.1016/j.jhydrol.2005.11.011, 2006.

International Commission On Large Dams: Register of dams, available at: http://www.icold-cigb.org/GB/World_register/data_base_presentation.asp, last access: 24 November 2016.

Islam, A., Bala, S., and Haque, M.: Flood inundation map of Bangladesh using MODIS time-series images, J. Flood Risk Manage., 3, 210–222, https://doi.org/10.1111/j.1753-318X.2010.01074.x, 2010.

Ji, L., Zhang, L., and Wylie, B.: Analysis of Dynamic Thresholds for the Normalized Difference Water Index, Photogram. Eng. Remote Sens., 75, 1307–1317, https://doi.org/10.14358/PERS.75.11.1307, 2009.

Leemhuis, C., Jung, G., Kasei, R., and Liebe, J.: The Volta Basin Water Allocation System: assessing the impact of small-scale reservoir development on the water resources of the Volta basin, West Africa, Adv. Geosci., 21, 57–62, https://doi.org/10.5194/adgeo-21-57-2009, 2009.

LeFavour, G. and Alsdorf, D.: Water slope and discharge in the Amazon River estimated using the shuttle radar topography mission digital elevation model, Geophys. Res. Lett., 32, L17404, https://doi.org/10.1029/2005GL023836, 2005.

Lehner, B., Liermann, C. R., Revenga, C., Vörösmarty, C., Fekete, B., Crouzet, P., Döll, P., Endejan, M., Frenken, K., Magome, J., Nilsson, C., Robertson, J. C., Rödel, R., Sindorf, N., and Wisser, D.: High-resolution mapping of the world's reservoirs and dams for sustainable river-flow management, Front. Ecol. Environ., 9, 494–502, https://doi.org/10.1890/100125, 2011.

Liebe, J. R., van de Giesen, N., and Andreini, M.: Estimation of small reservoir storage capacities in a semi-arid environment: A case study in the Upper East Region of Ghana, Phys. Chem. Earth Pt. A/B/C, 30, 448–454, https://doi.org/10.1016/j.pce.2005.06.011, 2005.

Liebe, J. R., van de Giesen, N., Andreini, M., Walter, M. T., and Steenhuis, T. S.: Determining watershed response in data poor environments with remotely sensed small reservoirs as runoff gauges, Water Resour. Res., 45, w07410, https://doi.org/10.1029/2008WR007369, 2009.

Liu, Y., Song, P., Peng, J., and Ye, C.: A physical explanation of the variation in threshold for delineating terrestrial water surfaces from multi-temporal images: effects of radiometric correction, Int. J. Remote Sens., 33, 5862–5875, https://doi.org/10.1080/01431161.2012.675452, 2012.

Mercier, F., Cazenave, A., and Maheu, C.: Interannual lake level fluctuations (1993–1999) in Africa from Topex/Poseidon: connections with ocean-atmosphere interactions over the Indian Ocean, Global Planet. Change, 32, 141–163, https://doi.org/10.1016/S0921-8181(01)00139-4, 2002.

Morris, C. S. and Gill, S. K.: Variation of Great Lakes water levels derived from Geosat altimetry, Water Resour. Res., 30, 1009–1017, https://doi.org/10.1029/94WR00064, 1994.

Müller, M. F., Yoon, J., Gorelick, S. M., Avisse, N., and Tilmant, A.: Impact of the Syrian refugee crisis on land use and transboundary freshwater resources, P. Natl. Acad. Sci. USA, 113, 14932–14937, https://doi.org/10.1073/pnas.1614342113, 2016.

Ponchaut, F. and Cazenave, A.: Continental lake level variations from Topex/Poseidon (1993–1996), Comptes Rendus de l'Académie des Sciences – Series IIA – Earth and Planetary Science, 326, 13–20, https://doi.org/10.1016/S1251-8050(97)83198-9, 1998.

Rodrigues, L. N., Sano, E. E., Steenhuis, T. S., and Passo, D. P.: Estimation of Small Reservoir Storage Capacities with Remote Sensing in the Brazilian Savannah Region, Water Resour. Manage., 26, 873–882, https://doi.org/10.1007/s11269-011-9941-8, 2012.

Rodriguez, E., Morris, C., Belz, J., Chapin, E., Martin, J., Daffer, W., and Hensley, S.: An assessment of the SRTM topographic products, Technical Report JPL D-31639, Jet Propulsion Laboratory, Pasadena, California, 2005.

Sawunyama, T., Senzanje, A., and Mhizha, A.: Estimation of small reservoir storage capacities in Limpopo River Basin using geographical information systems (GIS) and remotely sensed surface areas: Case of Mzingwane catchment, Phys. Chem. Earth Pt. A/B/C, 31, 935–943, https://doi.org/10.1016/j.pce.2006.08.008, 2006.

Solander, K. C., Reager, J. T., and Famiglietti, J. S.: How well will the Surface Water and Ocean Topography (SWOT) mission observe global reservoirs?, Water Resour. Res., 52, 2123–2140, https://doi.org/10.1002/2015WR017952, 2016.

Song, C., Huang, B., and Ke, L.: Modeling and analysis of lake water storage changes on the Tibetan Plateau using multi-mission satellite data, Remote Sens. Environ., 135, 25–35, https://doi.org/10.1016/j.rse.2013.03.013, 2013.

Vörösmarty, C. J., Sharma, K. P., Fekete, B. M., Copeland, A. H., Holden, J., Marble, J., and Lough, J. A.: The Storage and Aging of Continental Runoff in Large Reservoir Systems of the World, Ambio, 26, 210–219, 1997.

Wang, X., Gong, P., Zhao, Y., Xu, Y., Cheng, X., Niu, Z., Luo, Z., Huang, H., Sun, F., and Li, X.: Water-level changes in China's large lakes determined from ICESat/GLAS data, Remote Sens. Environ., 132, 131–144, 2013.

Wang, Y., Liao, M., Sun, G., and Gong, J.: Analysis of the water volume, length, total area and inundated area of the Three Gorges Reservoir, China using the SRTM DEM data, Int. J. Remote Sens., 26, 4001–4012, https://doi.org/10.1080/01431160500176788, 2005.

Wang, Y., Sun, G., Liao, M., and Gong, J.: Using MODIS images to examine the surface extents and variations derived from the DEM and laser altimeter data in the Danjiangkou Reservoir, China, Int. J. Remote Sens., 29, 293–311, https://doi.org/10.1080/01431160701253311, 2008.

Xiao, X., Boles, S., Frolking, S., Li, C., Babu, J. Y., Salas, W., and Moore, B.: Mapping paddy rice agriculture in South and Southeast Asia using multi-temporal MODIS images, Remote Sens. Environ., 100, 95–113, https://doi.org/10.1016/j.rse.2005.10.004, 2006.

Xu, H.: Modification of normalised difference water index (NDWI) to enhance open water features in remotely sensed imagery, Int. J. Remote Sens., 27, 3025–3033, https://doi.org/10.1080/01431160600589179, 2006.

Yan, Y.-E., Ouyang, Z.-T., Guo, H.-Q., Jin, S.-S., and Zhao, B.: Detecting the spatiotemporal changes of tidal flood in the estuarine wetland by using MODIS time series data, J. Hydrol., 384, 156–163, https://doi.org/10.1016/j.jhydrol.2010.01.019, 2010.

Yang, X., Zhao, S., Qin, X., Zhao, N., and Liang, L.: Mapping of Urban Surface Water Bodies from Sentinel-2 MSI Imagery at 10 m Resolution via NDWI-Based Image Sharpening, Remote Sensing, 9, 596, https://doi.org/10.3390/rs9060596, 2017.

Yoon, Y. and Beighley, E.: Simulating streamflow on regulated rivers using characteristic reservoir storage patterns derived from synthetic remote sensing data, Hydrol. Process., 29, 2014–2026, https://doi.org/10.1002/hyp.10342, 2015.

Zhang, G., Xie, H., Kang, S., Yi, D., and Ackley, S. F.: Monitoring lake level changes on the Tibetan Plateau using ICESat altimetry data (2003–2009), Remote Sens. Environ., 115, 1733–1742, https://doi.org/10.1016/j.rse.2011.03.005, 2011.

Zhang, H., Gorelick, S. M., Avisse, N., Tilmant, A., Rajsekhar, D., and Yoon, J.: A New Temperature-Vegetation Triangle Algorithm with Variable Edges (TAVE) for Satellite-Based Actual Evapotranspiration Estimation, Remote Sensing, 8, 735, https://doi.org/10.3390/rs8090735, 2016.

Zhang, S., Gao, H., and Naz, B. S.: Monitoring reservoir storage in South Asia from multisatellite remote sensing, Water Resour. Res., 50, 8927–8943, https://doi.org/10.1002/2014WR015829, 2014.

Zhu, Z. and Woodcock, C. E.: Object-based cloud and cloud shadow detection in Landsat imagery, Remote Sens. Environ., 118, 83–94, https://doi.org/10.1016/j.rse.2011.10.028, 2012.

Zhu, Z. and Woodcock, C. E.: Continuous change detection and classification of land cover using all available Landsat data, Remote Sens. Environ., 144, 152–171, https://doi.org/10.1016/j.rse.2014.01.011, 2014.

Zhu, Z., Wang, S., and Woodcock, C. E.: Improvement and expansion of the Fmask algorithm: cloud, cloud shadow, and snow detection for Landsats 4-7, 8, and Sentinel 2 images, Remote Sens. Environ., 159, 269–277, https://doi.org/10.1016/j.rse.2014.12.014, 2015.

Zwally, H., Schutz, B., Abdalati, W., Abshire, J., Bentley, C., Brenner, A., Bufton, J., Dezio, J., Hancock, D., Harding, D., Herring, T., Minster, B., Quinn, K., Palm, S., Spinhirne, J., and Thomas, R.: ICESat's laser measurements of polar ice, atmosphere, ocean, and land, J. Geodynam., 34, 405–445, https://doi.org/10.1016/S0264-3707(02)00042-X, 2002.

Appendix B

Quantitative analysis of contested water uses and management in the conflict-torn Yarmouk basin

Résumé

Le bassin versant du Yarmouk est partagé entre la Syrie, la Jordanie et Israël. Depuis le début de son développement dans les années 1960, le débit de la rivière Yarmouk a diminué de plus de 85% malgré la signature d'accords de gestion bilatéraux. La Syrie et la Jordanie se rejettent la responsabilité du déclin de la rivière et ont toutes deux développé leur propre récit explicatif : la Jordanie considère que la Syrie a violé leur accord de 1987 en construisant plus de barrages que ce qui était convenu, tandis que la Syrie rejette la faute sur le changement climatique. De fait, il est de plus en plus difficile de faire la distinction entre des facteurs naturels et des facteurs anthropiques à la source d'un changement de régime hydrologique, puisque les deux pays ne partagent aucune information, que ce soit sur les débits hydrologiques ou sur leur propre gestion des resources en eau. Nous utilisons la télédétection et la simulation multi-agents pour montrer que le récit de chaque pays est partiellement valide, mais qu'aucun des deux récits n'explique pleinement la diminution du débit du Yarmouk. Nos résultats révèlent que l'extraction des eaux souterraines par les agriculteurs syriens dans les hautes terres a considérablement diminué les débit de base et débit total de la rivière. En utilisant l'analyse de scénarios, nous montrons également que l'abandon et la destruction de barrages syriens après le début de la guerre civile en 2011 a conduit à une augmentation de 87% du débit. D'autres scénarios se tournent vers une période d'après-guerre future et suggèrent des rôles que les pays transfrontaliers pourraient avoir dans les efforts de reconstruction. La télédétection et la simulation multi-agents offrent des possibilités pour analyser quantitativement des bassins versants lorsque les États ne partagent pas d'information et il est très difficile de collecter des données terrain.

Quantitative analysis of contested water uses and management in the conflict-torn Yarmouk basin

Nicolas Avisse[a,1], **Amaury Tilmant**[a], **David Rosenberg**[b], **and Samer Talozi**[c]

[a]Department of Civil Engineering and Water Engineering, Université Laval, Québec, QC G1V 0A6, Canada; [b]Department of Civil & Environmental Engineering, Utah State University, Logan, UT 84322, USA; [c]Civil Engineering Department, Jordan University of Science and Technology, Irbid 22110, Jordan

This manuscript was compiled on February 15, 2018

The Yarmouk River basin is shared between Syria, Jordan, and Israel. Since its development started in the 1960s, Yarmouk River flows have declined more than 85% despite the signature of bilateral management agreements. Syria and Jordan blame each other for the decline and have both developed their own explanatory narratives: Jordan considers that Syria violated their 1987 agreement by building more dams than what was agreed on, while Syria blames climate change. In fact, it is increasingly difficult to distinguish between natural and anthropogenic factors that affect the flow regime as the two countries do not share information, on either hydrological flows or water management. We use remote sensing and multi-agent simulation to show that each country's narrative is partially valid, but that neither narrative fully explains the decrease in Yarmouk River flows. Our results reveal that groundwater extraction by Syrian farmers in highland areas has dramatically decreased base flows and total Yarmouk flows. Using scenario analysis, we additionally show that the disuse and destruction of Syrian dams since the 2011 start of the Syrian civil war led to an 87% flow increase. Subsequent scenarios look to a future post-war period and suggest roles that basin states can play in recovery efforts. The remote sensing and multi-agent simulation offer opportunities to quantitatively analyze river basins where the basin states do not share information and it is very difficult to collect on-the-ground field data.

remote sensing | Syria | transboundary waters | river basin closure

The Yarmouk River basin (YRB) is shared by three countries: Syria, Jordan, and Israel (Fig. 1). Since the 1960s, development in the basin has increased and the historical annual flow of 450–500 $hm^3 \cdot y^{-1}$ (million cubic meter per year; 1–4) has dropped by more than 85% to reach 60 $hm^3 \cdot y^{-1}$ in 2010. In 2013, flow rose to 120 $hm^3 \cdot y^{-1}$ with the Syrian civil war (Fig. 2).

The collapse of the Yarmouk flow occurred despite the signature of two bilateral agreements. The first one was signed in 1953 between Jordan and Syria (7), and updated in 1987 (5) essentially to recognize water uses and dams already built in Syria (8, 9). The 1987 version gives the right to Syria to retain water in 28 dams on the Yarmouk basin for a cumulated capacity of 164.64 hm^3, and allows Jordan to use water in the Wahda reservoir (a major reservoir that had yet to be built on the Yarmouk River; see Fig. 1) to irrigate crops in the Jordan Valley along the King Abdullah Canal (KAC) and to supply Amman with freshwater. No explicit limitation regarding groundwater withdrawals is mentioned in the document. The second agreement is the Treaty of Peace signed in 1994 between Jordan and Israel (10), which gives the two countries specific water rights on the Yarmouk waters: (*i*) Israel is entitled to a 25 hm^3 annual *allocation* while Jordan gets the rest of the flow; and (*ii*) Jordan has the possibility to store up to 20 hm^3 each year in Lake Tiberias during the Winter Period, and get it back at the entrance of the KAC in the Summer Period (*concession*). Technically, the sharing of water is operated at Adasiya (outlet of the YRB; see Fig. 1).

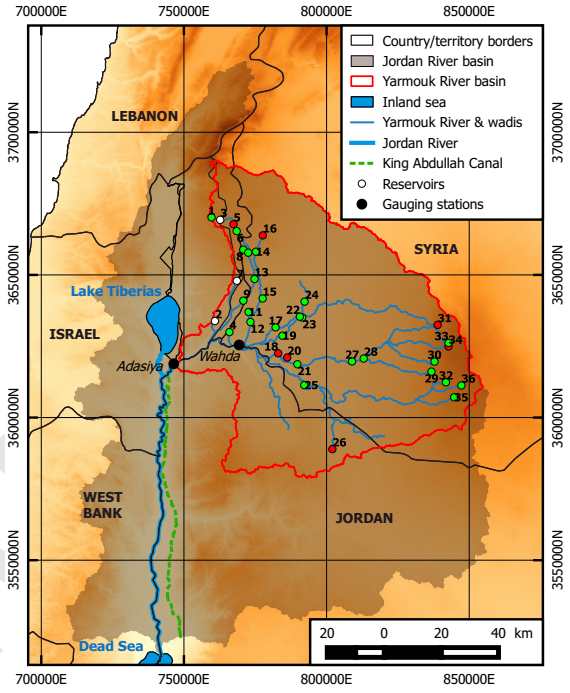

Fig. 1. The Yarmouk River basin as part of the Jordan River basin, with reservoirs other than Wahda detected using remote sensing – colors refer to the inclusion in the 1987 bilateral agreement between Syria and Jordan (5); see Fig. S6. All coordinates are expressed in the Coordinate Reference System (CRS) WGS 84/UTM zone 36N (EPSG:32636), in which 1 unit equals 1 m.

After considering surface water flow depletion caused by the Syrian reservoirs listed in the 1987 agreement, reduced groundwater triggered by irrigation from springs and projected wells in Syria, and irrigation return flows, the Jordanian Ministry of Water and Irrigation/Jordan Valley Authority (MWI/JVA; 11) expected inflows to the Wahda dam to attain 117.6 $hm^3 \cdot y^{-1}$. Yet, the flow monitored by MWI/JVA has never reached such a level before the Syrian civil war, and Jordan has been the first affected by the river decline due to (*i*) its downstream position as most springs and wadis (intermittent rivers) feeding the Yarmouk are located in Syria and the Israel-controlled Golan Heights, and (*ii*) the fact that it bears the brunt of the hydrological risk as per the Israel–Jordan Treaty (no matter the flow reaching Wahda, Jordan has to send the 25 $hm^3 \cdot y^{-1}$ *allocation* to Israel).

Jordan and Syria have both developed their own, competing, narratives to explain the decrease in Yarmouk flows: downstream Jordan considers that Syria violated their 1987

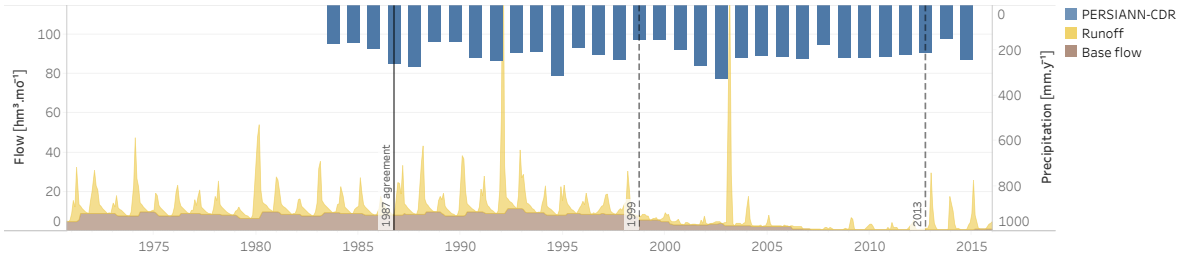

Fig. 2. Yarmouk River flow – expressed in terms of base flow (moving minimum) and runoff – measured at the station of the Wahda dam by the Jordanian Ministry of Water and Irrigation, and the Jordan Valley Authority; and PERSIANN-CDR precipitation upstream from that station. In situ measurements of the Yarmouk River flow at the Wahda dam, or Maqarin station before the dam's construction, and Adasiya (depicted in Fig. 1) are the only ground data available in the basin. For years following the 1960s, three stages can clearly be noticed: (i) a stationary regime before 1999; (ii) a sharp decrease of both the base flow and the runoff during the period 1999–2012; and (iii) the return of the runoff from 2013, when many Syrian refugees fled the civil war (6).

bilateral agreement by building more dams than what was agreed on, while upstream Syria blames climate change and particularly precipitation decrease (9). Each perspective is fostered by a few studies. Regarding the Syrian narrative, Salameh and Bannayan (2) estimate that rainfall dropped by 30% in the second half of the 20th century. Moreover, after comparing two periods, 1927–1954 versus 1968–1987, Beaumont (12) comes to the conclusion that natural runoff were, on average, 25% lower in the second period. The fact that three of the four most severe multi-year droughts in the region since 1901 occurred after 1990 is also attributed to climate change (13). Other analyses overlook such natural aspects and rather adopt the Jordanian narrative considering that the Yarmouk depleted because of excessive water abstractions and uncoordinated construction of dams in the Syrian part of the YRB (14, 15).

Work to clarify the causes of the flow decrease has become much more difficult since the start of the civil war in Syria. To the best of our knowledge, the study conducted by Al-Bakri (16) on the Jordanian part of the YRB is the only analysis that provides local information on land use and water withdrawals. However, detailed information on reservoir operation, canal diversions, irrigation requirements, and groundwater withdrawals is crucial to identify with precision the causes to flow regime changes, and to distinguish consistent study results from politically biased narratives.

We couple remote sensing and multi-agent simulation (MAS) to apply and validate the modeling approach in a river basin (the Yarmouk) where one country (Syria) is experiencing a civil war and limited ground data is available for use. We further use the validated model to test competing hypotheses and country narratives about the causes of a 60-year decline in stream flows, as well as possible future trajectories for flows after the civil war winds down. Results show the Yarmouk discharges decreased because of excessive groundwater withdrawals and declining precipitation, and suggest roles the riparian countries can play in post-war recovery efforts.

Significance Statement

For decades, it has been difficult for policy makers to independently understand and quantify the causes of hydrological changes in complex, non-cooperatively managed river basins with expanding water use, infrastructure, uncertain climate changes, and where it is difficult to collect on-the-ground data. In the Yarmouk basin, for example, which is shared between Syria, Jordan, and Israel, the annual outflow now corresponds to less than 15% of the pre-development era flow. The riparian countries have developed their own, contested, narratives to explain the decline of Yarmouk flows. This study uses remote sensing, multi-agent simulation, and scenario analysis to quantify the contributions of natural and anthropogenic factors to the decline of river discharges.

N.A. and A.T. designed research; N.A. performed research; N.A., A.T. and D.R. analyzed data; and N.A., A.T., D.R., and S.T. wrote the paper.

The authors declare no conflict of interest.

[1]To whom correspondence should be addressed. E-mail: nicolas.avisse@gmail.com and amaury.tilmant@gci.ulaval.ca

Basis for the Contested Political Narratives

Precipitation Decline. We measure an average PERSIANN-CDR (Precipitation Estimation from Remotely Sensed Information using Artificial Neural Networks - Climate Data Record; see *Materials and Methods*) precipitation for 1983–2015 over the YRB of 239 mm·y^{-1} – i.e. 64% of the 372 mm·y^{-1} estimated by Salameh and Bannayan for the pre-development stage (2). The decline is consistent with the 30% rainfall drop for the second half of the 20th century compared to the pre-development period considered by the same authors.

Unilateral Storage Development. Using a remote sensing method developed by Avisse et al. (17, see *Materials and Methods*), we detect 37 reservoirs in the YRB (Fig. 1): 25 are Syrian and listed in the agreement between Syria and Jordan (5), 1 is listed in the agreement but under Israeli control in the Golan Heights, 1 is the Wahda dam, and the remaining 10 have been unilaterally built in the basin. These last 10 dams have a cumulated storage capacity of 34.5 hm^3 in Syria, less than 0.1 hm^3 in Jordan, and 2.9 hm^3 in the Israel-occupied Golan Heights (Fig. S6). Many detected reservoirs are very small as they are found to have not stored more than 1 hm^3 in 30 years. 2 dams among the 28 listed in the agreement are not detected because they are too small or rarely filled with water. As a trade-off between representing the entire multi-reservoir system of the YRB, and taking into account dams that can significantly affect the Yarmouk River flow, only reservoirs with a capacity larger than 1 hm^3 are considered in the multi-agent model (Table S2).

The evolution of cumulated storage capacity and cumulated water stored in reservoirs of the YRB (except Wahda; see

Supporting Information) is presented in Fig. 3. These results enable us to do a first qualitative analysis of the impact of the construction of dams on the discharge observed downstream (Fig. 2). It is particularly interesting to notice that the pre-1995 growth of the cumulated storage capacity does not seem to have affected the hydrological regime of the river during the same period of time. However, precipitation data for years between the pre-development phase (pre-1960s) and 1983 is missing to consistently conclude on the impact of the new dams, as rainfall seems to have strongly varied during this period. On the contrary, while the cumulated storage capacity remained the same between 1999 and 2006, the runoff declined and the filling of the reservoirs was affected. The reasons behind these changes should then be found in the late 1990s multi-year drought (13) and/or in increasing water withdrawals for irrigation purpose (18). The consecutive low Yarmouk River flow and low reservoir water storage coincide with the 2007–2008 drought. Higher precipitation in the subsequent years (period 2009–2012), though, did not materialize in higher discharges downstream, as more water has been stored in the reservoirs. Finally, it seems clear that the disuse of many reservoirs in 2013, after the Syrian civil war started, led to less water stored in the YRB and to larger runoff discharges during the following years.

Causes of the Yarmouk River Flow Past Changes

We build a remote sensing-based PyNSim MAS model of the YRB (19, see *Materials and Methods*). PyNSim modeling infrastructure adopts an arc-node representation of the water resources system while enabling multi-level institutional arrangements. Base flow and runoff are distinguished in the modeling – the base flow corresponds to the groundwater flow reaching Wahda and Adasiya directly, and depends on groundwater withdrawals, irrigation return flows, and infiltration inside the wadis (see *Supporting Information*). Our model is first validated by comparing modeled and observed flows over 1983–2015 (period covered by PERSIANN-CDR data): we obtain high Kling-Gupta efficiencies (KGE' of 0.64 and 0.90 at Wahda and Adasiya respectively; see *Supporting Information* and Fig. S8). Different scenarios representing alternative theories (either narratives from the riparian countries, or complementary ideas that have yet to be fully explored) regarding the hydrological changes in the YRB are then designed and assessed using the PyNSim MAS model. The goal is to test the validity of these theories and to identify impacts on Jordan and Israel, considering water diversions downstream from the YRB as per the 1994 Treaty of Peace.

The five scenarios analyzed in this paper are:

No precipitation decline A higher precipitation is considered to produce the 422 $hm^3 \cdot y^{-1}$ natural flow at Adasiya that was expected by Jordan in the feasibility study of the Wahda dam (11). This scenario addresses the Syrian narrative.

Listed dams only Only dams listed in the Syria–Jordan agreement (i.e. all dams except Qunaitera and Avnei Eitan al-Golan; see Table S2) are modeled. This scenario addresses the Jordanian narrative.

No groundwater pumping development Crop water requirements in areas located far from reservoirs remain unchanged after the signature of the agreement between Syria and Jordan in 1987. This scenario addresses Syrian groundwater pumping ignored by the 1953 and 1987 Jordan–Syria agreements.

All dams active 2013–present All dams continue to operate in 2011 as in prior years. This scenario assumes conditions continue as though the Syrian civil war did not occur.

Aggregate effects Combination of the four prior scenarios with increased precipitation, only dams listed in the Syrian-Jordanian agreement, no groundwater development, and continued operation of the dams after 2011.

Impact on the Yarmouk River Flow. The analysis focuses on the inflow into the Wahda reservoir because (*i*) most dams and irrigated crops in the YRB are located upstream from that reservoir (Fig. S6), and (*ii*) the flow at Adasiya is strongly influenced by the operation of that reservoir.

Results are presented in Fig. 4*A*, with the simulated *historical* flow for comparison. It is particularly interesting to notice that the base flow still sharply decreases in 1999 with the *no precipitation decline* and *listed dams only* scenarios. It means that neither the reduced precipitation nor the unlisted dams caused that major hydrological change. On the contrary, the stationary base flow after 1999 with the *no groundwater development* scenario confirms that the growth of groundwater abstractions strongly impacted the base flow (groundwater-irrigated area rose from 49% in 1985 to 58% in 2000 in Syria as farmers could get low interest loans, well licenses were more easily delivered, and fuel was strongly subsidized; 20, 21). If groundwater pumping had not developed since 1987, the groundwater table would have remained at the same level and the base flow would not have been affected.

The difference between the annual flow for each scenario and the simulated *historical* flow is presented in Fig. 4*B*. This figure shows the impact of each scenario on the Yarmouk discharge. Until 1999, our simulations show that anthropogenic activity had little or no effect on the Yarmouk River flows. The main difference between the *historical* and *aggregate effects* flows lies in the precipitation decline. From 2000 onwards, however, the impact of human activities through large groundwater withdrawals is again particularly clear as the gap between the simulated *historical* and *no groundwater development* scenarios keeps increasing until the base flow completely disappears in 2006. In 2013, our modeling shows that the destruction/disuse of Syrian dams led to an increase of the runoff by 25.7 $hm^3 \cdot y^{-1}$ (i.e. +87%) on average over the period 2013–2015. This value is consistent with the ∼25 $hm^3 \cdot y^{-1}$ estimate from Müller et al. (6). It must be stressed that this sudden increase did not alleviate water scarcity in Jordan though, as more than 500,000 Syrian refugees entered the country during the same period of time (22). The simulation of the *listed dams only* scenario finally reveals that the impact of the unilateral construction of dams by Syria and Israel is marginal over the whole 1983–2015 historical period.

Moreover, provided that groundwater abstractions had remained at the 1987 level, Jordan would still have received a discharge close to the 117.6 $hm^3 \cdot y^{-1}$ that it expected to fill the Wahda reservoir (see *Introduction*). Indeed, with the simulation of the *no groundwater pumping development* scenario, the modeled flow reaching Wahda during the period 2006–2012 remains close to 100 $hm^3 \cdot y^{-1}$ higher than the ∼15 $hm^3 \cdot y^{-1}$

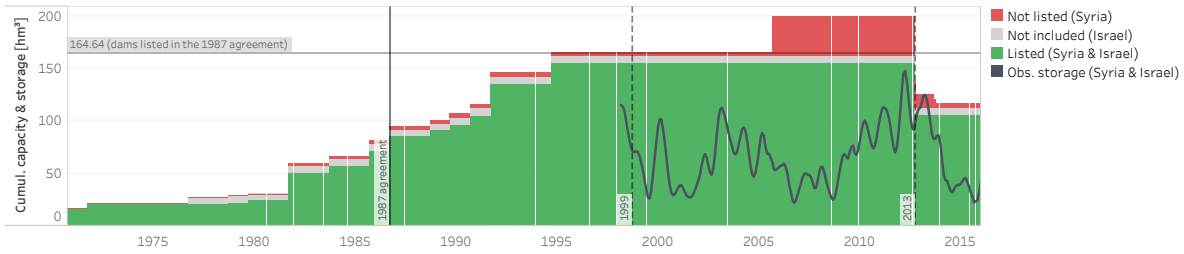

Fig. 3. Cumulated storage capacity and variations in Syria and the Israel-occupied Golan Heights. Capacities are sorted in terms of their inclusion in the Syria–Jordan agreement (5). Color codes for capacity categories are the same as in Fig. 1 and S6.

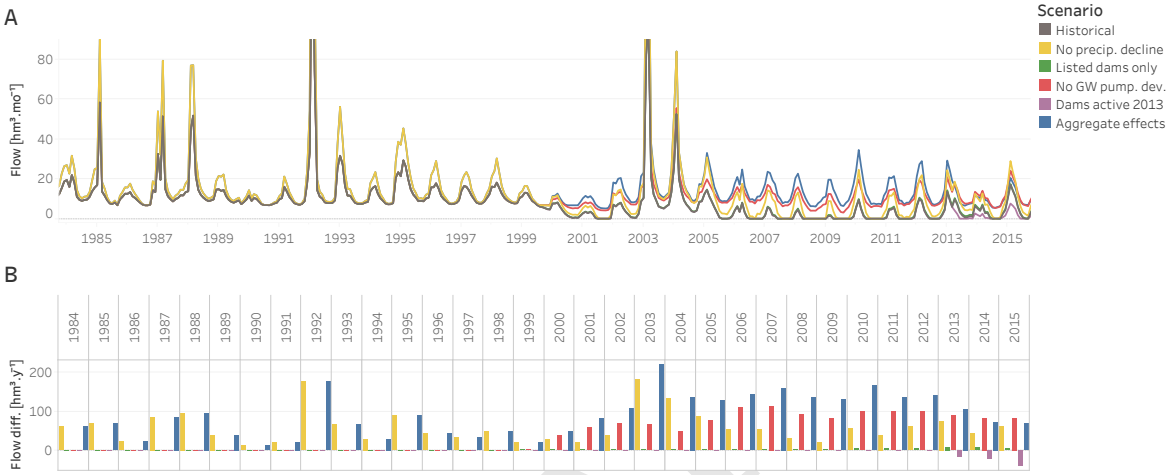

Fig. 4. (*A*) Simulation results at the Wahda dam location for the proposed scenarios, and (*B*) water year flow difference with the historical run.

measured by MWI/JVA during this period (Fig. 2). In other words, neither the uncoordinated construction of upstream reservoirs nor the significant decline in precipitation would yield, on average, less than 115 $hm^3 \cdot y^{-1}$ at the Wahda dam.

Consequences on the Water Transfers as per the 1994 Treaty of Peace. This section focuses on the effects that past hydrological changes and human development/management policies have had on the sharing of the flows at Adasiya as per the Jordanian–Israeli treaty (see *Introduction*). The analysis is conducted over the post-treaty period (1994–2015). All scenarios defined in the previous section are considered but the *all dams active* one since it only affects the Yarmouk flows after 2013. Results are presented in Table 1: (*i*) the flows eventually available for Jordan (through the KAC after the *concession* is sent back by Israel), (*ii*) the flows eventually available for Israel (share pumped to Lake Tiberias and remaining after the *concession* is sent back to Jordan), and (*iii*) the flows eventually available for the Jordan River (overflow from Yarmoukeem Pool). More information on these diversion systems is available in *Supporting Information* and Fig. S7.

Increased groundwater abstractions most affected Jordan and Israel (+23.6 and +42.9% respectively). By looking at average flows, we can also notice that Jordan would have received more additional water than Israel with any scenario. This assessment is consistent with the water rights' definition in the Treaty of Peace (see *Introduction*): Jordan bears the brunt of the hydrological risk and is therefore the first affected by the change in the flow regime. As for the uncoordinated construction of dams, Jordan is estimated to have lost 1.4 $hm^3 \cdot y^{-1}$, while Israel has lost 0.5 $hm^3 \cdot y^{-1}$ – a volume that represents 10% of the total storage capacity Israel controls in the Golan Heights. Flow to the Jordan River increases by +188.6% with the *no precipitation decline* and +53.5% with the *no groundwater development* because of recurrent Yarmoukeem Pool overflows.

Future Scenarios

We examine three future scenarios for the years 2016–2025 with the aim to identify (*i*) potential water flows of the Yarmouk as the Syrian civil war winds down, and (*ii*) how Jordan can support the post-war recovery to simultaneously assist Syrians and promote Jordan's own hydrological interests. Each scenario assumes precipitation is the same as for 2006–2015 (236 $mm \cdot y^{-1}$ on average, similar to the historical 239 $mm \cdot y^{-1}$ average). We recognize that future conditions (social, hydrological, and other) are highly uncertain in conflict areas such as the Yarmouk basin in Syria; and the precision of results critically depends on scenario assumptions. The principal value of these future scenarios is to compare results across conditions that may manifest in the post-war period and help basin states see what role, if any, they could play in recovery efforts:

Status quo The water resources system configuration remains the same as in 2015 (7 dams in disuse because of the Syrian civil war; see Table S2).

Re-operate dams Starting in 2018, Syrians independently rebuild and re-operate dams that fell into disuse to their prior capacities.

Table 1. Consequences of each scenario on the transfers as per the 1994 Treaty of Peace between Israel and Jordan (10).

Beneficiary's share		Historical	No precip. decline	List. dams only	No GW pump. dev.	Aggregate effects
Jordan	μ [hm^3·y^{-1}]	118.5	134.8	119.9	146.4	150.5
	Diff. [%]	-	+13.8	+1.2	+23.6	+27.0
Israel	μ [hm^3·y^{-1}]	39.7	54.9	40.2	56.7	67.7
	Diff. [%]	-	+38.3	+1.3	+42.9	+70.7
Jordan River	μ [hm^3·y^{-1}]	17.2	49.7	17.6	26.4	64.1
	Diff. [%]	-	+188.6	+2.4	+53.5	+272.8

μ and Diff. respectively are the average flow and the difference with the simulated historical flow for the period 1994–2015.

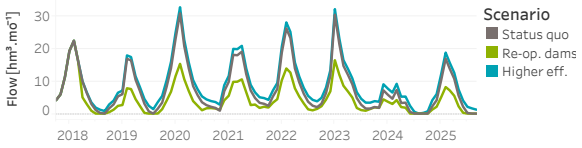

Fig. 5. Simulation results at the Wahda dam location for future scenarios.

Higher irrigation efficiency Donor organizations promote and support Syrian farmers to rebuild and redevelop their irrigation systems to increase efficiency by 10%, reaching 60% and 80% from surface water and groundwater sources respectively from 2018 onwards.

With respect to the *status quo* scenario, Fig. 5 shows that inflow to the Wahda dam would slightly increase with a *higher irrigation efficiency* in Syria. According to our simulations, Jordan and Syria would respectively receive 2.1 and 4.9 hm^3·y^{-1} more water than with the *status quo* of damaged Syrian dams remaining in disuse. Moreover, just as Jordan regularly buys water from Israel through a Lake Tiberias–KAC transfer, it could also be beneficial for Jordan to help Syrian farmers upgrade their irrigation networks so long as saved water flows to the Wahda dam. As for the scenario that considers the rehabilitation of the Syrian dams destroyed or damaged during the civil war, Jordan can expect the Yarmouk River to significantly decrease. In other words, compared to the *status quo* (i.e. damaged Syrian dams remain in disuse) the river would return to the 2010 low flow state. In this case, our simulations show that Jordan and Israel would respectively lose, on average, 18.7 and 6.8 hm^3·y^{-1}.

Discussion

A multi-agent simulation model of the entire Yarmouk River basin has been built from remote sensing products and two time-series of monthly flows near the outlet of the basin only. The model has been validated over the historical period 1983–2015 ($KGE' = 0.90$ at the Wahda dam station).

We have used the model to assess the contributions of natural and anthropogenic factors in the collapse of the Yarmouk flows. These factors are encapsulated in scenarios representing riparian countries' perspectives and other theories regarding the hydrological changes in that basin. Results indicate (*i*) that the unilateral construction of dams that are not listed in the 1987 agreement between Syria and Jordan (Jordanian narrative) has had a limited impact on the flow regime changes; (*ii*) that a 36% precipitation decrease since the first half of the 20th century (Syrian narrative) has largely, but partly, led to the river flow decline; and (*iii*) that groundwater overabstraction by Syrian highland farmers (theory hardly mentioned) has caused most of the decrease in the Yarmouk flows. Two reasons may explain why the third and main factor has not been publicly discussed by the riparians: it is not mentioned in the Jordanian–Syrian agreement (groundwater regulation is unfortunately largely ignored in international water law; 23); and until now, there has not been a tractable method to quantify the effects of groundwater extraction on stream flow, particularly a method that requires extremely limited ground data and that could be applied in a war-torn region. As for the flow increase in 2013, we have shown that the destruction/abandonment of some Syrian reservoirs led to a 25.7 hm^3·y^{-1} flow increase, which alleviated a small part of the previous decrease.

By modeling institutional interactions as per the 1994 Treaty of Peace between Jordan and Israel, we have assessed the relative contributions of these natural and anthropogenic factors on the sharing of the Yarmouk waters between the two countries. This has also been useful when testing future scenarios to estimate how Jordan and Israel can support the post-war recovery of Syria while promoting their own hydrological interests.

The approach developed in this paper is based on freely available remote sensing data and modeling tools (for land use, dams characterization method, precipitation, hydrological modeling and systems modeling). The tools and results can be used in basins where riparian countries and stakeholders share information or they do not. Outside parties can also use the tools and results with less reliance on basin parties for critical information. The methodology has the potential to target issues hampering an effective cooperation between parties, and to provide decision-support information in cases requiring further negotiations.

Materials and Methods

The modeling framework of this study relies on two components: (*i*) the use of remote sensing to retrieve both hydrological and anthropogenic data; and (*ii*) the development of a multi-agent simulation (MAS) model to adequately represent different human and institutional behaviors, and characterize various levels of interactions. The modeling tools and input datasets (except confidential data from MWI/JVA) are freely available on GitHub.

Remote Sensing. Remote sensing is used to retrieve hydrological and anthropogenic data for the MAS model without any detailed on-the ground measurement, observation, survey or interaction with water resources managers. The monthly PERSIANN-CDR precipitation product is used in this study. This global dataset covers the period from January 1983 onwards with a 0.25° spatial resolution. The method developed by Avisse et al. (17) is implemented to locate reservoirs, to assess their maximal storage capacities, and to

monitor their storage for validating the model. This method relies on Landsat satellite images and digital elevation models (DEMs) only and does not require any in situ data. Extrapolations from ground measurements in Jordan are also made to estimate evaporation – which is a major water loss according to MWI/JVA (11) – and sedimentation. The rainfall–runoff hydrological model GR2M (24) is chosen, because of its simple formulation, to estimate the natural flow at the outlet of the basin. This lump model relies on two parameters only (precipitation and evapotranspiration) to produce a discharge on a monthly basis. The resulting flow is then separated between base flow and runoff. The runoff is disaggregated to the location of each reservoir considered for the modeling (i.e. listed in Table S2) using a modified drainage area ratio; and the base flow is assimilated to the groundwater flow. Rivers, pipes, and canals between reservoirs and crops are obtained using DigitalGlobe and CNES/Airbus high resolution (∼1 m) imagery available via Google Earth, and elevation from a DEM. Irrigation water demand is calculated from remotely sensed land use maps, crop water requirements (25), precipitation and standard irrigation efficiencies. More detailed information on these remote sensing techniques is available in *Supporting Information*.

Multi-Agent Simulation. The PyNSim architecture (19) is chosen to develop the MAS model. It adopts an arcs and nodes configuration, which is particularly useful to represent the spatially distributed organization of agents inside the same system (26). Nodes symbolize reservoirs, aquifers, consumption sites, and diversion systems; and arcs symbolize rivers, pipes, canals, and groundwater transfers. The main asset of PyNSim, though, lies in the capacity to define different institutional levels of managing agents, from individual actors who manage one site to institutions who supervise interactions within the water resources system. Human decisions then complement the physical processes from a traditional arcs and nodes representation. All information on the building of the MAS model for our Yarmouk case study is described in *Supporting Information*.

ACKNOWLEDGMENTS. PERSIANN-CDR is developed by the Center for Hydrometeorology and Remote Sensing (CHRS) at the University of California, Irvine (UCI), and is available to the public as an operational climate data record via the NOAA NCDC CDR Program ftp. Landsat satellite images were obtained through the United States Geological Survey (USGS) EarthExplorer. SRTM (C-band) data were released by NASA, and are available at the US Geological Survey's EROS Data Center. We thank Jordan's Ministry of Water and Irrigation, and Jordan Valley Authority, for providing Yarmouk discharge records. This work was conducted as part of the Belmont Forum water security theme for which coordination was supported by the National Science Foundation under grant GEO/OAD-1342869 to Stanford University. Any opinions, findings, and conclusions or recommendations expressed in this material are those of the authors and do not necessarily reflect the views of the National Science Foundation. The authors acknowledge the financial support of NSERC through grant G8PJ-437384-2012.

1. Burdon DJ (1954) Infiltration rates in the Yarmouk basin of Syria-Jordan. *Association Internationale d'Hydrologie Scientifique* 2(37):343–355.
2. Salameh E, Bannayan H (1993) *Water resources of Jordan: present status and future potentials*. (Friedrich Ebert Stiftung, Amman), p. 183.
3. Hof FC (1998) Dividing the Yarmouk's waters: Jordan's treaties with Syria and Israel. *Water Policy* 1(1):81–94.
4. UN-ESCWA and BGR (2013) Inventory of shared water resources in Western Asia, (United Nations Economic and Social Commission for Western Asia and Bundesanstalt für Geowissenschaften und Rohstoffe, Beirut), Technical report.
5. Syria, Jordan (1987) Agreement between the Syrian Arab Republic and the Hashemite Kingdom of Jordan concerning the utilization of the Yarmuk waters.
6. Müller MF, Yoon J, Gorelick SM, Avisse N, Tilmant A (2016) Impact of the Syrian refugee crisis on land use and transboundary freshwater resources. *Proceedings of the National Academy of Sciences* 113(52):14932–14937.
7. Syria, Jordan (1953) Agreement between the Republic of Syria and the Hashemite Kingdom of Jordan concerning the utilization of the Yarmuk waters.
8. Rosenberg DE (2006) The Yarmouk River agreements: Jordan-Syrian transboundary water management, 1953 - 2004. *Arab World Geographer* 9(1):23–39.
9. Hussein H (2017) Whose 'reality'? Discourses and hydropolitics along the yarmouk river. *Contemporary Levant* 0(0):1–13.
10. Israel, Jordan (1994) Treaty of peace between the State of Israel and the Hashemite Kingdom of Jordan.
11. MWI/JVA (2002) Al-Wehdah dam project: Updated feasibility, (The Hashemite Kingdom of Jordan, Ministry of Water and Irrigation/Jordan Valley Authority, Amman), Technical report.
12. Beaumont P (1997) Dividing the waters of the river Jordan: An analysis of the 1994 Israel–Jordan Peace Treaty. *International Journal of Water Resources Development* 13(3):415–424.
13. Kelley CP, Mohtadi S, Cane MA, Seager R, Kushnir Y (2015) Climate change in the Fertile Crescent and implications of the recent Syrian drought. *Proceedings of the National Academy of Sciences* 112(11):3241–3246.
14. FAO (2009) *Irrigation in the Middle East region in figures: AQUASTAT survey - 2008*, FAO Water Reports. (Food and Agriculture Organization, Rome) No. 34, p. 402.
15. Yorke V (2016) *Jordan's Shadow State and Water Management: Prospects for Water Security Will Depend on Politics and Regional Cooperation*, eds. Hüttl RF, Bens O, Bismuth C, Hoechstetter S. (Springer International Publishing, Cham), pp. 227–251.
16. Al-Bakri JT (2015) Mapping irrigated crops and their water consumption in Yarmouk basin. A report for regional coordination on improved water resources management and capacity building, (Ministry of Water and Irrigation), Technical report.
17. Avisse N, Tilmant A, Müller MF, Zhang H (2017) Monitoring small reservoirs' storage with satellite remote sensing in inaccessible areas. *Hydrology and Earth System Sciences* 21(12):6445–6459.
18. Aw-Hassan A, Rida F, Telleria R, Bruggeman A (2014) The impact of food and agricultural policies on groundwater use in Syria. *Journal of Hydrology* 513:204–215.
19. Knox S (2014) PyNSim's documentation (http://umwrg.github.io/pynsim/; last access: 14 February 2017).
20. Kaisi A, Yasser M (2004) Participatory management of water resources for agricultural purposes in Syrian Arab Republic in *Participatory water saving management and water cultural heritage*. (Hamdy A. (ed.), Tüzün M. (ed.), Lamaddalena N. (ed.), Todorovic M. (ed.), Bogliotti C. (ed.)), pp. 243–253. Options Méditerranéennes : Série B. Études et Recherches; n. 48.
21. Gül A, Rida F, Aw-Hassan A, Büyükalaca O (2005) Economic analysis of energy use in groundwater irrigation of dry areas: a case study in Syria. *Applied Energy* 82(4):285–299.
22. UNHCR (2017) Syria regional refugee response: Inter-agency information sharing portal (http://data.unhcr.org/syrianrefugees/country.php?id=107; last access: 14 February 2017).
23. Eckstein Y, Eckstein GE (2005) Transboundary aquifers: Conceptual models for development of international law. *Ground Water* 43(5):679–690.
24. Mouelhi S, Michel C, Perrin C, Andréassian V (2006) Stepwise development of a two-parameter monthly water balance model. *Journal of Hydrology* 318(1):200–214.
25. Allen RG, Pereira LS, Raes D, Smith M (1998) *Crop evapotranspiration: Guidelines for computing crop water requirements*, FAO Irrigation and drainage paper. (Food and Agriculture Organization, Rome) No. 56, p. 300.
26. Harou JJ, et al. (2009) Hydro-economic models: Concepts, design, applications, and future prospects. *Journal of Hydrology* 375(3):627–643.
27. Barnes J (2009) Managing the waters of Ba'th country: The politics of water scarcity in Syria. *Geopolitics* 14(3):510–530.
28. Courcier R, Vénot JP, Molle F (2005) Historical transformations of the lower Jordan river basin (in Jordan): Changes in water use and projections (1950-2025) in *Comprehensive Assessment Research Report 9*. (Comprehensive Assessment Secretariat, Colombo).
29. World Bank (2001) Syrian Arab Republic irrigation sector report, (World Bank, Rural Development, Water and Environment Group, Middle East and North Africa Region), Report No. 22602-SYR.
30. Salman M, Mualla W (2008) Water demand management in Syria: centralized and decentralized views. *Water Policy* 10(6):549–562.
31. Delannoy JJ, Madeline P, Lhenaff R (2016) *Géographie physique: Aspects et dynamique du géosystème terrestre*. (Vuibert, Paris), p. 840.
32. Şen Z (2008) *Wadi hydrology*. (Taylor & Francis, Boca Raton), p. 368.
33. Chavez P (1996) Image-based atmospheric corrections revisited and improved. *Photogrammetric Engineering & Remote Sensing* 62(9):1025–1036.
34. Wu W, De Pauw E (2011) A simple algorithm to identify irrigated croplands by remote sensing, (GISU/ICARDA), Technical report.
35. Du C, Ren H, Qin Q, Meng J, Zhao S (2015) A practical split-window algorithm for estimating land surface temperature from Landsat 8 data. *Remote Sensing* 7(1):647–665.
36. Ibrahim WY, Batzli S, Menzel WP (2014) Agricultural policy effects on land cover and land use over 30 years in Tartous, Syria, as seen in Landsat imagery. *Journal of Applied Remote Sensing* 8(1):083506.
37. Bastiaanssen W (2015) Satellite-based estimation of evapotranspiration, soil moisture and biomass production for two irrigated areas in Jordan, (MWI), Report for the Ministry of Water and Irrigation.
38. Dastane NG (1974) *Effective rainfall in irrigated agriculture*, FAO Irrigation and drainage paper. (Food and Agriculture Organization, Rome) No. 25, p. 62.
39. Etana Syria (2015) The Yarmouk basin: Between conflict and development, (Etana Syria), Technical report.
40. CBSSYR (2004) 2004 census, (Central Bureau of Statistics Syria), Official document.
41. Barnaud C, Le Page C, Dumrongrojwatthana P, Trébuil G (2013) Spatial representations are not neutral: Lessons from a participatory agent-based modelling process in a land-use conflict. *Environmental Modelling & Software* 45(Supplement C):150–159.
42. Giuliani M, Castelletti A, Amigoni F, Cai X (2015) Multiagent systems and distributed constraint reasoning for regulatory mechanism design in water management. *Journal of Water Resources Planning and Management* 141(4):04014068.
43. Bousquet F, Le Page C (2004) Multi-agent simulations and ecosystem management: a review. *Ecological Modelling* 176(3):313–332.
44. Gupta HV, Kling H, Yilmaz KK, Martinez GF (2009) Decomposition of the mean squared error and NSE performance criteria: Implications for improving hydrological modelling. *Journal of Hydrology* 377(1):80–91.
45. Kling H, Fuchs M, Paulin M (2012) Runoff conditions in the upper Danube basin under an ensemble of climate change scenarios. *Journal of Hydrology* 424:264–277.
46. Giuliani M, Castelletti A (2013) Assessing the value of cooperation and information exchange in large water resources systems by agent-based optimization. *Water Resources Research* 49(7):3912–3926.

Supporting Information (SI).

.1. Incremental Naturalized Inflows to each Reservoir. The rainfall–runoff hydrological model GR2M (24) relies on two input datasets: precipitation and evapotranspiration. Precipitation directly comes from the PERSIANN-CDR satellite estimates, and evapotranspiration is calculated as the average of crop water requirements over the YRB from the land use maps that have been created, and using the single-crop coefficient method (see *Water Withdrawals*).

GR2M is calibrated with two parameters (a "production store" capacity and a percolation parameter) to minimize the sum of squared distances between simulated and "reference" naturalized water year flows of the Yarmouk River (i.e. from October to September). This "reference" naturalized flow is generated using a proportional calculation between precipitation averaged over the YRB for each water year, and historical precipitation and discharge of 372 mm·y^{-1} and 467 hm^3·y^{-1} respectively (2). Finally, because this study is principally aimed at analyzing policies in data-scarce areas, a few rare inconsistencies on simulated naturalized flows are corrected: when simulated naturalized flows are lesser than observed flows, the former are replaced by the latter.

A base flow is consecutively extracted from the final simulated flow at Adasiya, and assumed to amount to 9 hm^3·mo^{-1} as the 1st percentile of GR2M values. Considering the ratio between observed inflows to Adasiya and the Wahda dam location, the base flow is divided with the repartition 2 hm^3·mo^{-1} and 7 hm^3·mo^{-1} between these two stations respectively.

In order to better estimate inflows to each reservoir considered for the modeling (i.e. listed in Table S2), the PERSIANN-CDR precipitation is corrected to represent the rainfall effectively contributing to the runoff. Indeed, while the spatial resolution of PERSIANN-CDR is already relatively fine, it is still coarse compared to the size of some reservoirs' catchment: each pixel covers more than 650 km^2, which is for example almost four times the area of Qunaitera's incremental watershed where precipitation varies a lot. Thus, PERSIANN-CDR images are resampled to match Landsat resolution, and each precipitation value is weighted inside the YRB, using a gradient derived from isohyets (1, 2, 27), to form a *weighted precipitation* (P_w). A runoff factor is added to take into account the strong variability of infiltration inside the YRB (1) and produce a *contributive precipitation* (P_c).

The naturalized runoff at Adasiya estimated above with GR2M (i.e. total simulated flow minus groundwater flow) is then disaggregated to each reservoir's catchment, proportionally to the catchment's area and to the *contributive precipitation* P_c averaged over it, to get the inflows to each reservoir.

.2. Groundwater Dynamics. The mean annual usable recharge (R) of the Yarmouk aquifer is estimated to be around 125 hm^3·y^{-1} (28). Because the base flow of the Yarmouk at Adasiya did not vary much for all the duration of Jordanian records – unlike at the Wahda dam –, and because almost all crop areas are located upstream from the Wahda dam, all groundwater abstractions are assumed to be made in the aquifer upstream from the latter station, and all return flows to eventually reach it. The water balance of this aquifer at a given month t can then be expressed as:

$$\Delta Q_\mathrm{t} = R/12 - \sum_p \{\bar{x}_\mathrm{t}^\mathrm{p} - \bar{f}_\mathrm{t}^\mathrm{p}\} + \sum_w \bar{i}_\mathrm{t}^\mathrm{w} \qquad [1]$$

with $\bar{x}$ [hm^3] and $\bar{f}$ [hm^3] the groundwater withdrawals and return flows associated to each land use map's pixel p (see *Water Withdrawals*), and $\bar{i}$ [hm^3] the infiltration inside each wadi w (see *Wadis and Canals*), averaged over the last 24 months before t to consider a certain transit time inside the aquifer.

The base flow of the Yarmouk River at the Wahda dam location is assumed to be affected and to decrease when the water balance of the aquifer becomes negative, i.e. if:

$$X_\mathrm{t} > \frac{R/12 + I_\mathrm{t}}{1 - 0.3 \cdot (1 - \eta_\mathrm{i})} \qquad [2]$$

with X [hm^3] and I [hm^3] the sums of all groundwater withdrawals in the YRB and infiltration inside wadis, and η_i the irrigation efficiency (see *Water Withdrawals*). Simulations have a posteriori shown infiltration to be around 1.7 hm^3·mo^{-1} on average over the pre-1999 stationary regime period (see *Validation of the Modeling*). Consequently, we get from this value and Eq. 2 a threshold of approximately 14.8 hm^3·mo^{-1} for X above which the level of the aquifer lowers. In that case, the base flow at the Wahda dam location decreases by $|\Delta Q_\mathrm{t}|$.

.3. Wadis and Canals. Connections between reservoirs through wadis and canals/pipes represented in Fig. S6, are obtained from Google Earth and elevation from the SRTM-C DEM.

The maximal transfer capacity is calculated for each canal or pipe with the Manning-Strickler equation:

$$Q_\mathrm{p} = K_\mathrm{s} \cdot A_\mathrm{p} \cdot {R_\mathrm{h}}^{2/3} \cdot j^{1/2} \qquad [3]$$

where K_s [m$^{1/3}$·s^{-1}] is the Strickler coefficient, A_p [m^2] the cross sectional area of flow, $R_\mathrm{h} = A_\mathrm{p}/P_\mathrm{p}$ [m] the hydraulic radius (with P_p [m] the wetted perimeter), and j [m·m^{-1}] the hydraulic slope. By considering a canal in unfinished concrete ($K_\mathrm{s} = 60$ m$^{1/3}$·s^{-1}) and dimensions roughly determined using DigitalGlobe and CNES/Airbus imagery available via Google Earth (cross section of 1 m large and 0.5 m high; and $j = 0.1\%$), we get $Q_\mathrm{p} \simeq 1.00$ hm^3·y^{-1}. To this discharge is applied a canal conveyance yield (50%; 29, 30) to evaluate the quantity effectively reaching crops downstream.

As for the wadis, we considered 50% of losses in the transmission of water releases from one reservoir to another to account for infiltration (31). 75% of these losses are then assumed to recharge the aquifer (32).

.4. Storage Variations. Storage is assessed with the algorithm developed by Avisse et al. (17) from 1998 onwards, as Landsat images were not continually available for previous years, and for reservoirs large enough to apply the method (capacity > 1 hm^3 and maximal area > 0.5 km^2). For smaller reservoirs (i.e. Dar'a al-Sharqi, Al-Ghariyah al-Sharqiyah, Tafas, and Harran), the method's water area monitoring is combined to a linear storage–area relationship based on official storage capacities (5).

.5. Net Reservoir Evaporation. The net quantity of water that is evaporated at each month above each reservoir is assessed by deriving reservoirs' area from reservoirs' simulated storage (using the storage–area relationships presented in *Storage Variations*; 17), by considering the *weighted precipitation* P_w (see *Incremental Naturalized Inflows to each Reservoir*), and the same monthly reservoir evaporation as the one measured above the Wahda dam (11).

.6. Sedimentation. 0.6 hm^3 of sediments filled the Wahda dam since the dam started to store water. From this value and the 341 hm^3 of cumulated inflows that reached the reservoir since its completion in 2006, we roughly get a ratio of 0.0018 cubic meter of sediments per cubic meter of water. The same ratio is used to estimate at which rate Syrian reservoirs fill with sediments.

.7. Water Withdrawals. The focus is put on irrigation, as it accounts for 80% of water use in the Syrian part of the YRB (29). This usage is also more consumptive than industrial and household usages. Irrigation water demand is calculated from land use, crop water requirements, precipitation, and an assumption on efficiency.

Al-Bakri conducted a detailed study on land use in the Jordanian part of the YRB for the year 2014 (16). As we did not find any similar work or ground data for the rest of the basin, remote sensing is relied on to create a first land use map for 2014. Landsat products are chosen because their spatial resolution (30 m) is fine enough to delineate the small irrigated crop areas cultivated by farmers in the YRB. Satellite images are gathered to cover a period of one year over the basin. The Normalized Difference Vegetation Index (NDVI) is then computed from surface reflectance, which is estimated with the Dark Object Subtraction 1 (DOS1; 33) atmospheric correction applied to top of atmosphere (TOA) reflectance. A principal component analysis (PCA) is applied before conducting an unsupervised classification. Resulting classes are eventually associated to particular irrigated crops by using as a reference the irrigated crops areas obtained by Al-Bakri (16), and pictures taken by local people in the YRB and available in Google Earth. Irrigated olive trees are also distinguished from rainfed ones by analyzing land surface temperature anomalies (LST anomalies; 34) evaluated with a Split-Window algorithm (35). Because this whole land-use

map production step is quite cumbersome, and because by any means no ground data is available for years different than 2014, only two other maps are created using the same protocol – with a mask derived from the 2014 map to distinguish irrigated and rainfed olives – for key transition years in irrigation development policies (18, 30): 1984 and 1998. It can be noted that similar years are considered by Ibrahim et al. (36) to analyze the effect of agricultural policies on land use in Syria. No map is produced for the pre-development phase nor for years before 1984 because Landsat images are not available over the YRB for that period.

For each timestep and each pixel in a land use map, we estimate crop water requirements (ET_c) using the single crop coefficient method and parameters from the Food and Agriculture Organization of the United Nations (FAO) Penman-Monteith method (25). However, a correction factor calibrated with ground measurements in Jordan (16, 37) is applied to FAO's crop coefficient to take into account local conditions of irrigation and plant spacing. For years between 1984, 1998, 2006 and 2014, crop water requirements are interpolated from the three land use maps and by assuming an irrigated crop area twice as large in 2006 as in 1998 (6). ET_c for 1983 and 2015 is assumed to be the same as for 1984 and 2014 respectively. A crop irrigation deficit is injected to consider that only 60% of the crop demand is met (average deficit in the Jordan Valley). In order to account for surface runoff and deep percolation below the root zone, an *effective precipitation* (P_e) is computed from P_w (see *Incremental Naturalized Inflows to each Reservoir*) to estimate precipitation de facto available to crops (38). Irrigation efficiencies (η_i) of 50% for surface water and 70% for groundwater are considered to compute final water withdrawals (based on 14, 30). It must be noted that return flows to the aquifer are then estimated to account for 30% of irrigation losses. Water users are linked to water sources based on the land use maps and detailed imagery available in Google Earth. For irrigated crop areas close to reservoirs listed in Table S2 and built for irrigation purpose, farmers are assumed to withdraw water in reservoirs first to try to meet the demand; and then in aquifers if there is not enough water in the reservoirs (39).

Households near reservoirs are also considered as they are assumed to use the reservoir as their primary source of water. Water withdrawals for household consumption are then assessed using population data from the 2004 Syrian official census (40), a 5 $m^3 \cdot mo^{-1} \cdot cap^{-1}$ consumption extrapolated from the consumption of Jordanians, and the conveyance yield of 50% (see *Wadis and Canals*).

.8. Multi-Agent Simulation Model of the Yarmouk Basin. Multi-agent simulation (MAS) techniques have recently received a lot of attention due to their ability to capture decision-making at the agent level, be it an institution (e.g. a government agency, a riparian country) or a water user (e.g. a farmer, a household) as well as their interactions (41, 42). In a typical MAS, human agents are implemented as autonomous entities that make decisions in relation to one another and in response to hydrological and socioeconomic conditions (43). MAS are therefore well suited to model water resources systems characterized by multiple institutions with varying degrees of cooperation.

In our study area, the YRB and the Yarmoukeem Pool (YP)–Lake Tiberias–KAC water exchange systems make the water resources system environment (see the arcs and nodes configuration in Fig. S7*A*).

Fig. S7*B* illustrates the multi-agent configuration of the whole system created with PyNSim (see *Materials and Methods*). Local irrigation needs are assumed to be prioritized over other downstream needs in Syria (39) and the occupied Golan Heights (no cooperation between Israel and Syria). Upstream reservoirs release water to downstream reservoirs only when their maximal storage capacity is reached: the standard operation policy (SOP) is consequently adopted to represent the management of these reservoirs (the relevance of this choice is discussed in *Validation of the Modeling*). As for the Wahda dam operator, it releases water from the reservoir only when the inflows make the simulated storage larger than the storage that has been measured on the ground by JVA (validation step; see *Validation of the Modeling*); or more water in case the outflow is not sufficient to satisfy the *allocation* (scenario simulation step; see *Consequences on the Water Transfers as per the 1994 Treaty of Peace*). These controllers basically follow the instructions of their respective institutional supervisors, while preserving the water balance and physical constraints of each diversion system.

.9. Validation of the Modeling. The PyNSim MAS simulation model is first run to recreate the observed flow at the Wahda dam and Adasiya over the historical period. Results are presented in Fig. S8.

Qualitatively, the model reproduces well the seasonality of the Yarmouk River flow. More importantly with regard to the objective of this study, it replicates well the three periods initially identified at the Wahda dam station (Fig. 2): (*i*) the stationary period before 1999, (*ii*) the subsequent collapse of both the base flow and the runoff, and (*iii*) the return of the runoff in 2013. The fact that the simulated base flow collapses in 1999, at the exact same time as in the observations, also validates the reasoning behind the definition of a threshold on groundwater abstractions (see *Groundwater Dynamics*). The slight difference in the rate of the base flow reduction may be explained either by errors on irrigation requirements estimates (or a change in irrigation efficiency), or by the simplistic representation of the aquifer's dynamics in the modeling. The contrasted quality of the results for certain years (e.g. 1990, 2004, 2014 at Wahda; or 1993 at Adasiya) may be caused by errors in PERSIANN-CDR data, by the difficulty to locally calibrate this precipitation dataset (or the GR2M model), or by a few temporary changes in the operation of the Syrian reservoirs.

The remote sensing storage monitoring (see *Storage Variations*) is used to discuss the validity of the SOP. By comparing the simulated monthly cumulated storage in Syria and the occupied Golan Heights to remote sensing observations, we obtain a correlation coefficient of 0.67. This means that the simulated human decisions concerning reservoir operation are significantly correlated with the decisions that reservoir managers actually took between 1998 and 2015. Differences between model estimates and remote-sensed values are potentially influenced by errors on the assessment of natural inflows, land use, irrigation requirements, crop–water source association, reservoir operation, or just remote-sensed storage estimates.

As for the results at the outlet of the YRB, the modified Kling-Gupta efficiency-statistic (KGE' in Eq. 4; 44, 45) is chosen to take into account the strong variability of the Yarmouk River flow, and to measure the quality of the simulated flows:

$$KGE' = 1 - \sqrt{(r-1)^2 + (\beta-1)^2 + (\gamma-1)^2} \qquad [4]$$

where r is the correlation coefficient between simulated and observed flows, $\beta = \mu_s/\mu_o$ is the bias ratio with μ the mean discharge, $\gamma = CV_s/CV_o = (\sigma_s/\mu_s)/(\sigma_o/\mu_o)$ is the variability ratio with CV the coefficient of variation and σ the standard deviation, and s and o indices stand for *simulated* and *observed* data respectively.

We then obtain KGE' values of 0.64 and 0.90 for discharges at Adasiya and the Wahda dam respectively. These high values confirm the validity of the modeling.

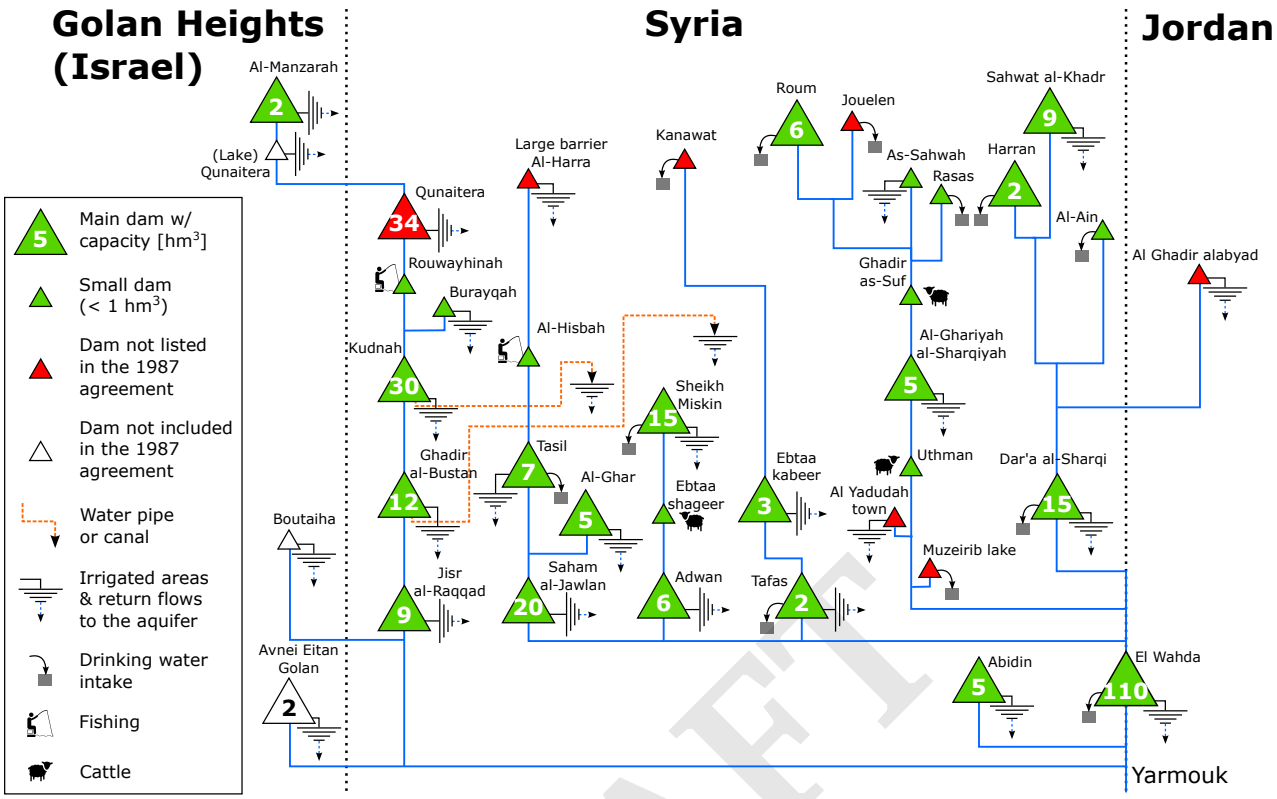

Fig. 6. Reservoirs, usages, wadis and canals detected in the Yarmouk River basin using remote sensing.

Table 2. Dams considered in the modeling.

Name	Operator's country	Listed?	Coordinates [East, North]	Completion year	Disuse year	Capacity [hm^3]	$\bar{q}_{nat}$ [hm^3·y^{-1}]
Al-Manzarah	Israel	Yes	223485, 282845	1982	-	2.3	0.3
Avnei Eitan al-Golan		-	223991, 246480	1982	-	2.3	0.5
Abidin		Yes	228895, 242487	1989	-	5.5	0.4
Qunaitera		No	231404, 280519	2006	2013	33.9	9.3
Jisr al-Raqqad		Yes	234093, 253358	1991	-	11.0	1.4
Kudnah		Yes	236056, 270196	1992	-	30.0	5.4
Al-Ghar		Yes	235663, 249285	1990	2013	5.5	0.5
Saham al-Jawlan		Yes	236335, 245880	1995	-	20.0	0.6
Ghadir al-Bustan		Yes	237999, 260863	1987	-	12.0	1.9
Tasil		Yes	240680, 253980	1984	-	6.6	7.7
Adwan	Syria	Yes	245080, 243840	1986	2013	5.7	3.0
Ebtaa kabeer		Yes	254499, 247077	1972	2013	3.5	8.9
Sheick Miskin		Yes	255463, 252644	1982	2013	15.0	30.1
Roum		Yes	305526, 237106	1977	-	6.4	0.3
Sahwat al-Khadr		Yes	277060, 218989	1986	-	8.8	0.6
Dar'a al-Sharqi		Yes	254714, 223397	1970	2013	15.0	31.1
Tafas		Yes	247434, 240864	1982	-	2.1	6.9
Al-Ghariyah al-Sharqiyah		Yes	271627, 231346	1982	2013	5.0	11.7
Harran		Yes	304324, 223335	1980	-	2.0	0.3
El Wahda	Jordan	Yes	232104, 237922	2007	-	110.0	64.4

Coordinates are expressed in WGS 84/UTM zone 36N (EPSG:32636). $\bar{q}_{nat}$ are naturalized incremental runoffs to the reservoirs averaged over the historical period.

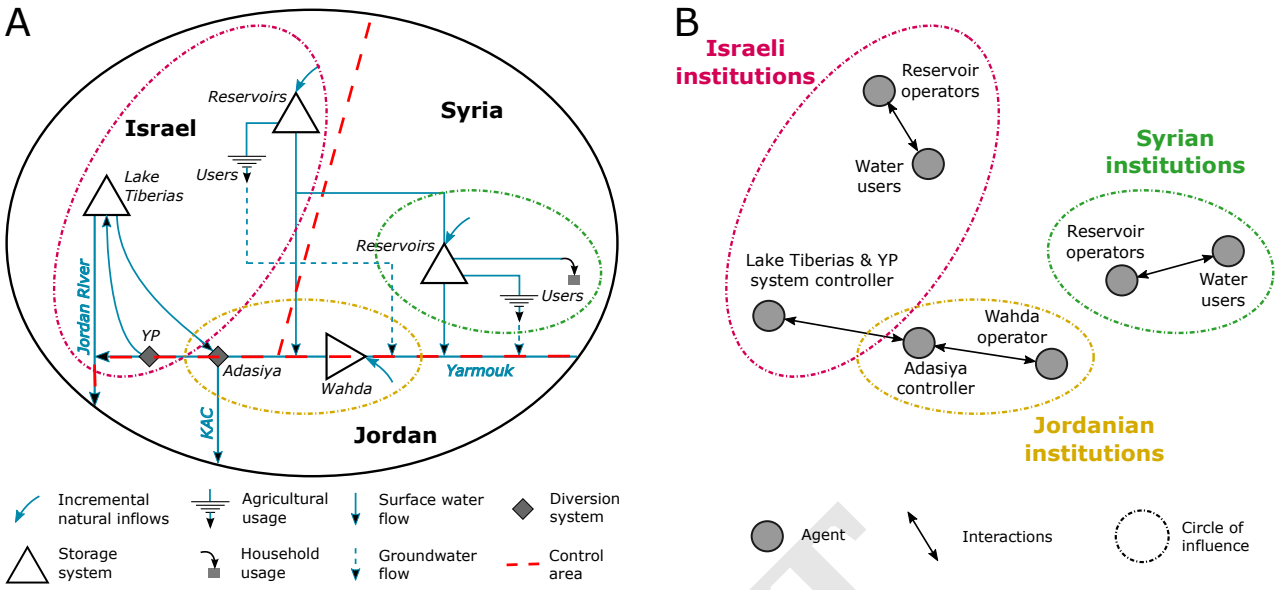

Fig. 7. (*A*) Schematic of the water resources system considered in this study. The reservoir system is a simplified version of the complex multi-reservoir system of Fig. S6. The exchange system at Adasiya separates the flow between *alpha* (diversion to the KAC) and *beta* (natural route), and the Israeli system at the Yarmoukeem Pool (3.5 km downstream from Adasiya along *beta*) sends up to 4.5 $m^3 \cdot s^{-1}$ to Lake Tiberias, essentially to supply the *allocation* and *concession*. This *concession* is eventually sent back to the KAC from Lake Tiberias as per the treaty between Israel and Jordan. Flows above 4.5 $m^3 \cdot s^{-1}$ go to the Jordan River. (*B*) Associated multi-agent representation with supervising institutions from each riparian country – based on a generic MAS representation (46). Main reservoirs' operators are considered as independent (i.e. stakeholders with their own interests) storing water from the inflows, releasing water to meet certain demands (through water user agents), or spilling water in case they overflow. Other agents characterize Jordanian and Israeli controllers of the diversion systems at Adasiya and the Yarmoukeem Pool. Institutions are also created to represent the supervising managers in each country. Since Jordan and Israel interact to transfer water as per the Treaty of Peace, the circles of influence of the two countries' institutions overlap. The circles of influence of Syrian and Jordanian institutions do not overlap because there is no effective cooperation between the two countries, despite the signature of the 1987 agreement (9).

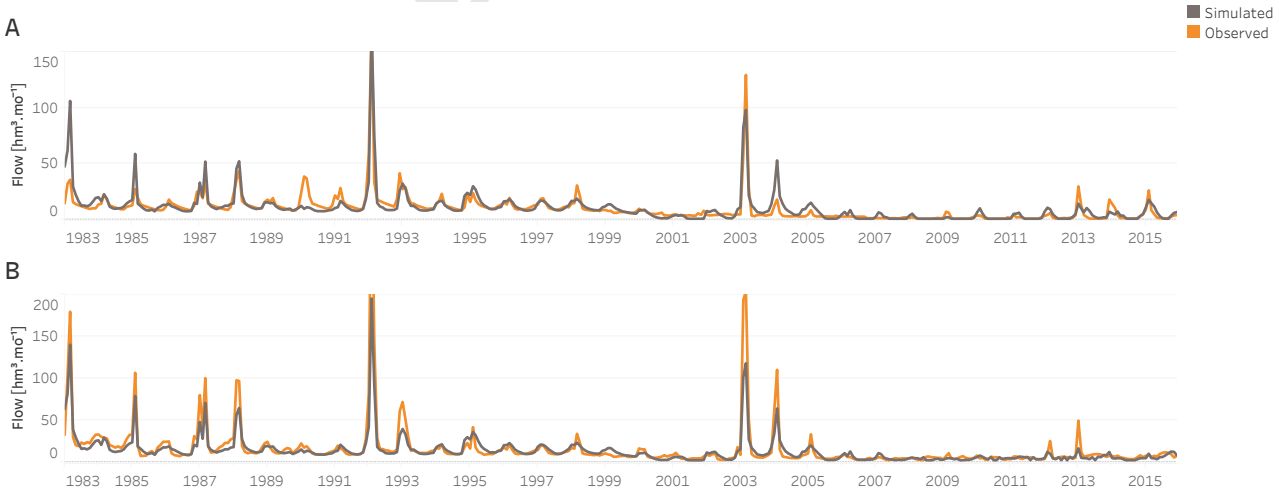

Fig. 8. Measured flows and simulation results of the historical run at (*A*) Wahda and (*B*) Adasiya stations.

Appendix C

A New Temperature-Vegetation Triangle Algorithm with Variable Edges (TAVE) for Satellite-Based Actual Evapotranspiration Estimation

Hua Zhang[1], Steven M. Gorelick[2], Nicolas Avisse[3], Amaury Tilmant[3], Deepthi Rajsekhar[2] and Jim Yoon[2]: A New Temperature-Vegetation Triangle Algorithm with Variable Edges (TAVE) for Satellite-Based Actual Evapotranspiration Estimation, Remote Sensing, 8, 735, doi:10.3390/rs8090735, 2016.

[1] Department of Engineering, School of Engineering and Computing Sciences, Texas A&M University, Corpus Christi, TX 78412, USA

[2] Department of Earth System Science, Stanford University, Stanford, CA 94305-2115, USA

[3] Department of Civil Engineering and Water Engineering, Université Laval, Québec, QC G1V 0A6, Canada

Résumé

L'estimation de l'évapotranspiration réelle (AET), qui est variable dans l'espace, est un défi majeur pour la gestion régionale des ressources en eau. Nous proposons une nouvelle méthode de télédétection, l'algorithme du triangle à bords variables (TAVE), pour générer des estimations d'AET journalières, à partir de données satellitaires de température de la surface terrestre et d'indice de végétation NDVI. Le TAVE saisit l'hétérogénéité de l'AET à travers différentes zones de même altitude, et permet une certaine variabilité dans la détermination des valeurs locales des classes extrêmes humide et sèche (connues sous le nom de bords). Comparé aux méthodes du triangle traditionnelles, TAVE introduit trois caractéristiques uniques : (i) la discrétisation du domaine en zones d'altitude qui se superposent ; (ii) un bord humide variable qui est une fonction de la zone d'altitude ; et (iii) des valeurs variables pour un paramètre d'effets combinés (tenant compte des résistances aérodynamique

et de surface, du gradient de pression de vapeur, et de la disponibilité de l'humidité du sol) le long des bords sec et humide. Avec ces caractéristiques, TAVE répond efficacement à l'influence combinée du terrain et du stress hydrique sur les estimations d'AET dans un environnement semi-aride. Nous démontrons l'efficacité de cette méthode dans l'un des pays les plus secs au monde – la Jordanie, et la comparons à la méthode du triangle traditionnelle (TA) et à un produit d'AET mondial (MOD16) sur différentes types d'utilisation des terres. Pour les terres irriguées, TAVE a produit des résultats similaires à ceux de la méthode du coefficient de culture unique (-3%), par rapport à une surestimation importante de TA (+234%) et à une sous-estimation de MOD16 (-50%). Dans les régions forestières (non-irriguées, consommatrices d'eau), TA et MOD16 ont produit des écarts moyens d'AET 15,5 fois et -3.5 fois plus importants que ceux déterminés par TAVE. Puisque TAVE possède une structure simple et des exigences de données faibles, il fournit un moyen efficace de satisfaire le besoin grandissant d'estimations d'évapotranspiration dans des régions semi-arides pauvres en données. Cette étude constitue une étape réellement nécessaire pour la quantification par satellite de la consommation agricole d'eau en Jordanie.

Appendix D

Impact of the Syrian refugee crisis on land use and transboundary freshwater resources

Marc François Müller[1,2], Jim Yoon[1], Steven M. Gorelick[1], Nicolas Avisse[3], and Amaury Tilmant[3]: Impact of the Syrian refugee crisis on land use and transboundary freshwater resources, P. Natl. Acad. Sci. USA, 113, 14932–14937, doi:10.1073/pnas.1614342113, 2016.

[1] Department of Earth System Science, Stanford University, Stanford, CA 94305, USA

[2] Department of Civil & Environmental Engineering & Earth Sciences, University of Notre Dame, Notre Dame, IN 46556, USA

[3] Department of Civil and Water Engineering, Université Laval, Quebec, QC, Canada G1V 0A6

Résumé

Depuis 2013, des centaines de milliers de réfugiés ont migré vers le sud en direction de la Jordanie pour échapper à la guerre civile syrienne qui a débuté à la mi-2011. L'évaluation des impacts des conflits et migrations sur l'utilisation des terres et les ressources en eau transfrontalières dans une zone de guerre active reste un défi important. Cependant, les analyses spatiale et statistique de l'imagerie satellitaire sur la période récente de migration massive des réfugiés syriens montrent des changements rapides dans l'utilisation des terres, ainsi que l'utilisation et la gestion de l'eau dans le bassin de la rivière Yarmouk–Jordanie partagé par la Syrie, la Jordanie et Israël. Le conflit et l'émigration qui s'en est suivie ont entraîné une diminution de $\sim$50% à la fois dans l'agriculture irriguée en Syrie et dans la rétention des pluies hivernales dans les barrages syriens, ce qui a provoqué un apport d'eau supplémentaire inattendu à l'aval en Jordanie pendant la période de migration des réfugiés. En comparant les périodes pré- et post-migration, l'abandon syrien des terres irriguées est responsable pour moitié de l'augmentation du débit du cours d'eau, l'autre moitié étant attribuable à la récupération

d'une grave sécheresse. Malgré cette augmentation, le débit du Yarmouk à l'entrée de la Jordanie est toujours nettement inférieur au volume prévu par la Jordanie en vertu des accords bilatéraux de 1953, 1987 et 2001 avec la Syrie.

Appendix E

Freshwater distribution model of the Water Authority of Jordan

My first contribution to the Jordan Water Project was the development of an optimization model to represent the distribution of freshwater in the Water Authority of Jordan (WAJ) network presented in Fig. E.1.

It has been assumed that WAJ takes yearly decisions to monthly distribute water between the 12 governorates of the country with the objective of (1) minimizing the deficit (i.e. difference between the demand and the supply), and (2) minimizing the costs for transferring the water between the governorates. The problem has been mathematically formulated as:

$$Z^* = \min_{q,\delta} \left\{ \sum_i \sum_m \left[C_\delta \cdot \delta_{\mathrm{i,m}}^2 + \sum_j C_\mathrm{q} \cdot q_{\mathrm{i,j,m}} \right] \right\} \tag{E.1}$$

subject to:

$$d_{\mathrm{i,m}} = \sum_j \left(q_{\mathrm{j,i,m}} - q_{\mathrm{i,j,m}} \right) + \sum_s r_{\mathrm{i,s,m}} + \delta_{\mathrm{i,m}} \quad \forall (i,m) \tag{E.2}$$

$$\sum_m r_{\mathrm{i,s,m}} \leq R_{\mathrm{i,s}} \quad \forall (i,s) \tag{E.3}$$

$$q_{\mathrm{j,i,m}} \leq 3600 \cdot 24 \cdot 31 \cdot 10^6 \cdot V_{\max} \cdot \pi \cdot \frac{D_{\mathrm{j,i}}^2}{4} \quad \forall (j,i,m) \tag{E.4}$$

with Z^* the minimum total costs depending on the transfers $q_{\mathrm{i,j,m}}$ (hm^3) from governorate i to j at month m, d (hm^3) and δ (hm^3) the monthly demand and deficit within a governorate, C_q and C_δ the costs associated to transfers and deficits (empirically put at 1 and 10^5 JOD/hm^3 to prioritize the objectives), r (hm^3) the monthly supply from a source s (i.e. surface water or groundwater) inside a governorate, R (hm^3) the yearly water availability associated to a certain source in a certain governorate, $V_{\max}$ the maximum water velocity inside a pipe (roughly put at 1 m^3/s), and $D_{\mathrm{j,i}}$ the main pipe diameter from governorate j to i. d, R and D are input data from WAJ; while q, δ and r are decision variables. Eq. E.2 then ensures the water balance is satisfied inside a governorate, Eq. E.3 ensures that

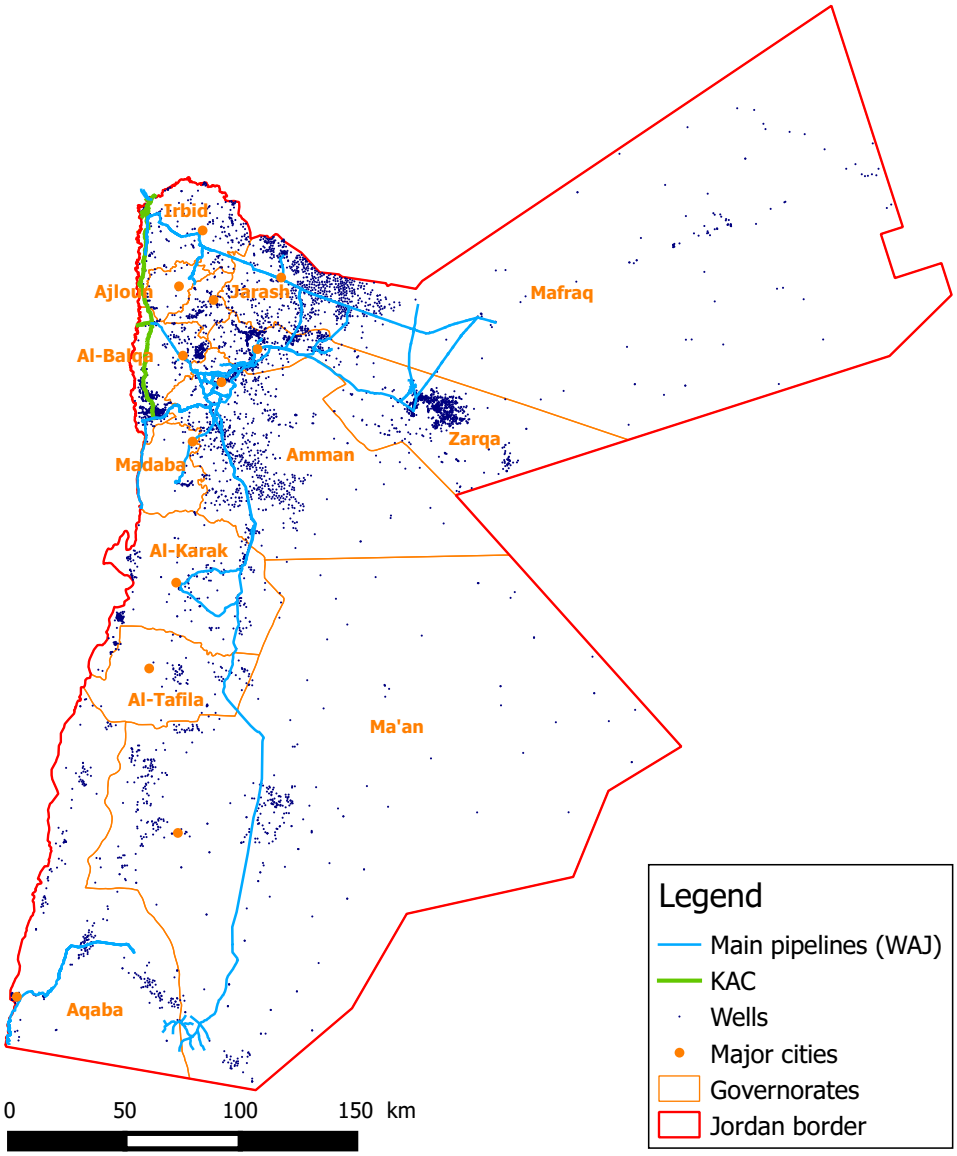

Figure E.1: Inter-governorate network of the Water Authority of Jordan. The major cities have the same name as their respective governorate.

the supply does not exceed the availability, and Eq. E.4 that the transfers do not exceed the conveyance system capacities.

The model was first applied to the year 2013 for which data on monthly WAJ transfers per governorate is available. The results indicated significant discrepancies when looking at particular transfers, even if the yearly water balance was satisfied. Pumping costs and differences in elevation between governorates have also been considered, but I had difficulties in estimating the related energy costs that may vary a lot both in space and time. Further work on this part of the project has thus focused on maintaining to some extent the same transfers from month to month to get simulated flows as close as possible to the transfers that had been monitored by WAJ.